



Politecnico di Torino

Laurea Magistrale in Ingegneria per l'Ambiente e il Territorio

Behavior and Spread of Carbon Iron Particles in a 2D Confined Aquifer Model

Host Institution:

University of Stuttgart, Vegas-Research Facility for Subsurface Remediation

Supervisor: Prof. Tiziana Tosco

External supervisors: Dr. Jürgen Braun M.Sc Giulia Giannelli (University of Stuttgart)

Candidate: Antonio Manzo

Acknowledgment:

For the realization of a work is always necessary a help, this help can be in different way and for this reason is necessary to thank the people that allowed me to arrive where I am now.

Inizio in italiano, poichè le prime persone che mi vengono in mente fanno parte della mia famiglia. Grazie ai miei genitori ed ai miei fratelli che mi hanno sempre spinto a realizzare ciò che volevo fare, spronandomi e consigliandomi.

Un ringraziamento ai ragazzi del centro sociale sindacale di Solofra, sempre disponibili ad avere una chiacchierata a distanza o farmi pesare meno questi anni lontano dal paese di origine con chiamate insaspettate per sapere come stesse andando e se “mi fossi già fatto i soldi”.

Un ringraziamento speciale al Gagliardo, sempre disponibile ad ospitarmi a Firenze nei miei primi traumatici mesi a Torino.

Un ringraziamento ai coinquilini ed i compagni di corso di Torino, che mi hanno sopportato come conviventi e colleghi e che mi hanno aiutato a superare le tante ansie della vita universitaria.

I think that it is better to thank in English my professor Tiziana Tosco, that gave me the possibility to do this experience in Germany, always available to help and solve doubts.

It is important to thank also the Erasmus friends, people that make me like I was at home also if I was far from my hometown.

Jetzt werde ich versuchen, mich auf Deutsch bei allen Leuten von Vegas zu bedanken, die mir geholfen haben, mir Ratschläge gegeben und mich unterstützt haben, auch wenn es nicht immer einfach war.

vielen Dank an Dr. Jürgen Braun, der mich in seinem Institut aufgenommen hat.

Ed ultima, ma non meno importante, devo ringraziare assolutamente Giulia Giannelli, perchè oltre ad essere un'ottima supervisor non mi sarei aspettato che sarebbe stata anche un'ottima amica.

Maybe I did not insert a lot of name, or a lot of words but honestly I appreciate everyone with a great feeling of gratitude. So if you arrived to read up to here, thank you too.

Abstract:

Injection of iron particles in contaminated sites is one of the most useful methods of land reclamation, for this reason, the study of iron particles diffusion in the soil is necessary to realize facilities increasingly performing.

In this work, the behavior and spread of Carbon Iron particles were analyzed in a 2D confined aquifer model. Before to start the experiment, Carbon Iron features were analyzed by means of sedimentation tests and a viscometer. Initially, it was necessary to set up a 2D confined aquifer model and study its hydraulic conductivity. Two tracer tests were done for this purpose using a fluorescent dye called uranine. In the first tracer test, the concentration of uranine was in μg concentration and it was detected by optical fibers, the second one had a concentration in mg and the uranine was visible under neon lighting. After that, the features of the 2D model were known and the experiment phase started.

Three different suspensions were injected to perform visual tests with a qualitative comparison. Initially, it was observed the behavior of a solution of water and uranine after that, a solution of Carboxymethyl cellulose and uranine was injected. In the end, 2g/l of Carboxymethyl cellulose and 20g/L of Carbon Iron was injected. After the Carbon Iron injection and the visual analysis, the 2D confined aquifer model was drained and a sample collection was carried out to obtain the concentration of the Carbon Iron components. This last part of the work allows a qualitative analysis and the possibility to understand the diffusion of the Carbon Iron in an aquifer.

List of Abbreviations:

AC: activated carbon

CI: Carbon Iron

CMC: carboxymethyl cellulose

DNAPL: dense non aqueous phase liquid

NAPL: Non aqueous phase liquid

nZVI: nano-sized zerovalent iron

PV: pore volume

TI: total iron

TOC: total organic carbon

TIC: total inorganic carbon

DOC dissolved organic carbon

POC: purgable organic carbon

NPOC: non-purgable organic carbon

TC total carbon (NPOC+TIC+POC)

SSM: solid sample modul

ZVI: zerovalent iron

Contents:

1	INTRODUCTION	1
1.1	Goals.....	3
2	THEORETICAL BACKGROUND AND GOALS.....	5
2.1.1	Colloids transport.....	5
2.1.2	Colloids deposition	6
2.1.3	Material and reaction involved	7
3	SEDIMENTATION TESTS	10
3.1	Suspensions: materials and preparation	10
3.2	Hydrometer tests.....	13
3.3	Sedimentation tests: experimental procedure.....	15
3.3.1	Density measurements for CMC solutions	17
3.3.2	Sedimentation test results: Carbon Iron in water	18
3.3.3	Sedimentation test results: CMC stabilized Carbon Iron.....	20
3.3.4	Study of results.....	23
3.4	Samples	24
4	DYNAMIC VISCOSITY.....	36
5	TRACER TESTS	41
5.1.1	Filling of the flume	46
5.2	Tracer test with optical fiber	50
5.3	Visual tracer test.....	54
6	EXPERIMENT	59
6.1	Injection set-up	60
6.1.1	Suspension preparation	62
6.2	Injection.....	64
6.2.1	Water and uranine injection	64
6.2.2	Water, uranine and CMC injection	68
6.2.3	CI and CMC injection	70
6.2.4	Comparison of the result.....	73
6.3	Sample collection	79
6.3.1	Total Iron values	81
6.3.2	Total Organic Carbon values	86
7	CONCLUSION.....	89
	Appendix 1, sedimentation test procedure:.....	91
	Appendix 2, CI properties from producer:.....	93
	Bibliography.....	95

List of Figures:

Figure 2.1 Conceptual view of (a) initial deposition kinetics, (b) the blocking effect and (c) the filter ripening effect (Kretzschmar, Borkovec, Grolimund, & Elimelech, 1999).....	6
Figure 2.2 DNAPL reduction mechanism promoted by ZVI modified from (Di Molfetta & Sethi, 2012)	9
Figure 3.1 Carboxymethyl cellulose	11
Figure 3.2 Production information CMC	11
Figure 3.3 Solutions preparation (from left to right): insertion of CMC; addition of degassed water, mixing of CMC and degassed water with the mixer (turrax9).	12
Figure 3.4 Hydrometer: (Casagrande) DIN 18123	13
Figure 3.5 Execution of sedimentation test.....	16
Figure 3.6 Solutions density measurement in time	17
Figure 3.7 Suspensions density and temperature as a function of time for 20g/L CI with no stabilizer	18
Figure 3.8 Time lapse of 20g/L CI sedimentation test.....	19
Figure 3.9 Suspensions density and temperature measured in the time. Continue and dashed lines are respectively density and temperatures values.	20
Figure 3.10 20g/L of I and 2g/L of CMC after 50 minutes from the beginning of the test	21
Figure 3.11 Suspensions density measure in the time and analogy between the different suspensions	23
Figure 3.12 Sedimentation test: the cross indicate the samples that were analyzed.....	25
Figure 3.13 Samples analysis of the different suspension	29
Figure 3.14 Samples results for the Test 1	30
Figure 3.15 Samples results for the Test 2	32
Figure 3.16 Sample results for the Test 3	34
Figure 4.1 Viscometer: ANTON PAAR Gray-Austria, type RHEOLAB MC 1	36
Figure 4.2 Moment vs RPM for the different suspensions	37
Figure 4.3 Viscosity values obtained by the viscometer.....	38
Figure 4.4 Shear stress vs Rounds Per Minute for the different suspensions	39
Figure 5.1 Base-flow set up	41
Figure 5.2 Front view of the flume structure	42
Figure 5.3 Degassed water reservoirs	43
Figure 5.4 From left to right: magnetic inductive flow meter; pressure and temperature transducer and measure software.....	44
Figure 5.5 Optical fibers in wells 4, 5 and 6	45
Figure 5.6 Flume filling with the use of a funnel (on the left), and sand compaction (on the right).46	46
Figure 5.7 From left to right: GEBA, Dorsilit n°8 bentonite and bentonite in powder	47
Figure 5.8 Injection of CO ₂	50
Figure 5.9 Fluorescence vs time: test with optical fiber	51
Figure 5.10 Concentration vs time: test with optical fiber.....	52
Figure 5.11 dark room.....	54
Figure 5.12 Visual test time lapse	57
Figure 6.1 Central port located at the back of the flume.....	59
Figure 6.2 Injection set-up, the blue arrows show the flow direction.....	60
Figure 6.3 Peristaltic pump	61
Figure 6.4 Preparation of uranine suspensions with a mixer (turrax9).....	62
Figure 6.5 Concrete machine used to prepare the CI suspension	62

Figure 6.6 HQd fiel case: oxygen and temperature meter	63
Figure 6.7 Pressure measure (Δh) of water and uranine injection	65
Figure 6.8 Uranine and water injection after 24 minutes.....	65
Figure 6.9 Outflow samples: uranine solution	66
Figure 6.10 Spread with injection of water and uranine (24% of PV fill up).....	67
Figure 6.11 Pressure measure (Δh) of water, uranine and CMC injection	68
Figure 6.12 Water, uranine and CMC injection after 24 minutes.....	69
Figure 6.13 Outflow samples: CMC solution	69
Figure 6.14 Spread with injection of water uranine and CMC	70
Figure 6.15 CI and CMC injection.....	71
Figure 6.16 Outflow samples: CI and CMC suspension.....	71
Figure 6.17 Spread with injection of CI and CMC	72
Figure 6.18 Spread areas of the three different suspensions	74
Figure 6.19 From left to right: final area occupied by the water and uranine; CMC suspension; CI suspension	75
Figure 6.20 Breakthrough curves for different suspension and for the solution modified from (Di Molfetta & Sethi, 2012)	76
Figure 6.21 Pressure measurements (Δh) during the injection of the two solutions	77
Figure 6.22 Draining of the flume, the orange x shows which samples were analyzed	79
Figure 6.23 Numeration of the analyzed samples.....	81
Figure 6.24 Time lapse of the draining process	85
Figure 6.25 Ratio between the CMC and AC concentration	88

List of Tables:

Table 2.1 Properties of Carbon Iron. Source: Safety data sheet by the UFZ Leipzig.....	7
Table 3.1 VEGAS degassed water parameters	10
Table 3.2 Suspensions referring to the Figure 3.12	24
Table 3.3 Samples collection time in the different sedimentation tests.....	26
Table 3.4 Total Iron and Total Organic Carbon measures in the sedimentation test samples. The values have all the same unit of measurement except for (*) values in mg/L	28
Table 5.1 Flume's layers from the top to the bottom.....	46
Table 5.2 Properties of GEBA sand.....	48
Table 5.3 Properties of Dorsilit n°8	48
Table 5.4 Parameters of the bed.....	49
Table 5.5 Result of the tracer test: porosity and hydraulic conductivity	53
Table 5.6 Hydraulic conductivity in each well	53
Table 5.7 Porosity evaluation with the visual test	58
Table 6.1 Values of oxygen concentration and temperature during the mixing phase.....	63
Table 6.2 Retention factor for the different suspensions	73
Table 6.3 Evaluation of the Darcy velocity in the two side of the flume: P is the pressure, L is half length of the flume, i is the hydraulic gradient, k is the permeability coefficient and vd is the Darcy velocity.....	78
Table 6.4 Concentration and absolute values in the flume samples	82
Table 6.5 Evaluation of the missing concentration of activated carbon in the different areas	86
Table 6.6 TOC: concentration of CMC and AC and their ratio in the flume	87

1 INTRODUCTION

In the history of mankind, the largest civilizations and city centers always developed near water sources because of its important role in the human health and economic purposes, such as irrigation and industries.

However, the amount of “usable water, the so called fresh water, is really small if compared to all water on Earth. As a matter of fact, salty water from seas and oceans represents 96,5% of Earth’s water and another 1% is constituted by salty water located in estuaries and groundwaters. Fresh water amounts to 2,5% of which 1,7% being not available as it is located in ice caps and 0,8% only available for human purpose” (Lauren F. Greenlee, 2009).

The available fresh water (0,8%) is stored in superficial bodies such as lakes, streams and, rivers, as well as in the subsurface, in the aquifers.

“An aquifer is an underground layer of water bearing rock”. (National Geographic Society, s.d.).

The aquifers have fissures where the liquid and the gases can go through and the water is preserved in the fissures.

“Surface water and groundwater are both important sources for community water supply needs.” (ENCYCOLPAEDIA BRITANNICA, s.d.) Characteristics of groundwater are usually more suitable for drinking water than the ones of superficial water, which normally requires more complicated and expensive water treatments. So, groundwater is a major clean water source.

In light of this, it appears clear that groundwater is one of the most important resources and must be protected. Unfortunately, the effects of industrial human activities on the environment and in particular on the quality of the groundwater have been in the past century underestimated or in certain cases completely neglected. Nowadays pollution of the underground water is a matter of fact. Accountability for restoring previous quality standards and for remediation strategies arose in the last decades only.

On the one hand, management measures are required in order to control diffuse sources of water pollution, those inputs, and impacts which occur over a wide area and are not easily attributed to a single source. They are often associated with particular land uses (urban, agricultural, forestry), as opposed to individual point source discharges. The assessment of the chemical status of groundwaters in Germany, based on data from the EEA (European Environmental Agency) monitoring network in 2010, indicates that 37% of groundwater bodies severely polluted by nitrates and pesticides from agriculture; the highest concentration can be found near farmland and settlement areas (Arle, et al., 2013). Furthermore, natural element to be found in the subsoil such as arsenic, lead and sulphate threaten human health (Arle, et al., 2013).

On the other hand, effective remediation strategies are necessary when facing point sources water pollutions.

Farms and natural elements are not the only cause of pollution, also the industries can degrade the quality of the underground water. An investigation conducts in Sicily show that on 72 aquifer 47%

1. INTRODUCTION

was in a bad chemical state due to the discovery of chlorinated solvents (Abita, Palumbo, Costa, Nicolosi, & Pellerino, 2017).

Industrial processes release chlorinated solvents that are slightly soluble in water and not degradable (Vanzetti, Giangoglio, & Sesia, 2016).

The pollutants are classified chemically by organic and inorganic. Organic pollutants are those substances that have at least one carbon atom of organic origin. Inorganic pollutants are metals originated by industrial waste, landfill and mining effluents and also nitrate, nitrates, sulphates, fluorides and cyanides (Di Molfetta & Sethi, 2012).

The physical classification is equally important to identify the different pollutants: the first physical aspect to take in consideration is the miscibility, that is the capacity to create with the water a single substance. The second one is the pollutants' density compared to that of water (Di Molfetta & Sethi, 2012).

In order to decontaminate aquifer from unwanted substances several technologies are today available:

- Pump and Treat: wells extract water from the aquifer so as to clean it. This technique is useful against the NAPL even so, pump and treat process is not feasible with residual saturated NAPL (Di Molfetta & Sethi, 2012).

The most common problem that can be observed with this technology is the rebound; it is an increase of pollutants in the aquifer due to the end of the pumping process but also the long reclamation times. This technology is very expensive both for the installation cost and for the times of fulfillment (Di Molfetta & Sethi, 2012).

- Permeable reactive barriers (PRB): a barrier made of millimetric iron is built in the aquifer after an excavation phase. The barrier has a hydraulic conductivity lower than the aquifer to facilitate the water flow in order to allow reaction that degrades and immobilizes the pollutant (Di Molfetta & Sethi, 2012).

This technique is used often because it does not need any external labor or energy inputs. Nonetheless, a plume situated under the building or a plume that has moved off property boundaries could be impossible to restore. Moreover, it can have a high cost due to the depth of the plume (R.Gavaskar, 1999).

- Removal of the pollutant by skimmer: the skimmer is a device inserted into piezometers or trench drain that capture the pollutant in the aquifer. The extracted substance is stored in special containers. (Di Molfetta & Sethi, 2012).

The advantage is that this technology can capture the pollutant without water but the disadvantages are that it works only on LNAPL and that its component needs a lot of maintenance (Di Molfetta & Sethi, 2012).

- Bioslurping: the extraction of NAPL and water carried out with a vacuum pumping. The extraction of water, air, and pollutant allows aerobic biodegradation phenomena of contaminants. This technique reduces the energy consumption of the reclamation work (Di Molfetta & Sethi, 2012).

- Air sparging and biosparging: vertical well in the aquifer inject air pressure. It is possible to add systems in the unsaturated layer to capture polluting vapors. The reclamation occurs with the phenomena of stripping of the pollutant in the aqueous phase, volatilization of the adsorbed component and biodegradation of the contaminant by aerobic metabolism. When the biodegradation phenomena are the most important in the process of reclamation it is possible to use the word biosparging (Di Molfetta & Sethi, 2012).

This technology is very effective but great depth of the aquifer can create prohibitive costs moreover, the characteristics of the aquifer must be homogeneous to avoid preferential paths ways causing the decrease of effectiveness (Di Molfetta & Sethi, 2012).

These technologies act on the plume, however, a better plan of the act should be found and remedy the source area of the pollutant because in this way it is possible avoiding the formation of a plume in the aquifers.

A better technique is the injection of zerovalent iron particles with the dimension of micrometer or nanometer because the little dimensions allow injecting directly into the aquifers consequently, these particles can affect directly on the plume or also on the source pollutant area, “the use of zerovalent iron micro and nano-particles is one of the most promising technologies for groundwater remediation” (Tosco, Gastone, Luna, & Sethi, 2015).

The problem of this technology is not connected with the decontamination result but about the particles spreads in the pore of the aquifer, because agglomeration of particles can cause clogging in the fissures causing inefficient remediation facilities.

To allow the diffusion of the micro and nano-particles in an aquifer is necessary to use a stabilizer. The purpose of the stabilizer is to increase the negative surface charge, in this way the iron particles decrease their agglomeration tendency caused by the magnetic attraction.

Furthermore, when the iron particles are injected they must remain in suspension for a necessary time to allow the spread in the aquifer for an optimal distance from the injection point (Tosco, Gastone, Luna, & Sethi, 2015).

1.1 Goals

The purpose of this work is studying the transport of Carbon-Iron particles in a 2D confined aquifer model (flume). A similar experiment was already carried out in the past in less controlled conditions with a suspension of 20g/L of CI and 4g/L of CMC (Giannelli, 2014). This concentration showed a high mobility of the Carbon Iron particles. Therefore, for this new experiment was decided to decrease the stabilizer concentration to 2g/L. Furthermore, the 2014 experiment was conducted with three different injection and four injection points, the current experiment will perform a single injection with a single injection point because getting the same results would mean that a single injection is more advantageous.

In the end, the spread area of the single injection can be a very useful information for the remediation operations to carry out more performing reclamation facilities

1. INTRODUCTION

Before to start the experiment it was decided to study some important parameters that could influence the results of the work:

- Chapter 3 includes the study of colloidal stability. The gravity and cohesion forces act on the suspension. Therefore, sedimentation tests were carried out to observe transport and sedimentation phenomena, because they could cause clogging in the tube of injection and an extreme mobility in an aquifer. With these tests, an initial comparison between the suspension used in the last experiment and what we are doing was also possible. Moreover, suspension samples were collected to have more representative information about the sediment particles and those that hold in suspension. Therefore, the samples were analyzed to know the Total Iron and Total Organic Carbon (TOC) concentration.
- Chapter 4 describes the viscosity of the different suspension and solutions injected in the flume. A viscometer was used to know the data and to make some comparison between the injected substances because the viscosity is connected to the coefficient diffusion in an aquifer.

After obtaining the information about the sedimentation rate and the viscosity, the successive part of the experiment is focused on the flume:

- Chapter 5 focuses on the experiments aimed at characterizing the flume from the hydrodynamic point of view. Hence, to have more precise information about the porosity and also the hydraulic conductivity of the flume two tracer tests has been performed. The first test was made with a concentration of $1000\mu\text{g/L}$ of uranine and the second one with 2g/L of uranine.
- Chapter 6 describes the injection experiment using initially two solutions and, in the end, the Carbon Iron suspension. The purposes of the different tests were to observe:
 - the behavior of a tracer: water and 1g/L of uranine;
 - the behavior of CMC solution: water, 1g/L of uranine and 2g/L of CMC
 - the behavior of CI suspension: water, 2g/L of CMC and 20g/L of CI.

In the end, solid samples were collected for a quantitative analysis. The purpose is to understand how the CI spreads in the flume and the concentration of Total Organic Carbon (TOC) and Zero-Valent Iron (ZVI) in different points of the flume

2 THEORETICAL BACKGROUND AND GOALS

The mobility and transport of particles are crucial factors for the environmental redevelopment that used the injection of particles in the subsoil. The particles are inserted in a colloidal suspension and they are injected in the aquifer so, it is possible the water restoration in the contaminated plume or also in the source area (Tosco, Gastone, Luna, & Sethi, 2015).

Therefore, is necessary to start with some theoretical notions, useful for better understanding the situation in an aquifer.

Little particles are transported between the fissures in an aquifer called colloids. They are commonly defined as small particles or other entities with dimension roughly between 1 nm and 1 μm (Ruben Kretzschmar, 1999).

2.1.1 Colloids transport

Colloidal particles have some unique properties. First, they have very large specific surface areas ($>10 \text{ m}^2/\text{g}$) and represent important sorbents for environmental contaminants. Second, particle transport by diffusion can be faster than by sedimentation (Ruben Kretzschmar, 1999).

The transport phenomenon is subject to numerous factors. The most obvious is the flow of the water but also the superficial adsorption and volatilization influence the movement of the particles. In the end, also biotic organisms can influence the transport. Furthermore, both the aquifer features and the variation of the form and dimension of the particles influence the diffusion in the fissures (Di Molfetta & Sethi, 2012).

So it is clear that the transport of colloids is a considerable aspect to understand. Below is a transport equation of colloidal particles in porous media 1D model (Ruben Kretzschmar, 1999):

$$\frac{\partial C}{\partial t} = D_p \frac{\partial^2 C}{\partial x^2} - v_p \frac{\partial C}{\partial x} - \frac{\rho_b}{\varepsilon} \frac{\partial S}{\partial t} \quad (1)$$

$$\frac{\rho_b}{\varepsilon} \frac{\partial S}{\partial t} = k_d C - \frac{\rho_b}{\varepsilon} k_r S \quad (2)$$

In this set of equation we have:

- $C(x,t)$ colloidal particle concentration in suspension;
- $S(x,t)$ deposit colloidal particles per unit mass of the porous matrix;
- x travel distance;
- t time;
- D_p hydrodynamic dispersion coefficient for colloidal particles;
- v_p average interstitial velocity of colloidal particles;
- ρ_b solid matrix bulk density;

- ε porosity;
- k_d colloid deposition;
- k_r release rate coefficients.

2.1.2 Colloids deposition

The particles in the aquifer can be affected by different phenomena. The dynamic process of attachment and detachment are governed by physical laws that operate at the scale of grains and pores (Tosco, Bianco, & Sethi, 2018).

It is possible to see three different processes in Figure 2.1:

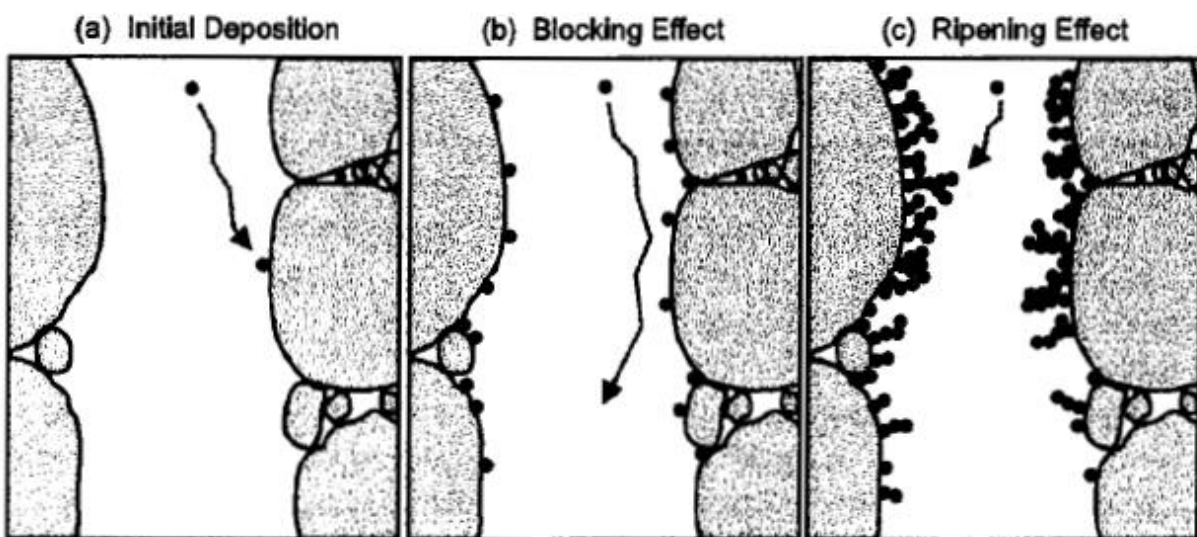


Figure 2.1 Conceptual view of (a) initial deposition kinetics, (b) the blocking effect and (c) the filter ripening effect (Kretzschmar, Borkovec, Grolimund, & Elimelech, 1999)

Initial deposition occurs when particle-particle and particle-collector interaction energies are similar. Blocking happens when particle-particle interaction energies are repulsive and, in the end, ripening occurs when particle-particle interaction energies are attractive. This means that particles tend to attract to the suspended one until they create a clogged phenomenon (Tosco, Bianco, & Sethi, 2018).

In addition to the size and density of colloidal particles, there are important factors that influence deposition which is of flow velocity, ionic strength and fluid viscosity (Kretzschmar, Borkovec, Grolimund, & Elimelech, 1999).

With the use of polymers, it is possible to change the viscosity of the suspension that has a non-Newtonian behavior. In this way, the colloids suspensions in water are stabilized (Tosco, Bianco, & Sethi, 2018).

Colloid release rates could be very small, with some chemical conditions. In this case, is possible wrote the equation 1 in another way (Kretzschmar, Borkovec, Grolimund, & Elimelech, 1999):

$$\frac{\partial C}{\partial t} = D_p \frac{\partial^2 C}{\partial x^2} - v_p \frac{\partial C}{\partial x} - k_d C \quad (3)$$

2.1.3 Material and reaction involved

Information from previous subchapters is useful to the study of particles that are put in polluted aquifers, to better understand how they can spread in an underground water system.

For the forecast of our study, the focus is on the Carbon Iron® particles.

“Carbon Iron® is an air-stable in situ reagent developed at the Helmholtz Centre of Environmental Research UFZ targeting halogenated organic contaminants or heavy metals in ground water” (Sweeney & Harries, 2016).

Carbon Iron® particles are composed of activated carbon colloids that are doped inside with nano iron structures. These two materials together make it possible to have an efficient subsurface transport of the reagent particles (Sweeney & Harries, 2016).

The properties of this material are shown in Table 2.1.

Table 2.1 Properties of Carbon Iron. Source: Safety data sheet by the UFZ Leipzig

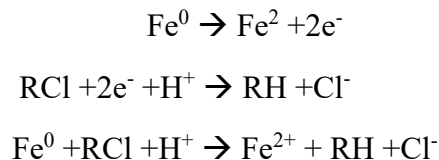
Properties	
Appearance	solid
Color	black
d₁₀ (nm)	550
d₅₀ (nm)	1340
d₉₀ (nm)	3630
Bet surface (m²/g)	594
ρ₀ (g/cm³)	3,3
ξ zeta potential (mV) pH=7	(-7,-23)
sedimentation rate (cm/h)	0.17
Zerovalent iron - Fe(0) (w/w%)	(10-25)
Total iron (w/w%)	(25-30)
Carbon-C (w/w%)	(50-60)
Solubility in water	insoluble
Moisture (w/w%)	<1,5
pH in water	6,8-7,4

Activated carbon is not only cheap but also compatible with the environment, its role is to decrease the surface charge of the iron particles furthermore, the AC collects hydrophobic pollutants, for this reason, it works efficiently for the DNAPL pollutants (Giannelli, 2014).

2. THEORETICAL BACKGROUND AND GOALS

The subsurface transport is guaranteed also with the use of polymers, one of the most common is the carboxymethyl cellulose (CMC). This is an anionic water-soluble polymer derived from cellulose, it has a hydrophilic behavior and its non-toxic make it a perfect stabilizer to use in sensible environmental like the aquifer (proekosrl, s.d.). Its high viscosity is another reason to use this polymer that gives a maximum stability for pH between 7 and 9 values.

When the carbon iron deposits in the fissures, the nano iron reacts with the pollutant and it starts an oxidation-reduction process. The Fe^0 oxidizes to Fe^{2+} reducing halogenated hydrocarbon substances with the elimination of chloride ions (Di Molfetta & Sethi, 2012):



In the end, it is possible to observe two main reaction mechanisms :

- subsequent hydrogenolysis, when a chloride ion is eliminated by two electrons and a hydrogen ion which strikes the solvent molecule;
- reductive β -elimination;

In Figure 2.2 is possible to observe the degradation paths:

2. THEORETICAL BACKGROUND AND GOALS

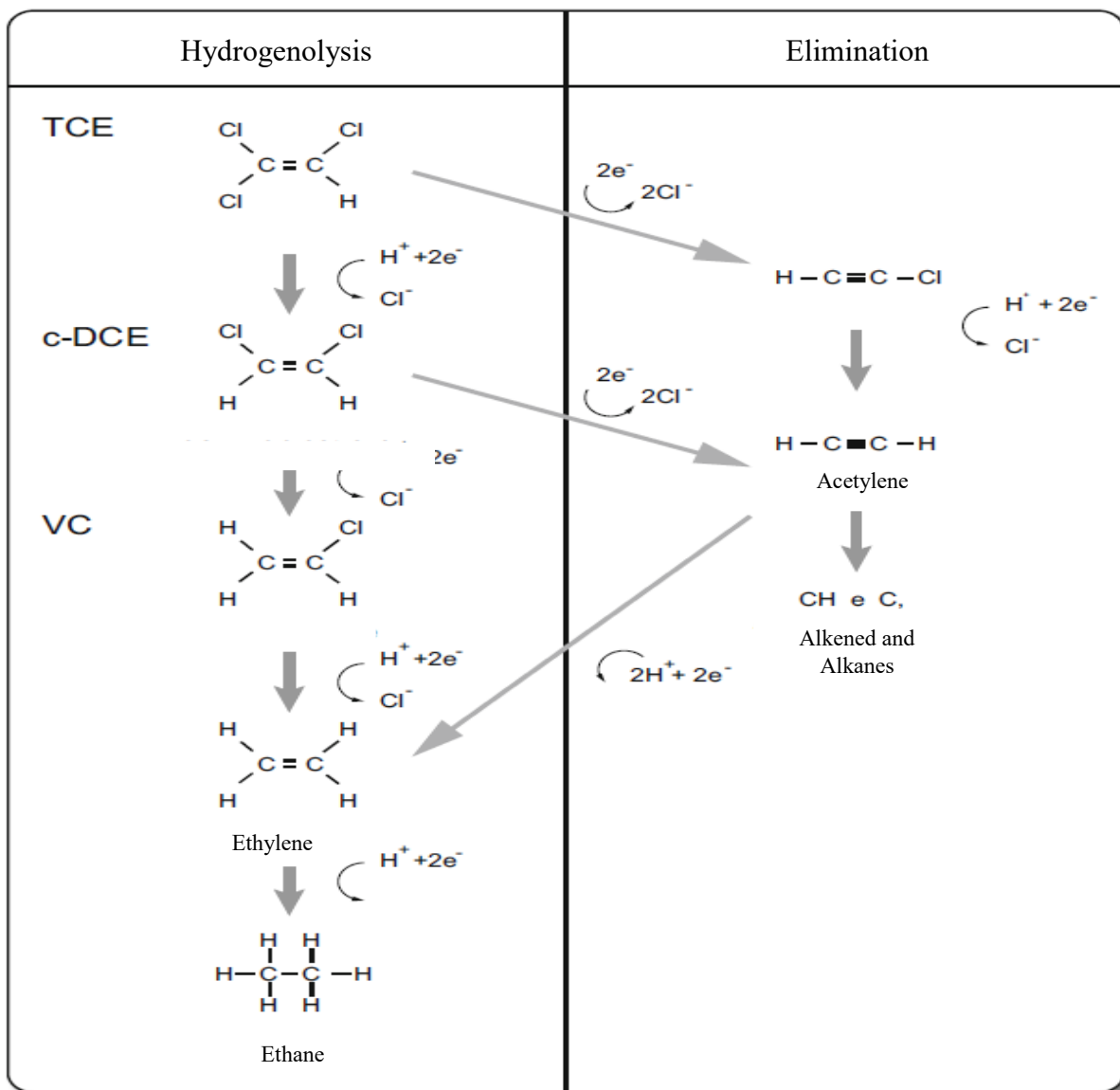


Figure 2.2 DNAPL reduction mechanism promoted by ZVI modified from (Di Molfetta & Sethi, 2012)

This process can become less strong with time because the Fe can be oxidized by the dissolved oxygen in an aquifer or because the iron is in contact with the water:



That causes an increase in pH water values because this reaction generates ions OH^- . When the pH increases, there are clogging and reactivity reduction phenomena. They are caused by the formation of precipitants (Di Molfetta & Sethi, 2012).

3 SEDIMENTATION TESTS

To obtain the particle size distribution there are different methodologies, for example, the Politecnico of Torino uses the magnetic susceptibilities of the suspension to study the quantity of iron particles that are subject to sedimentation phenomena. The magnetic field applied to the suspension gives back the magnetized component.

In the Vegas institute was decided to conduct sedimentation tests, they are standard laboratory procedures for the determination of the particle size distribution of soil with a periodic measurement of the density. When it is used for this purpose, there is a specific method to understand the percentages of the different soil components that could be observed in *Appendix 1*.

Nonetheless, the aim of the sedimentation test in this thesis is not the study of the soil distribution but to determinate the stabilization time for suspensions of Carbon Iron and Carboxymethyl Cellulose stabilizer in degassed water.

3.1 Suspensions: materials and preparation

The suspensions in these experiments are made with three components:

- **Degassed Water:** water with a low oxygen concentration. This is the same water that will be used to saturate the flume. In Vegas, the freshwater flows into columns which then come in contact with a vacuum that removes the dissolved oxygen. In Table 3.1, it is possible to see the degassed water parameters.

Table 3.1 VEGAS degassed water parameters

Degassed water	
pH	7,97 (9°C)
E.Coli	nd
Oxygen [mg/L]	
TOC [mg/L]	1
Nitrate [mg/L]	4,2
Nitrite [mg/L]	<0,005
Sulfate [mg/L]	34
Calciumcarbonate [mmol/L]	1,6
electrolytic conductivity [μ S/Cm]	333 (25°C)
Sodium [mg/L]	5,2
Calcium [mg/L]	48
Magnesium [mg/L]	8
Potassium [mg/L]	1,4
Chloride [mg/L]	7

- **Carboxymethyl cellulose ($\text{CH}_2\text{CO}_2\text{H}$):** CMC is the substance that has the purpose of stabilizing and to improve the mobility of the CI particles. It also increases the electrostatic repulsion. In addition, the CMC is appealing because it is very cheap non-toxic. It is also

3. SEDIMENTATION TESTS

biodegradable so, for this reason, it must be protected from sunlight. Dow Chemical Company produce this organic salt in powder, The CMC has a minimum purity of 99,5%. It is used also in food under E number to modify viscosity or like a thickener, to stabilize the emulsion some products like ice cream. However, the CMC use is not only observable in the food production but also in other sectors as paper products, textile sizing, and detergents.



Figure 3.1 Carboxymethyl cellulose

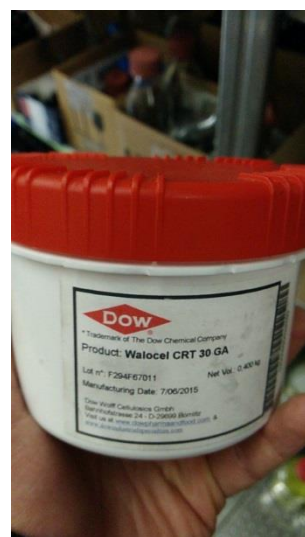


Figure 3.2 Production information CMC

- **Carbon Iron:** CI is a material developed and manufactured by the UFZ Leipzig composed by active carbon (AC) and nano zero valent iron (nZVI). The first one is a sorbent and the second one a reactant. It is composed of 22,3% of reactive iron and 50% of activated carbon. The particles size have $d_{50} < 1,5\mu\text{m}$. The characteristics of the CI used in the experiment are available in *Appendix 2*.

3. SEDIMENTATION TESTS

Four suspensions and three solutions were made to know the sedimentation rate, the preparation procedure is explained below:

1. Initially, the different concentrations of CMC were put in 1L containers with degassed water. So to create the suspensions in order to avoid the aggregation of CMC, a mixer (turrax9) was used for 5 minutes with a velocity between 20 and 21,5rpm. In this way, it was made the six solutions with 2g/L, 4g/L and 6 g/L of CMC, two for each concentration.
2. CI has been added in these solutions. Two solutions were available for each concentration, the first one to conduct the sedimentation test and the second one to carry out a sample collection. The suspensions with 20g/L of CI has been mixed again for 5 minutes with a velocity between 16 and 18rpm.

For the suspensions, sedimentation test was necessary to repeat the point 1 without adding the CI. Instead, for the solution with only 20g/L of CI and no CMC, it was necessary just accomplish again the point 2.



Figure 3.3 Solutions preparation (from left to right): insertion of CMC; addition of degassed water, mixing of CMC and degassed water with the mixer (turrax9).

Summary of the solutions and suspension prepared:

1. 1L water and 2g/L of CMC;
2. 1L water and 4g/L of CMC;
3. 1L water and 6g/L of CMC;
4. 1L water and 20g/L of CI;
5. 1L water, 2g/L of CMC and 20g/L of CI;
6. 1L water, 4g/L of CMC and 20g/L of CI;
7. 1L water, 6g/L of CMC and 20g/L of CI

These solutions and the suspensions were prepared in the same conditions to have a good comparison of the results.

3.2 Hydrometer tests

The hydrometers are tools used for measuring the relative density of a liquid. It has a heavy area at the lower end and a top where it is possible to measure the density value. For all the length of the hydrometer, there is a measurement bar with density values.

The bottom of the test tube is filled with lead shots. All the hydrometers have always the same amount of lead shots.

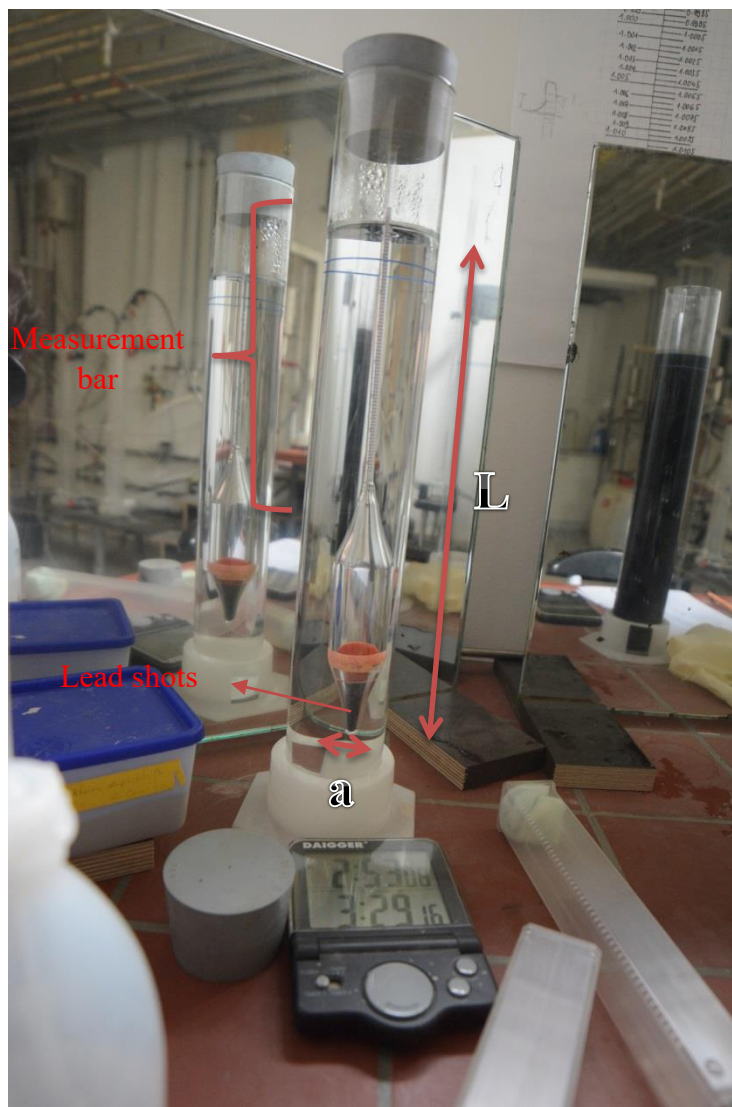


Figure 3.4 Hydrometer: (Casagrande) DIN 18123

To explain the principle of the hydrometer it is possible to conduct two different tests, one with water (w) and another one with oil (o).

The hydrometer is inserted in the cylinder with the water. The density measure (L) is taken when the tool is stabilized. L corresponds to the length between the level where the liquid intersects the measuring bar and the bottom of the hydrometer.

3. SEDIMENTATION TESTS

The hydrometer will increase the level of the water inside the tubes and it gives the value L_w of the tube inside water.

The area of the cross-section of the test tube (a) and the density of water (ρ_w) are known.

So it is possible to know the volume of water displaced $\rightarrow V_{w\text{-disp}} = a L_w$ (Archimedes principle)

The weight of the displaced water will be $\rightarrow W_{w\text{-disp}} = V_{w\text{-disp}} \rho_w g = a L_w \rho_w g$

Where ρ_w is the density of the water and g is the acceleration due to gravity.

In the end, the Archimedes principle says that:

$$\text{Weight of the loaded test tube} = \text{Weight of water displaced} = a L_w \rho_w g$$

The previous argument is applicable to all the liquids. The length of the tube inside another liquid and the density are the only parameters that can change.

Therefore, for the oil is possible to write:

$$\text{Weight of the loaded test tube} = \text{Weight of oil displaced} = a L_o \rho_o g$$

So, if there are not removals or additions of lead shots from the hydrometer, the weight of the loaded test tube is the same for both the cases.

Therefore, it is possible to write:

$$a L_w \rho_w g = a L_o \rho_o g \rightarrow L_w \rho_w = L_o \rho_o$$

$$\frac{L_w}{L_o} = \frac{\rho_o}{\rho_w}$$

This last equation means that if the L_o increases, the ρ_o must decrease to allow the occurrence of the equation.

In other words, the length is inversely proportional to the density:

$$L \propto \frac{1}{\rho}$$

This explains how is possible that a length can give information about density.

3.3 Sedimentation tests: experimental procedure

Appendix 1 gives the following test indications to carry out the tests:

- Use of two cylinders, the first one for the 1L suspension and the second one filled up with 1L of deionized water;
- The cylinder with the suspension was manually combined for one minute to avoid settlement at the bottom. After that the interval timer was started;
- When the hydrometer was moved by the suspension, a slow movement is necessary to avoid the resuspension of sedimented CI particle,
- It is necessary to wait for 20–30 seconds prior to taking a measurement by the hydrometer to allow for the stabilizing of the instrument.

The measurements that were collected through the hydrometer were taken each minute in the first 10 minutes of the sedimentation tests; during this time the hydrometer was not removed from the cylinder.

After that, measurements were collected every 5 minutes for 110 minutes; in this part of the test the hydrometer was extracted and inserted into a cylinder of deionized water to perform a control measurement on the calibration of the instrument. Moreover, temperature measurements of the suspension were collected with a mercury thermometer. It was inserted in the top of the liquid to avoid disturbing the system. Each measurement was taken after the stabilization of the instrument.

In the end, measurements were read every 20 minutes for 360 minutes.

The tests had a total duration of 480 minutes.

In the end, samples were collected at different from a replicate of each suspension (to avoid disturbing the density measurement) for additional characterization.

3. SEDIMENTATION TESTS

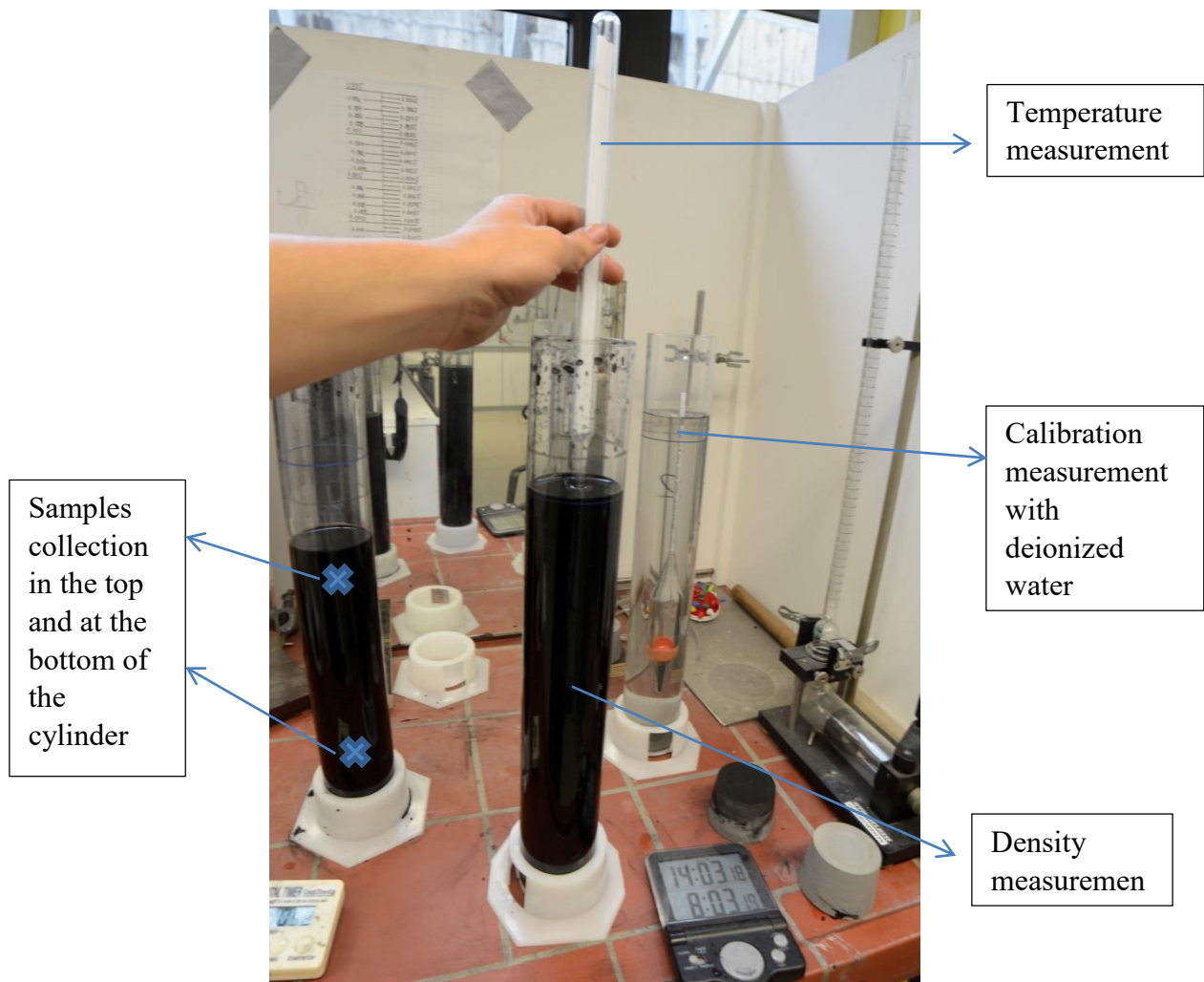


Figure 3.5 Execution of sedimentation test

The results of the hydrometer measurements in the next sub-chapters do not need calibration because the measurements of the deionized water are always equal to the density of water at 20°C (0,998g/cm³).

The results are reported and discussed in the next paragraphs.

3.3.1 Density measurements for CMC solutions

The results of the density measurement for the different CMC solutions in the absence of CI particles are shown in the figure below.

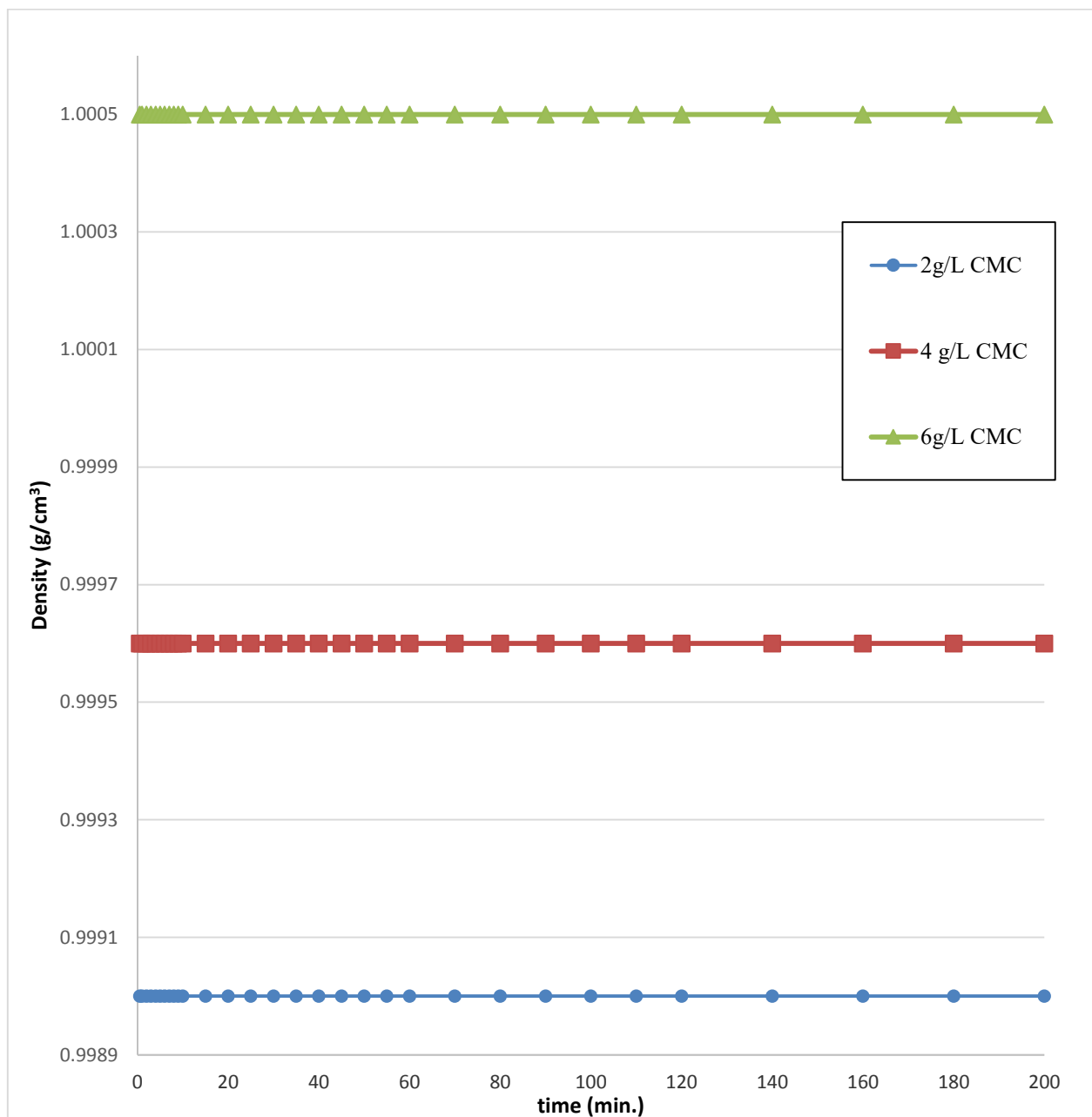


Figure 3.6 Solutions density measurement in time

It is possible to observe how the different solutions do not change in the time. Therefore, it means that the solutions are in a stable condition.

These tests were carried out just for 200 minutes because of the clear achievement of constant density values.

3.3.2 Sedimentation test results: Carbon Iron in water

In Figure 3.7 the behavior of the suspension made with 20g/L of CI in water without stabilizer is shown.

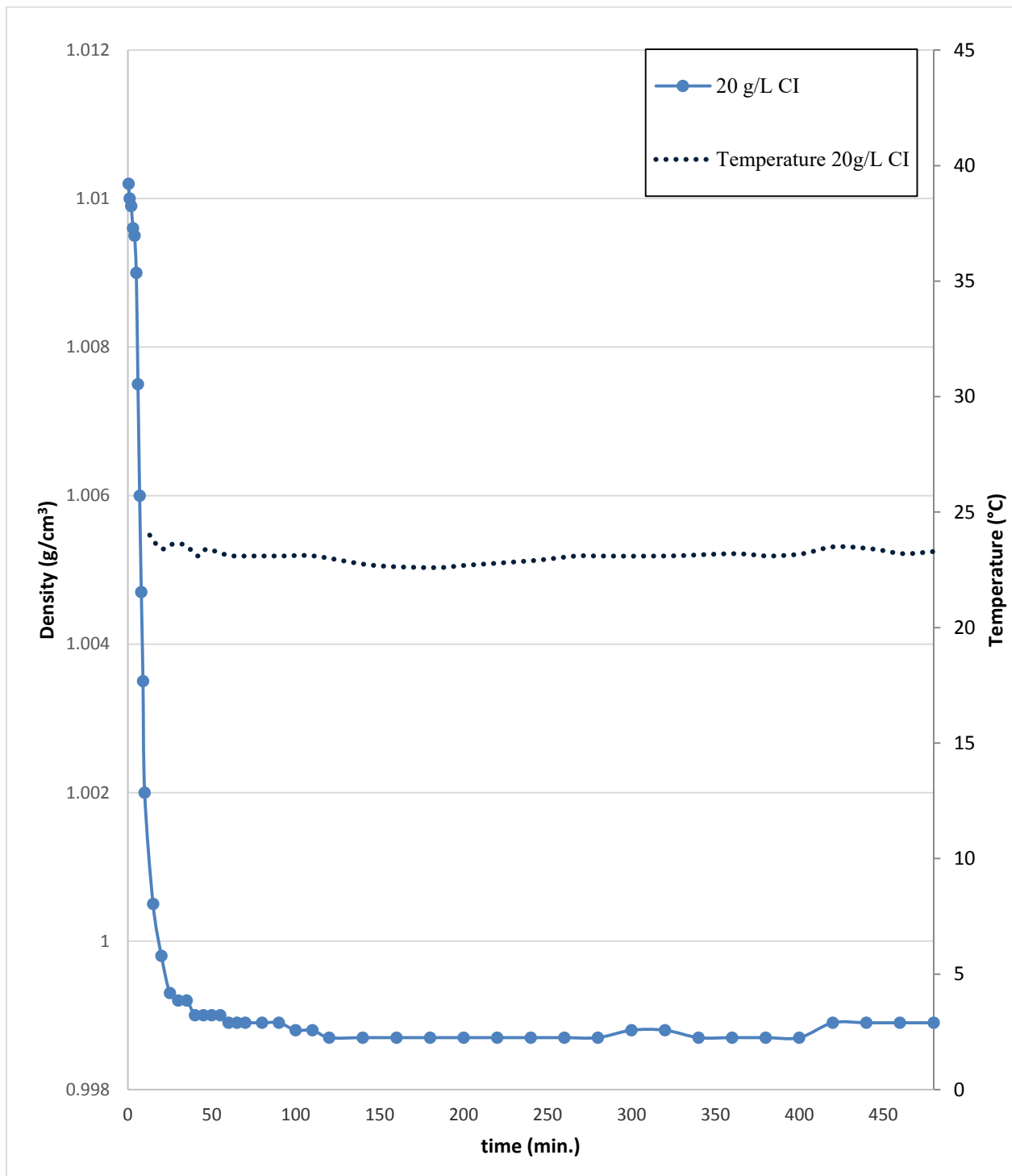


Figure 3.7 Suspensions density and temperature as a function of time for 20g/L CI with no stabilizer

3. SEDIMENTATION TESTS

It is easy to notice that the suspension density without a stabilizer has a rapid decrease, this means that a rapid sedimentation of the heavy CI particles occurs.

The temperature has an almost constant value and this is a perfect situation because high variations of temperature may affect the density measurement.

After 25 minutes from the start of the test, the solution is completely sedimented and a constant trend continues until the end of the test.

This phenomenon was perfectly visible during the test, as shown in the next picture of Figure 3.8, showing a clear separation between the water and CI elements.

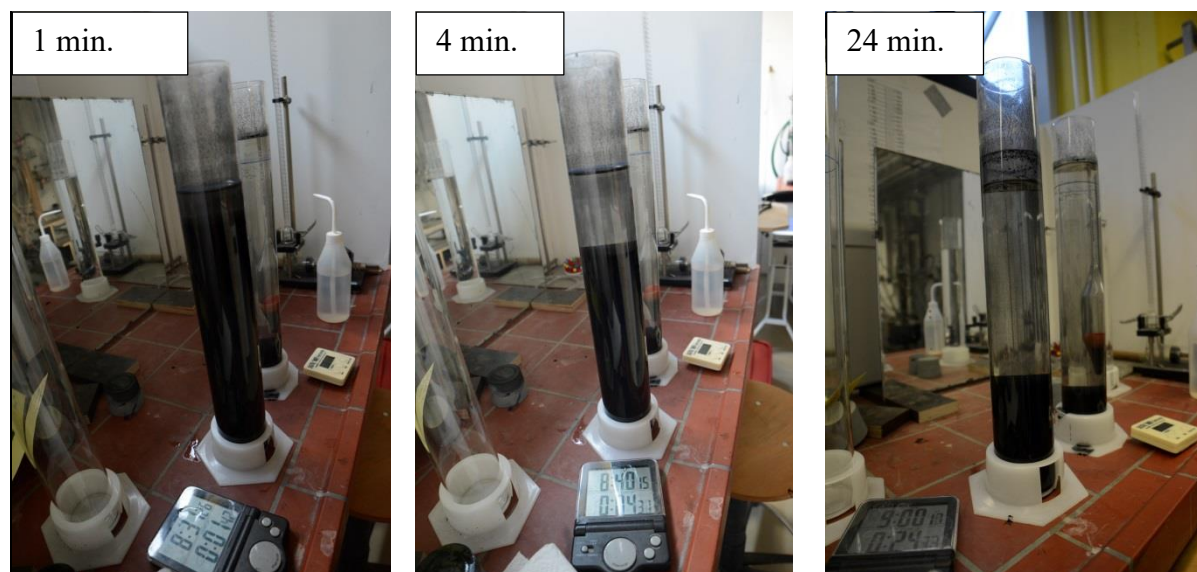


Figure 3.8 Time lapse of 20g/L CI sedimentation test

Obviously, this suspension without stabilizer has a complete sedimentation in a short time. Therefore, it cannot be adopted in field operation.

3.3.3 Sedimentation test results: CMC stabilized Carbon Iron

In this case, the three different tests had a duration of 480 minutes but a last value of density was measured for each suspension after more than 800 minutes from the start of the tests, to further confirm the results. These values did not have a variation of density consequently the suspensions certainly reached steady state condition.

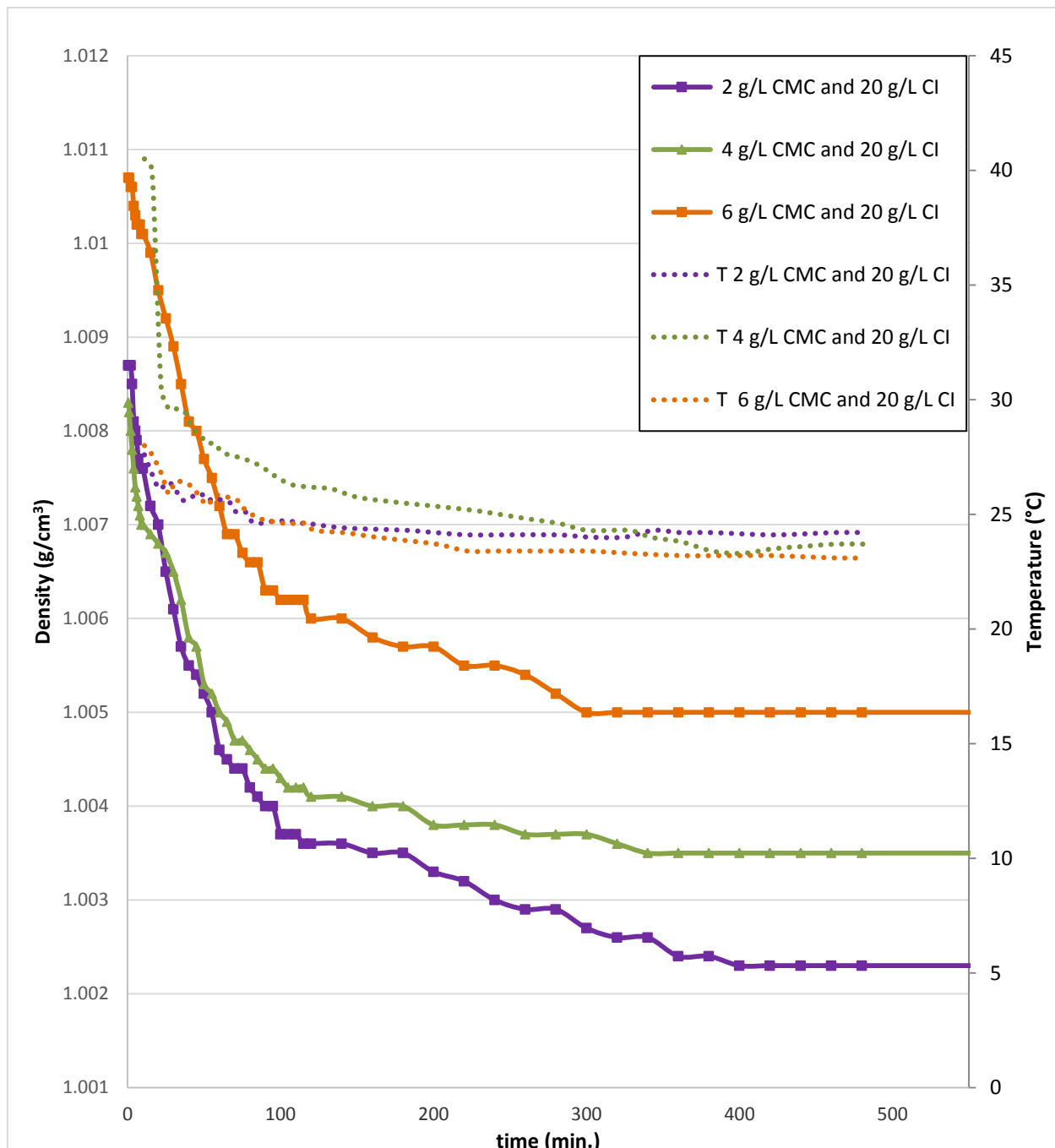


Figure 3.9 Suspensions density and temperature measured in the time. Continue and dashed lines are respectively density and temperatures values.

3. SEDIMENTATION TESTS

It is possible to observe that all the suspensions have a similar behavior. There is the first phase of sedimentation due to a fast change of density values, the second phase with a slower decrease and a final part with almost constant density.

The graph also shows that by using CMC, sedimentation is slower compared to the 20g/L CI in pure water. Indeed, it is possible to notice in Figure 3.10 how 20g/L of CI and 2g/L of CMC is after 50minuts from the beginning of the test.



Figure 3.10 20g/L of I and 2g/L of CMC after 50 minutes from the beginning of the test

From the Figure 3.10 is clear that the CI particles remain in suspension and it is impossible to observe the sedimentation phenomenon visually.

Returning to the Figure 3.9 however, it is important to notice that in the first part of the graph the density values are higher for the suspension with a lower concentration of particles (2 and 4g/L of CMC). This anomaly can be explained observing the values of temperatures.

The water density has not high variation between 20°C and 25°C ($0,998\text{g/cm}^3$ and $0,997\text{g/cm}^3$ respectively) so, the density of the suspensions can be considerate exact. For the suspension with 4g/L of CMC the first part has an error because comparing with the density of the water between 20°C and 40 °C there is a higher variation of water density ($0,998\text{g/cm}^3$ and $0,992\text{g/cm}^3$ respectively).

It is known that temperature affects the volume of a liquid, higher temperatures cause an increase of the volume, thus a decrease of the density occurs and the sedimentation results faster than a suspension with lower temperature.

3. SEDIMENTATION TESTS

So, it is possible to observe that density values in the first part of the tests have some anomalies because there are different temperatures:

$$T_{2CMC} < T_{4CMC} \rightarrow V_{2CMC} < V_{4CMC} \rightarrow D_{2CMC} > D_{4CMC}$$

Even so, after the stabilization of the temperature values the different density return in the expected condition:

$$D_{2CMC} < D_{4CMC}$$

However, these anomalies for the first part of the graphs are not a problem because the purpose of the sedimentation test was to study the trend of the different curve and not the specific values of density.

In the end, it is possible to say that the high variation of temperature values in the sedimentation tests are due to mixing process thus, the sedimentation phenomenon in the first part of the tests is faster than the end part.

3.3.4 Study of results

To understand better the behavior of the suspensions it is necessary focusing on the suspensions density.

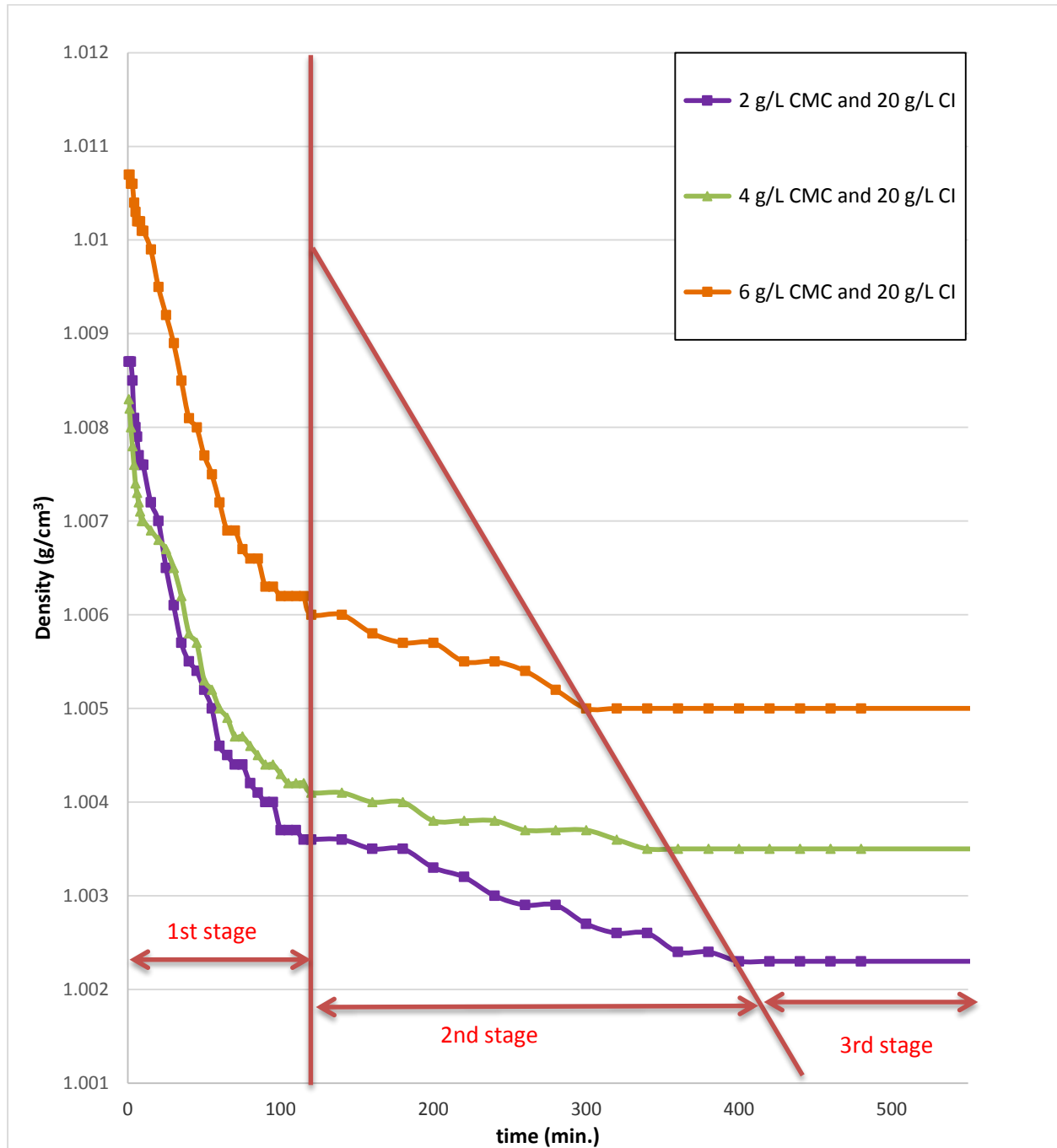


Figure 3.11 Suspensions density measure in the time and analogy between the different suspensions

In the Figure 3.11 is possible to divide the trend of the different suspensions into three parts.

Initially, in the first stage, there is a rapid decrease that it is equal for all the different suspensions. It is possible to see that this phase ends for all the tests approximately at the same time (120 minutes),

regardless of the CMC concentration applied. This means that in the first part of the graphic, we have the most significant sedimentation phenomena, which could cause clogging in the flume.

This part of the graphs is connected with the heavier iron particles that fall for the gravity effect.

In the second stage the decay became slower, this means that the particles are continuing to sediment.

With the increase of the CMC concentration, this time became minor until, the solutions achieve the third stage, the stable phase.

3.4 Samples

The samples collection has the purpose to know the Total iron and the Total Organic Carbon (TOC) that sediment during the tests. In the Figure 3.12 is possible to see the collection times. All the samples were of 40ml.

Table 3.2 Suspensions referring to the Figure 3.12

Test N°	Suspension	
	CMC g/L	CI g/L
1	0	20
2	2	20
3	4	20

3. SEDIMENTATION TESTS

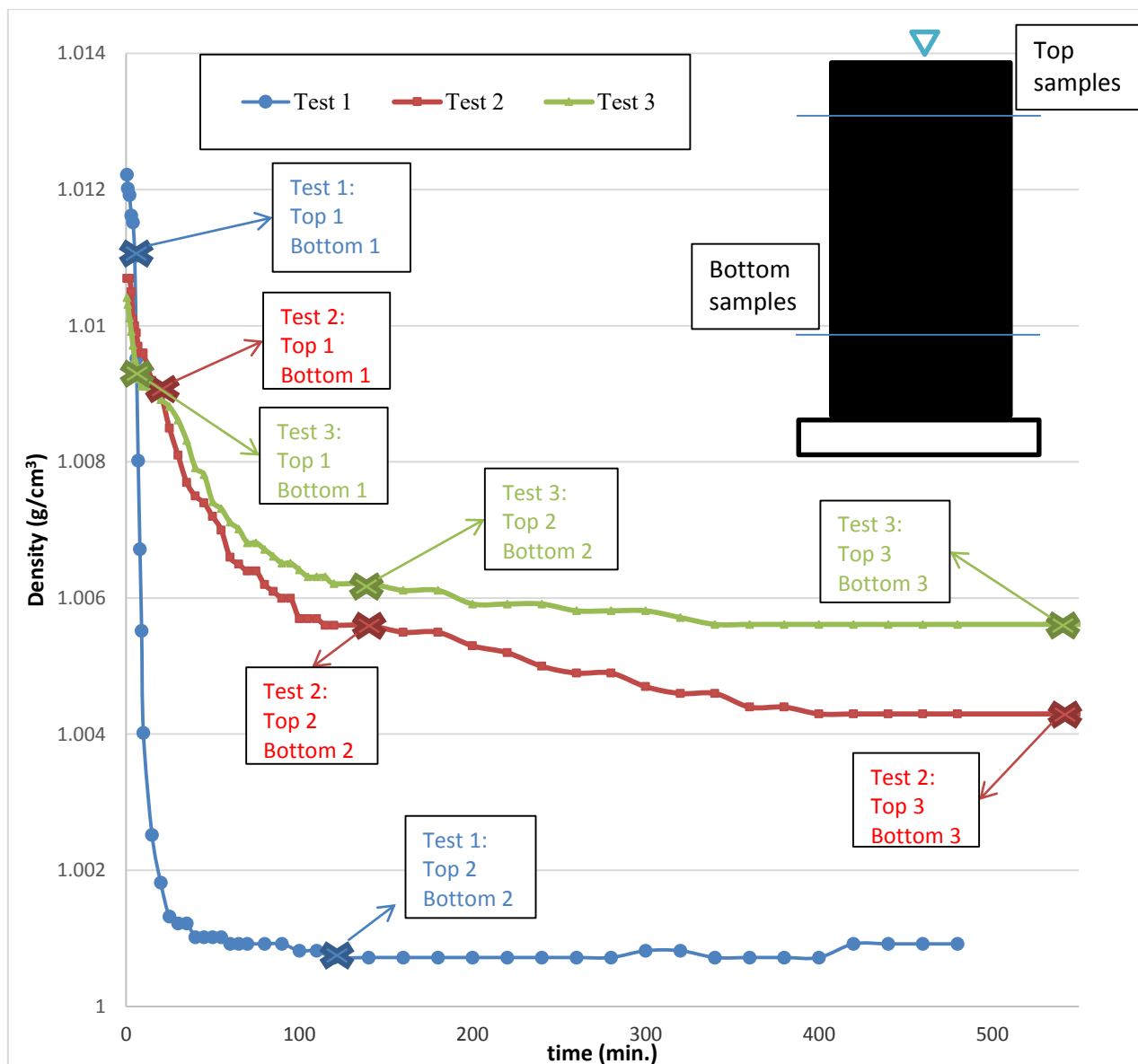


Figure 3.12 Sedimentation test: the cross indicate the samples that were analyzed

In the Figure 3.12 is described when the samples were collected.

For the Test 1 (20g/L CI and 0g/L CMC) just two couple was taken:

- At the beginning of the 1st stage (Top and Bottom 1);
- In the 2nd stage because for this suspension it is already the stable phase (Top and Bottom 2).

In the Test 2 (20g/L CI and 2g/L CMC) and 3 (20g/L CI and 4g/L CMC) there are three stages, for this reason, it was decided to take three couples of samples, one for each stage:

- ❖ At the beginning of the 1st stage:
 - 2 samples for the Test 2 (Top and Bottom 1);
 - 2 samples for the Test 3 (Top and Bottom 1).
- ❖ Between the end of the 1st stage and at the beginning of the 2nd stage:

3. SEDIMENTATION TESTS

- 2 samples for the Test 2 (Top and Bottom 2);
 - 2 samples for the Test 3 (Top and Bottom 3).
- ❖ At the end of the 3rd stage:
- 2 samples for the Test 2 (Top and Bottom 3);
 - 2 samples for the Test 3 (Top and Bottom 3).

In the Table 3.3 there are the time and the name of the samples taken along the sedimentation test.

However, before to start the collection of the samples for each test the different suspensions were analyzed for total iron and total organic carbon values at the times 0.

Table 3.3 Samples collection time in the different sedimentation tests

Test 1 (20g/L CI)	
	min.
Sample 1	0
Top 1	5
Bottom 1	6
Top 2	120
Bottom 2	121
Test 2 (2g/L CMC and 20g/L CI)	
	min.
Sample 2	0
Top 1	9
Bottom 1	10
Top 2	140
Bottom 2	141
Top 3	1000
Bottom 3	1001
Test 3 (4g/L CMC and 20g/L CI)	
	min.
Sample 3	0
Top 1	7
Bottom 1	8
Top 2	140
Bottom 2	141
Top 3	1453
Bottom 3	1454

The samples analysis gives two values:

- The Total Iron (Fe_{tot});
- The Total Organic Carbon (TOC).

The measurement procedure is summarized below.

The measurement of the total iron was determined according to ISO 6332-1988, DIN 38406 E1-1:

1. Samples were diluted individually in ultrapure water;
2. A defined volume was taken from the dilution and pipetted into a 10mL flask;

3. SEDIMENTATION TESTS

3. 0.5mL of ammonium acetate glacial acetic acid solution, 0.2mL of hydroxyl ammonium chloride and 0.2mL of 1,10-phenanthroline were added;
4. It was waiting 20 minutes for the reaction time;
5. The total iron measurements were taken with a photometer at 510nm.

For the TOC, two different methodologies were used, one for the top samples of the Test 1 in Table 3.3, and another methodology for the other samples because the top samples of the Test 1 had a very low concentration of Carbon Iron (it is possible to observe the Figure 3.8).

Therefore, the calculation procedure of the TOC in the samples with a low concentration of CI was:

1. The samples were filled into TOC vials or, if necessary, diluted beforehand in ultrapure water;
2. The TOC measurements were taken with an IR detector and with the sum method (measurement of TIC, acid, HCl and NPOC).

For the other samples the TOC procedure was:

1. The samples were strongly shaken;
2. 1mL (or less) were pipetted into TOC boats and weighed;
3. The samples were left in drying cabinet (105°C) until dry;
4. The TOC was measured with SSM IR detector, constant at 800°C

The used devices were:

- TIC/NPOC: TOC of company elementar LiquiTOC;
- TC: TOC from SHIMADZU, TOC-5000A + SSM;
- Total iron: Photometer by Perkin Elmer Lambda 14, cuvette quartz glass, 1cm

The results are shown in Table 3.4.

3. SEDIMENTATION TESTS

Table 3.4 Total Iron and Total Organic Carbon measures in the sedimentation test samples. The values have all the same unit of measurement except for (*) values in mg/L.

Test 1 (0g/L CMC)			Test 2 (2g/L CMC)			Test 3 (4g/L CMC)		
Sample 1			Sample 2			Sample 3		
Fe _{tot} (g/L)	1,787		0,67			1,341		
TOC (g/kg)	3,839		1,192			1,754		

Suspension 20 g/L Cl ⁻								
Test 1 (0g/L CMC)			Test 2 (2g/L CMC)			Test 3 (4g/L CMC)		
Top		Top			Top			
1 (5min.)	2 (120min.)	1 (9min.)	2 (140min.)	3 (1000min.)	1 (7min.)	2 (140min.)	3 (1453min.)	
Fe _{tot} (g/L)	0,006	0,57*	0,425	0,058	0,062	0,054	0,095	0,082
TOC (g/kg)	5,5*	4,4*	1,352	1,064	0,948	1,674	1,359	1,272
Bottom			Bottom			Bottom		
1 (6min.)	2 (121min.)	1 (10min.)	2 (141min.)	3 (1001min.)	1 (8min.)	2 (141min.)	3 (1453min.)	
Fe _{tot} (g/kg)	2,242	0,749	0,571	0,15	0,125	0,036	0,242	0,091
TOC (g/kg)	2,936	1,152	1,400	0,537	1,270	1,066	1,347	1,481

To compare the Top TOC values with the Bottom ones of the Test 1 it was decided to use the density of the water to have an equal unit of measurement. This hypothesis can be considered correct because in this samples there is a separation between water and Cl⁻ suspension.

$$5,5 \text{mg/L} = 0,0055 \text{g/Kg}$$

$$4,4 \text{mg/L} = 0,0044 \text{g/Kg}$$

$$0,57 \text{mg/L} = 0,00057 \text{g/Kg}$$

The analysis of the different suspensions at the time 0 are shown in the Figure 3.13.

3. SEDIMENTATION TESTS

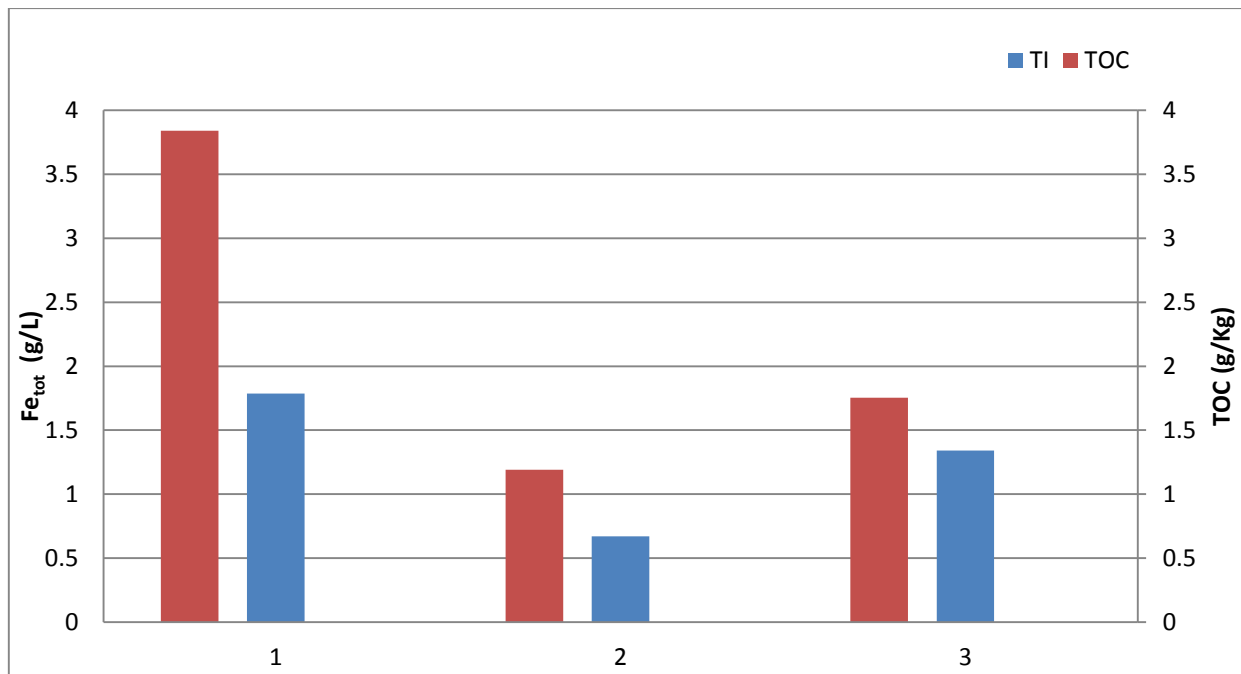


Figure 3.13 Samples analysis of the different suspension

The results show not expected values:

- For the different suspension, an equal value of Carbon Iron was used, this means that the values of Fe_{tot} must be for all the test equal to 4,44g but this does not happen. The concentration of total iron is lower than the expected quantity. Therefore, the Total iron concentration is different for the different suspensions.
A possible explanation is that the iron particles and the activated carbon are divided before to start the mixing.
- In the samples 1 was not used CMC however, the TOC values are bigger than other samples where there is activated carbon and CMC.

However, the sum of the top and bottom samples of the different suspensions can be compared with the analysis in the Figure 3.13 to be sure about the correctness of the data.

In the next figures, it is possible to observe how Fe_{tot} and TOC change in the time for the different tests.

All the graphs have the same size except the Top Test 1 because the results have values completely different and it is necessary a different range to observe the results.

Moreover, it is possible a comparison of the Total Iron in all the tests but this is not possible for the TOC measure because in the Test 1 the TOC is referred just to the Active Carbon that surrounds the Iron particles and in the Test 2 and 3 The TOC is referred both to AC and CMC polymers.

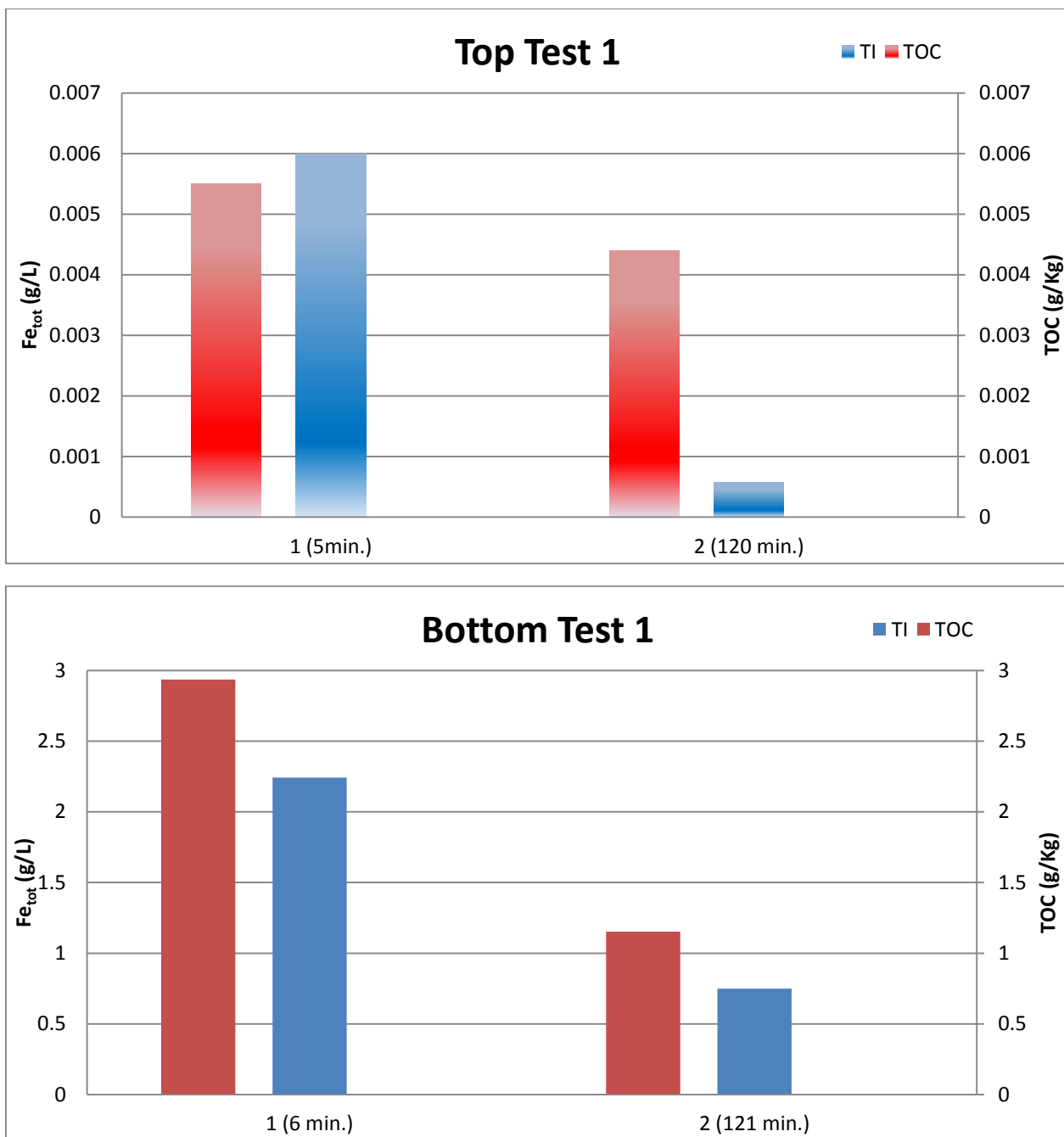


Figure 3.14 Samples results for the Test 1

It is possible considerate the Top of the suspension as water alone because the values of TOC and TI are near to the 0g/Kg.

As expected, in the bottom samples there is a higher concentration of Total Iron caused by a strong sedimentation process.

With a ratio it is possible to observe if there is a separation between the total iron and the activated carbon; values near the unity means sedimentation absent:

3. SEDIMENTATION TESTS

$$\frac{Fe_{totBottom\ 2}}{Fe_{totBottom\ 1}} = 0.33$$

$$\frac{TOC_{Bottom\ 2}}{TOC_{Bottom\ 1}} = 0.39$$

$$\frac{Fe_{totTop\ 2}}{Fe_{totTop\ 1}} = 0.095$$

$$\frac{TOC_{Top\ 2}}{TOC_{Top\ 1}} = 0.8$$

In the top of the cylinder the TOC remains almost constant and the iron decrease almost completely. In the bottom the sedimentation phenomenon of TOC and Fe_{tot} is quite similar however, the TOC tend to remain in suspension more than the total iron. In the end, the Figure 3.12 shows that between the two samples there is a big variation of density, therefore, the higher sedimentation of the iron and the big variation of density show that the iron particles sediment and the AC remains in suspension.

In the end, the TOC and Fe_{tot} in the initial part of the sedimentation test (5 and 6 minutes) are quite similar to the values in the samples 1 and they change completely in the 3rd stage of the test so, it is clear that the particles of iron and the activated carbon sediment in the bottom of the cylinder, deeper than the analysis point called Bottom.

3. SEDIMENTATION TESTS

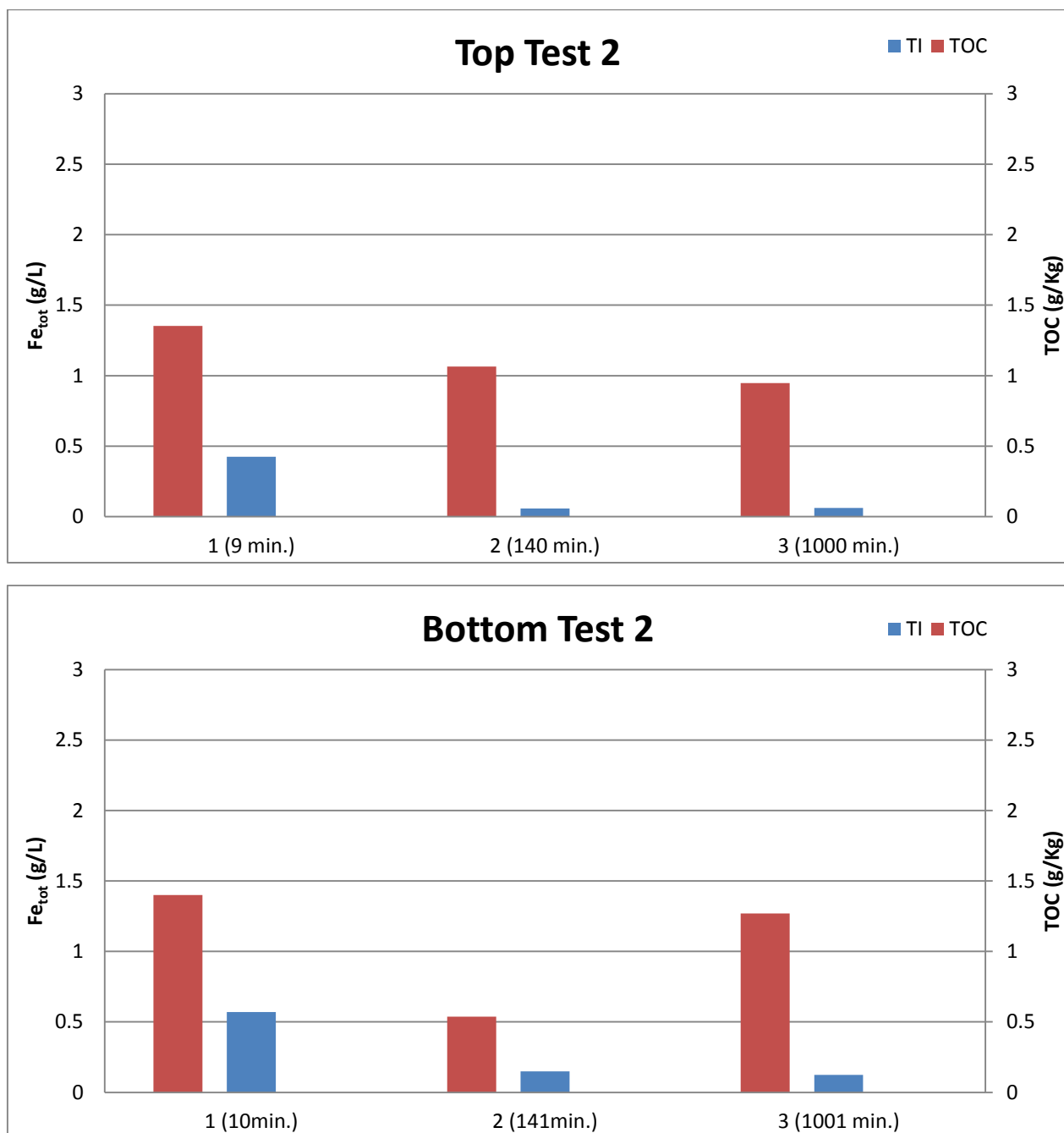


Figure 3.15 Samples results for the Test 2

In the Test 2 samples were taken in each stage of the sedimentation process.

In the 1st stage, the Fe_{tot} concentration is higher in the bottom than in the top due to the gravity force that influences the heavy iron particles, while the CMC and the AC particles remain longer in the suspension.

3. SEDIMENTATION TESTS

In the Top 1 sample (9 min.) the TOC and Fe_{tot} are higher than the Top 1 sample in Figure 3.14. Moreover, in the Bottom 1 sample (10 min.) is vice versa. This happens because the CMC polymer increases the TOC values and the capacity of CI particles to stay in suspension. Consequently, the distribution of the Fe_{tot} in the cylinder is more uniform than in the previous case.

In the Top 2 sample (140 min.) the 2nd stage starts. The sedimentation phase is ended and the cohesion force begins to act on the suspension. In fact, the differences between the Top 2 and Top 3 are not relevant and it is possible to say that the suspension is stabilized.

The same thing happens in the Bottom samples, where the Fe_{tot} decreases at the start of the 2nd stage and remains almost constant in the 3rd stage. The TOC in the Bottom samples initially decreases and then increases but it is possible to considerate this a constant trend because the Bottom 2 (141 min.) sample is an outlier. Indeed, in the Top samples 2 and 3 there is a little decrease of TOC and it cannot explain the high increase of TOC values in the Bottoms samples.

3. SEDIMENTATION TESTS

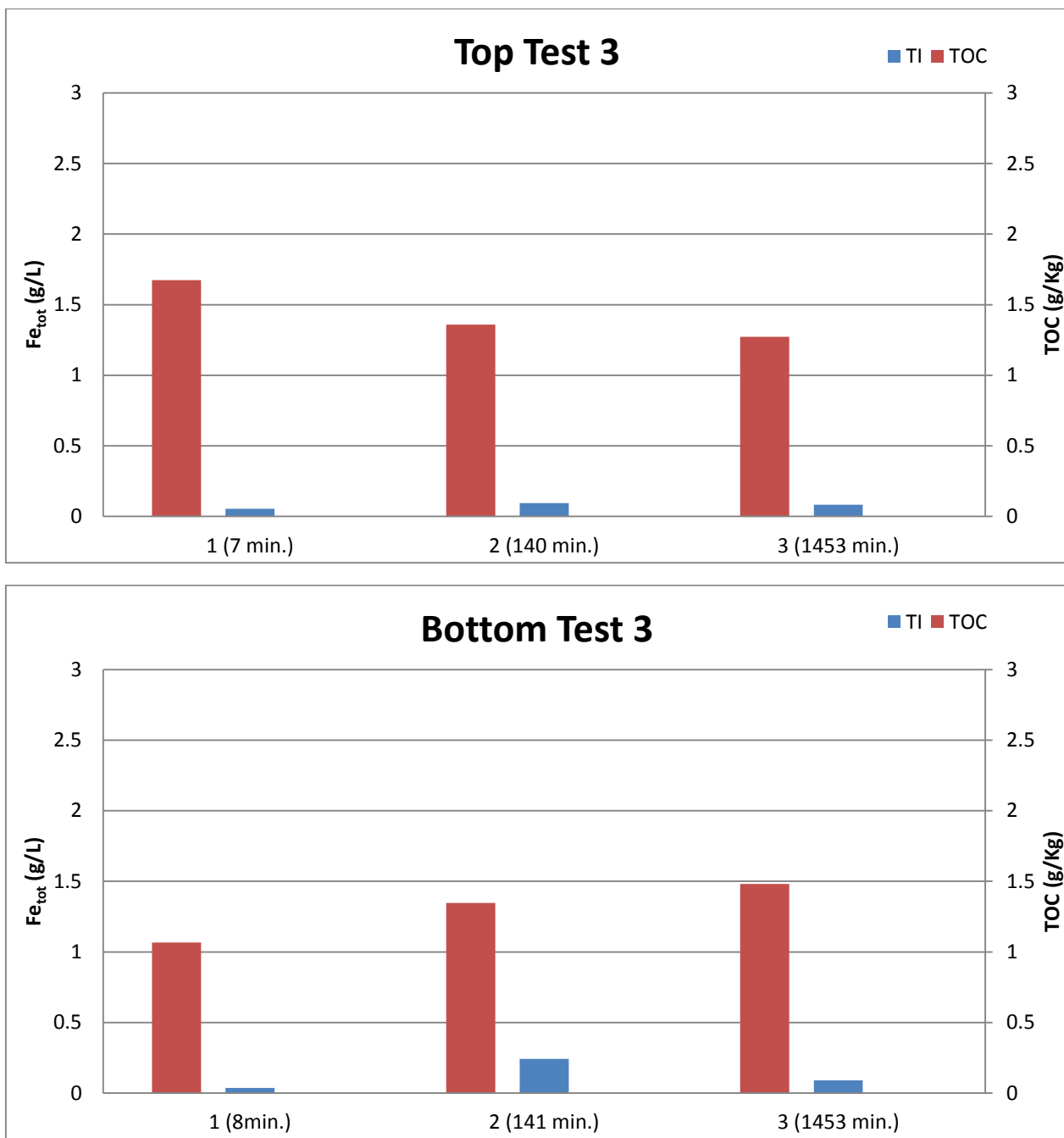


Figure 3.16 Sample results for the Test 3

For the last Test, the values of TOC in the Top and Bottom samples decrease and increase respectively how was expected because with the increase of the CMC the particles take more time to sediment. Instead, the values of Fe_{tot} remain constant for all the tests in the Top and Bottom samples both.

In previous tests, the Fe_{tot} trends were decreasing consequently it is possible that the Top and Bottom 1 (7-8 min.) could be outliers.

The study of the samples shows that the CI have disjunction of its elements and that with the increase of CMC the concentration of Fe_{tot} is not constant in the 1st stage suspension, but only at the start and

3. SEDIMENTATION TESTS

at the end of the 2nd and 3rd stage. Obviously, the TOC became higher because there were more CMC particles. However, the two suspensions with different values of CMC do not show big differences about the sedimentation process of the iron particles because the final values of Fe_{tot} in the Test 2 and 3 in the last samples (Test 2: Top and Bottom 3; Test 3: Top and Bottom 3) are almost the same. Thus, the difference about the two suspensions is the mobility: when a suspension is injected in an aquifer is advisable to have a low mobility to avoid the dispersion of the CI. For this reason, it is a good decision to use a lower concentration of stabilizer (2g/L of CMC than 4g/L used in the PhD work by Giannelli, 2014).

Since the Test 3 results about bottom Fe_{tot} seem to be outliers, it is advised to consider only Test 1 and Test 2 results to a more accurate analysis.

4 DYNAMIC VISCOSITY

The viscosity explains the measure of a fluid resistance to a gradual deformation by shear stress or tensile stress. The viscosity of suspensions depends on the temperature, solid fraction, the maximum solid fraction of the particulate phase, on shear rate, particle diameter, and viscosity of the suspending liquid (Konijn, Sanderink, & Kruyt, 2014).

For the experiment, it is relevant to know this factor because the diffusion of the suspensions in the flume depends on the diffusion coefficient D that it is related to the viscosity η . It is possible to expect a high diffusion coefficient for fluids that have a low viscosity (Atkins, 2000):

$$\eta \propto 1/D$$

The viscometer was used to analyze this parameter for the suspensions and the solution described in chapter 1.1. The temperatures of the different samples were kept similar ensure comparability.

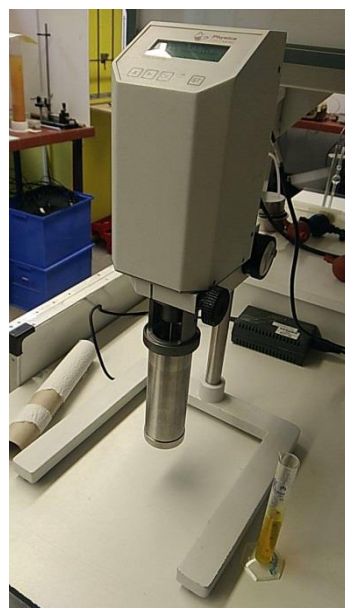


Figure 4.1 Viscometer: ANTON PAAR Gray-Austria, type RHEOLAB MC 1

The viscometer has the purpose to calculate the dynamic viscosity. The tool has two cylinders: the first one “a” inside of the second one “b”. The cylinder “a” rotates due to the engine torque.

A liquid is put between the two cylinders. When the cylinder “a” starts to rotate the tool measures the moment of resistance due to the shears force of the liquid on the cylinder “b”.

The viscometer changes the rotational speed and it gives for each velocity a shear force referred to the unit area of the rotation cylinder “a”.

Knowing the dimension of the cylinders, the velocity of rotation and the shear force the tools can evaluate the viscosity of the liquid.

4. DYNAMIC VISCOSITY

Viscometer used for the measurements is a Rheolab MC1 (anton paar), which ensures correct measurements above $500\mu\text{Nm}$. Also, very high moments turbulent flow is generated in the suspensions, that causes incorrect measurements.

Moreover, the moments excessively high produce a turbulent flow in the suspensions that cause the recording of false values because of rheology laws act in a laminar state.

In the Figure 4.2 is showed the relation between the moment and the rounds per minute.

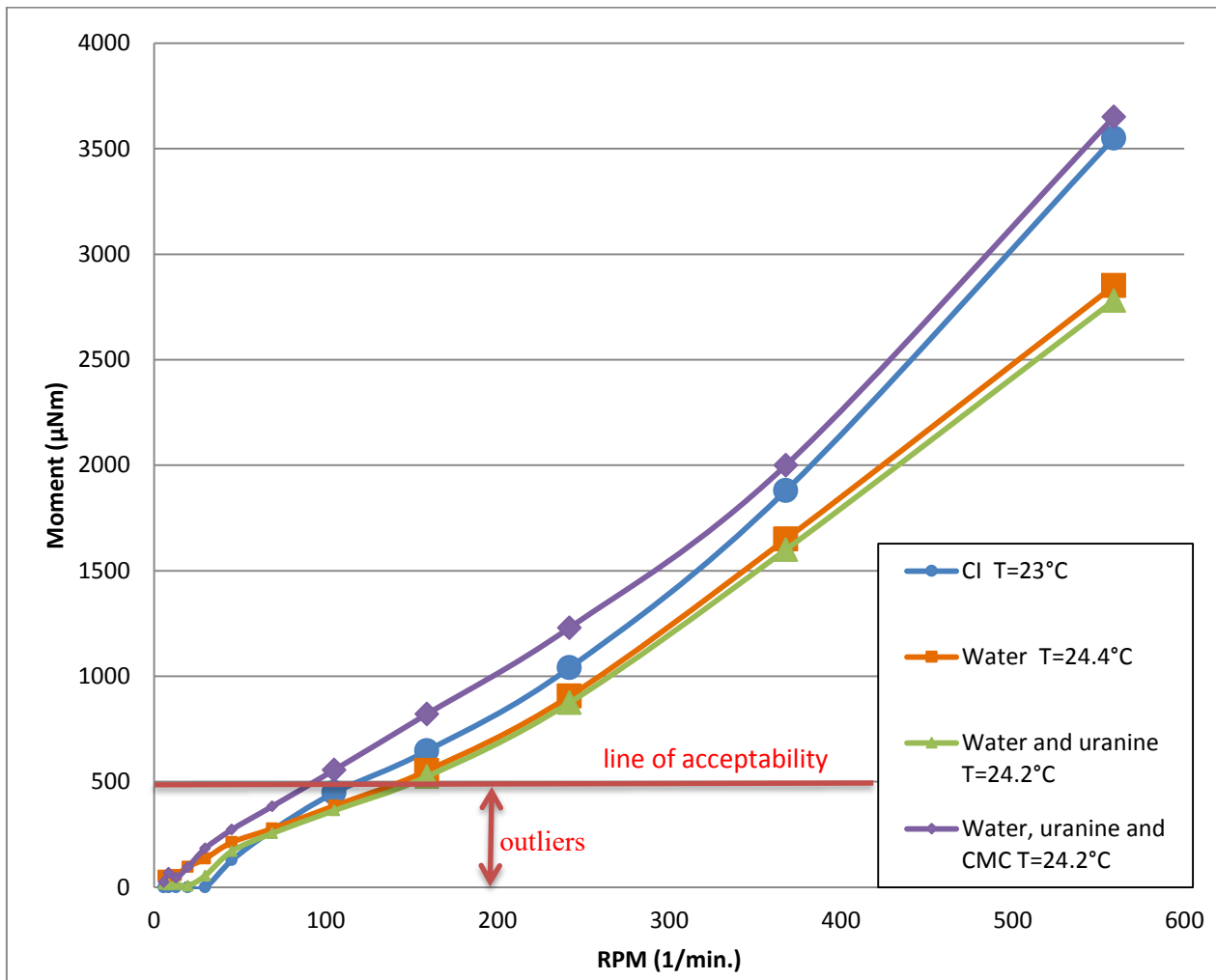


Figure 4.2 Moment vs RPM for the different suspensions

It is possible to observe that the suspension with CMC has five acceptable values and the other suspensions just four. Furthermore, the first values of the water suspensions are very close to the line of acceptability differently by CI suspension thus, it is predictable that the CMC and CI suspensions are having the higher representativeness than water samples.

So, knowing the values not influenced by error it is possible to analyze the viscosity graph.

4. DYNAMIC VISCOSITY

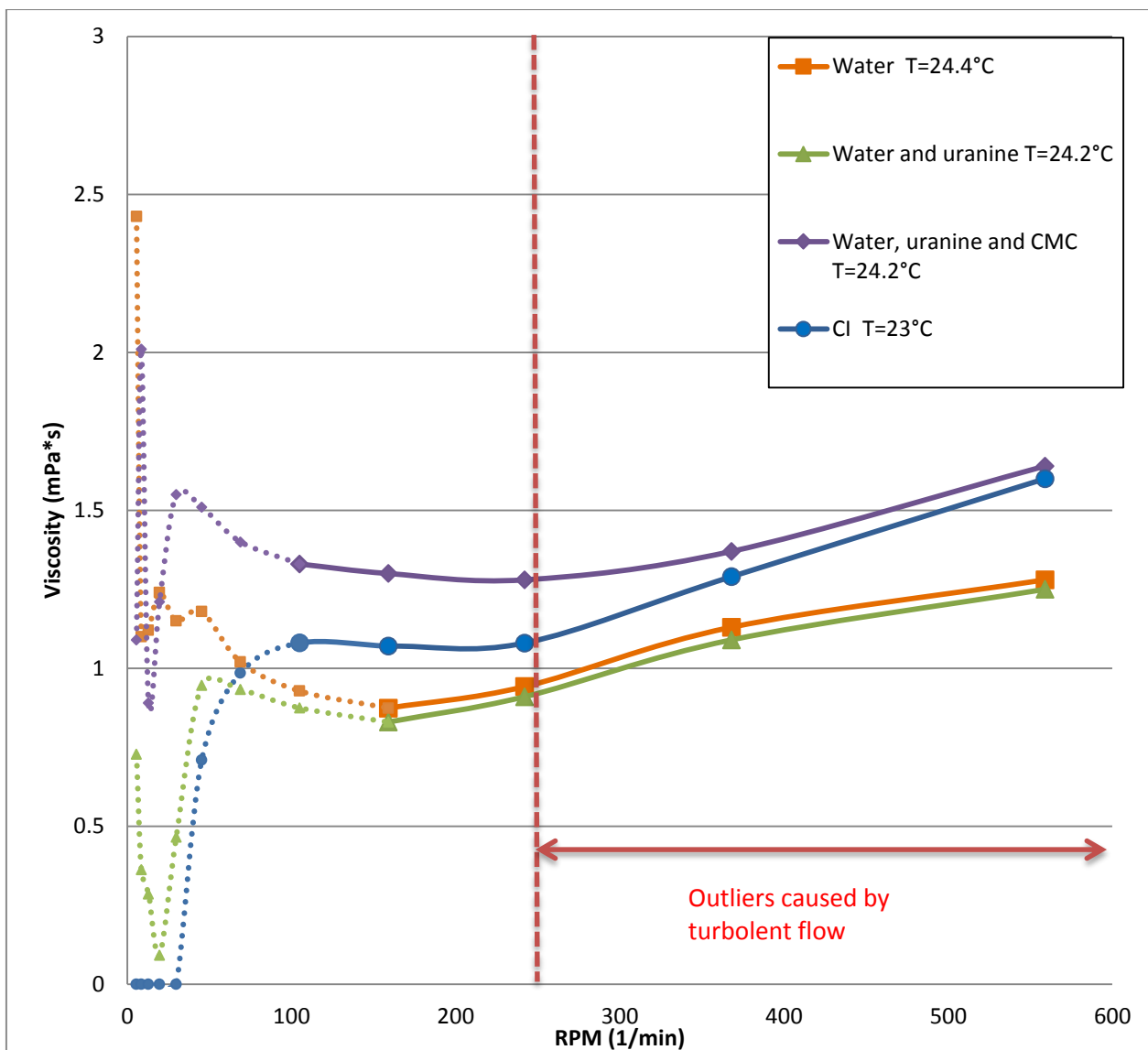


Figure 4.3 Viscosity values obtained by the viscometer

From the Figure 4.3 is noticeable that the uranine does not change the viscosity value of the water but also that 20g/L of CI and 2g/L of CMC suspension has a viscosity lower than just 2g/L of CMC. This last result is not anomalous because, the viscosity of CMC solution was evaluated many times during this work with different samples and, the results had always a viscosity higher than the CI solution.

It is evident from the results that the CMC increases the viscosity of a suspension. However, it is also worth to note that, when the CI is added to the solution, the viscosity decreases slightly because a fraction of the dissolved CMC sorbs onto the CI, therefore reducing the overall concentration of free CMC affecting the suspension viscosity.

With the Figure 4.4, it is possible to see the relation between shear stress and the round per minute. The correct values are shown with a continuous line while the outliers are represented with a dashed line.

4. DYNAMIC VISCOSITY

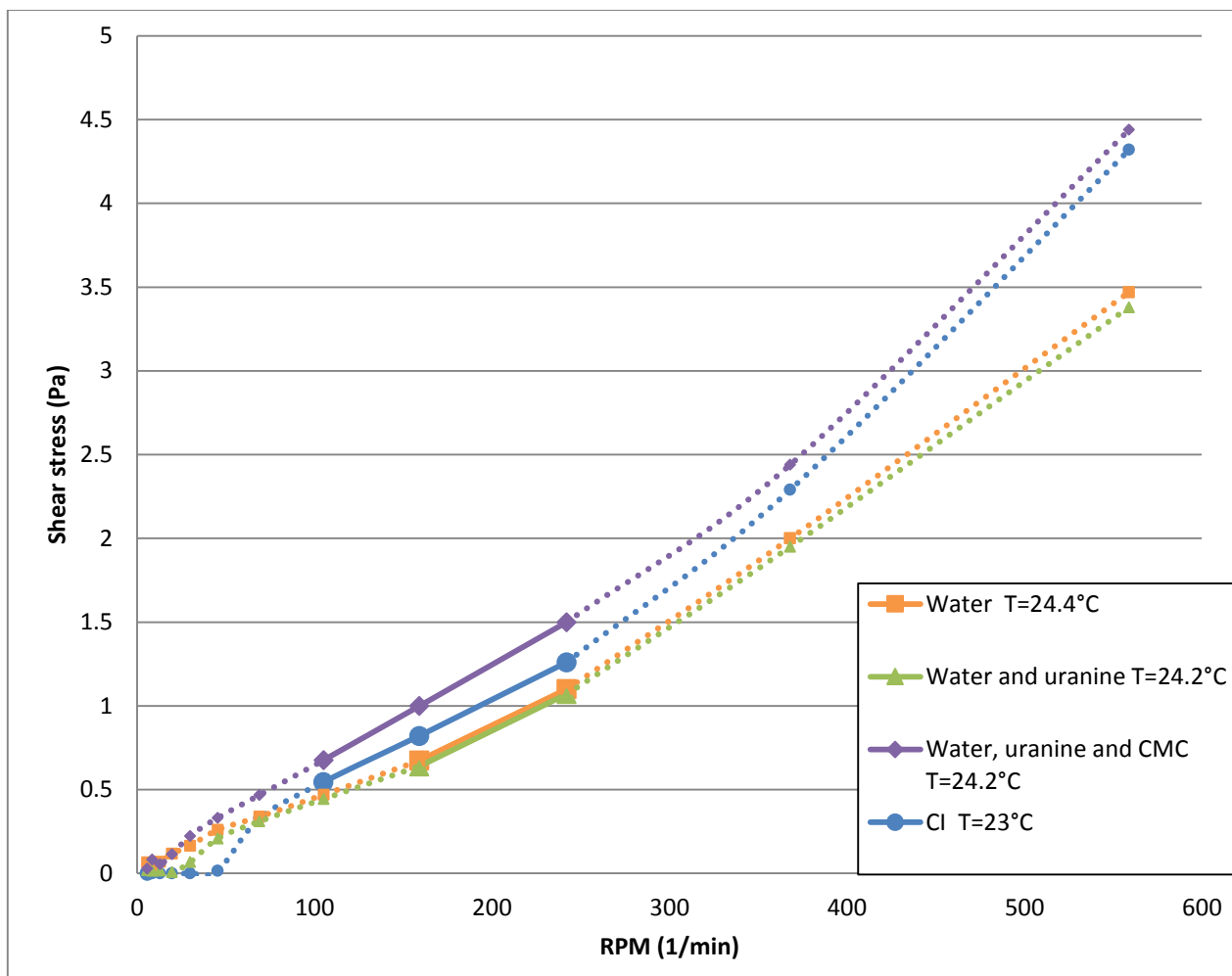


Figure 4.4 Shear stress vs Rounds Per Minute for the different suspensions

Observing the Figure 4.3 and Figure 4.4 it is evident that the suspensions have a constant trend in the range of measures not subject to errors. Thus, the different fluids belong to the category called Newtonian.

It is important to say that the viscosity measurements, and consequently the coefficient diffusion of the suspensions, are not the same in the fluid in bulk and when flowing through the porous media. Consequently, it is possible to distinguish an effective and a real diffusion coefficient. This happens because a free fluid has more space to move and to spread, while in a porous medium wall effects are not negligible, the cross section available for flow is reduced, and flow paths are tortuous (multiphysics CYCLOPEDIA, 2015).

Despite this difference, it is possible to assume that the relationship between the different solutions does not change: both for a fluid in the bulk and in the porous medium it is true that:

$$\eta_{CMC} > \eta_{CI} > \eta_{water} \rightarrow D_{CMC} < D_{CI} < D_{water}$$

Where η is the viscosity and D the density respectively of the:

- CMC: solution of 2g/L of CMC polymer in water;

4. DYNAMIC VISCOSITY

- Water: water and uranine;
- CI: suspension of 2g/L of CMC and 20g/L of CI

5 TRACER TESTS

The purpose of the tracer tests is to estimate the fundamental hydrodynamic properties of the porous medium.

The flume is made of stainless steel, it has a volume of 84L. Its dimensions are:

- Length L= 100 cm;
- Height H= 70 cm;
- Width B = 12 cm.

Since the width is smaller than the other two dimensions, the flume can be considered a bi-dimensional flow. It has 3 in-flow wells and 3 out-flow wells (numbered in Figure 5.2 as W1 to W6).

BASE-FLOW SETUP

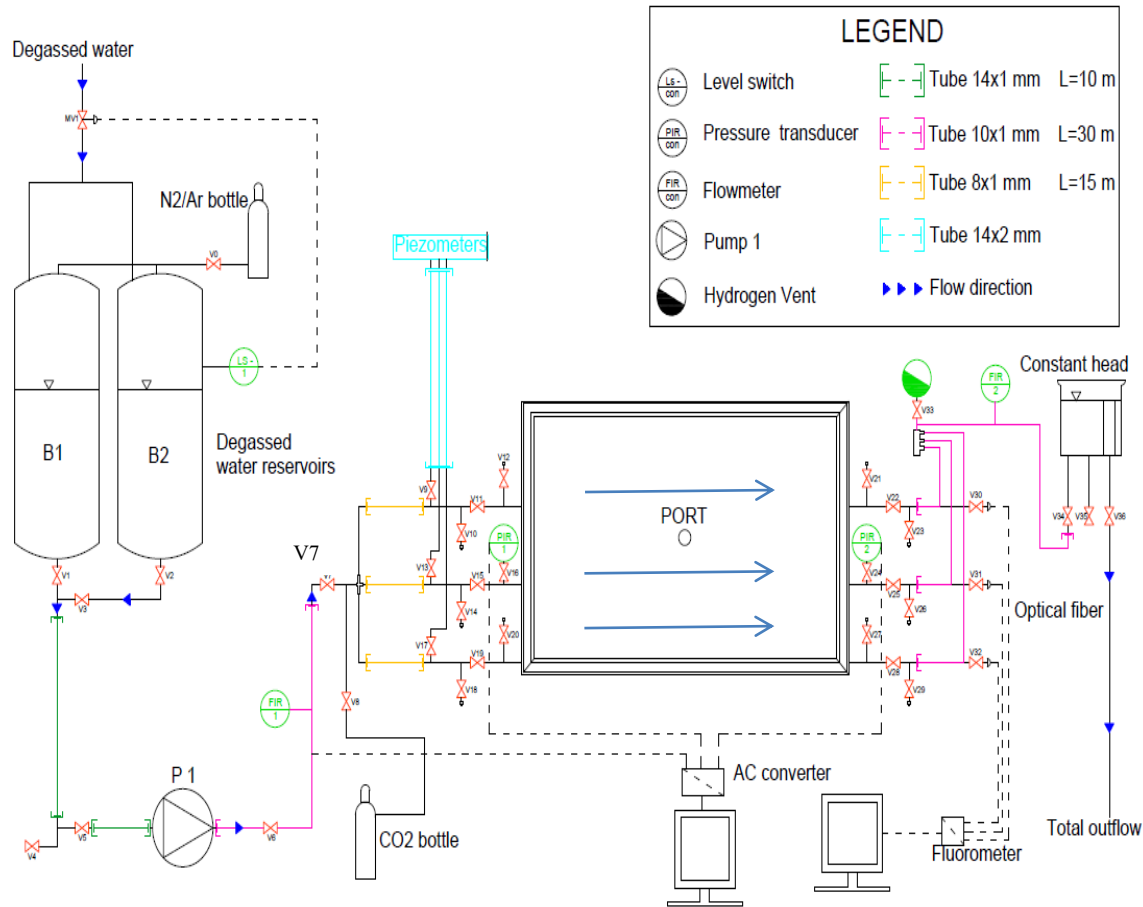


Figure 5.1 Base-flow set up

The tests were performed in the flume applying the following boundary conditions:

5. TRACER TESTS

- Constant inflow: 16,3L/h and 9,06L/h respectively for the tests with a higher and lower tracer concentration;
- Outflow: constant head placed at 87 cm from the flume base and a constant flow equal to the inflow.

These tests are executed with the injection of uranine, a biologically degradable substance that in certain concentration can be observed with the help of neon lamps.

The Figure 5.2 shows the project of the base-flow set up.

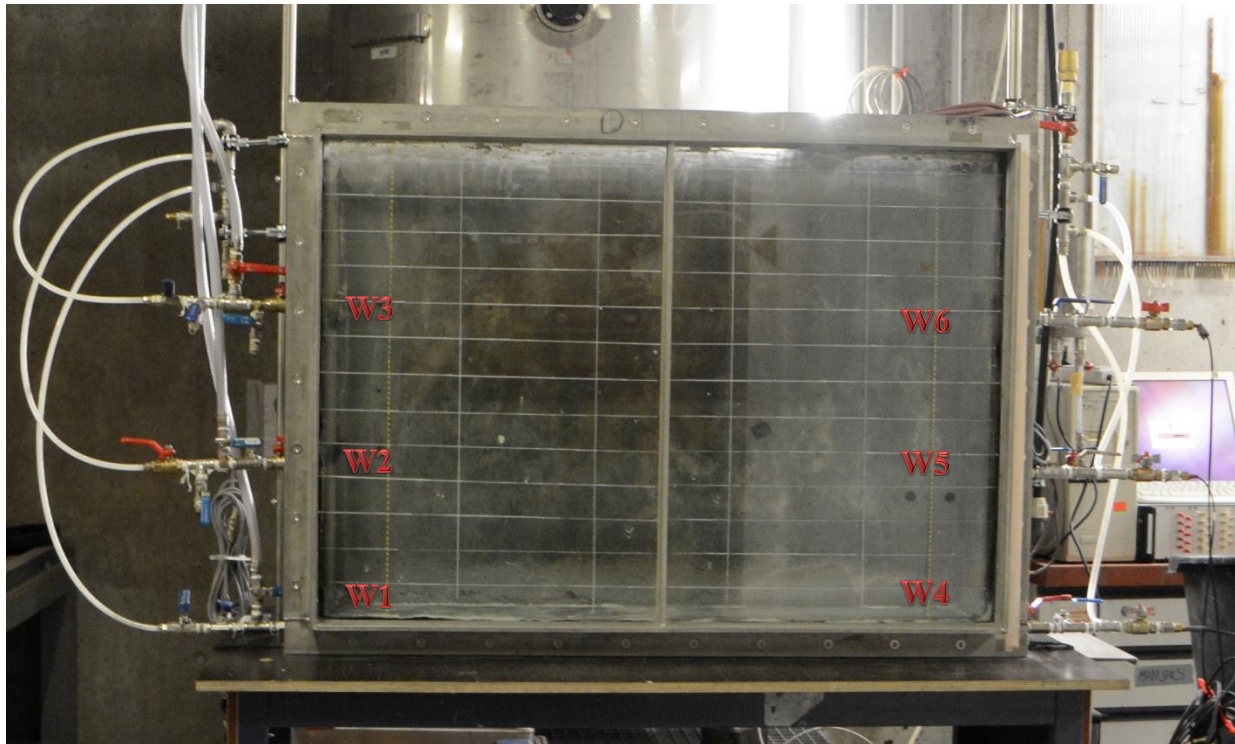


Figure 5.2 Front view of the flume structure

The degassed water is stored in reservoirs; they provide the water for the flume. Through a pump (YTRON-Z homogenizer-shear pump) the degassed water entered in the flume.



Figure 5.3 Degassed water reservoirs

The flow, temperature, and pressure are measured continuously. The inflow values are measured with a magnetic inductive flow meter. The water passes through a magnetic field where the voltage changes. This voltage is proportional to the mean flow velocity.

Two pressure and temperature transducer (ADZ Nagano, sensortechnik SML 20 sn:11403090004) are emplaced in the wells 2 and 5 (Figure 5.2). Furthermore, there are three piezometers that can give pressure values in each in-flow wells. In the end, the software ProfiLab Expert 4.0 produced by ABACOM Ingenieursellschaft allows the digital collections of the data

All these tools can be seen in Figure 5.4.

5. TRACER TESTS

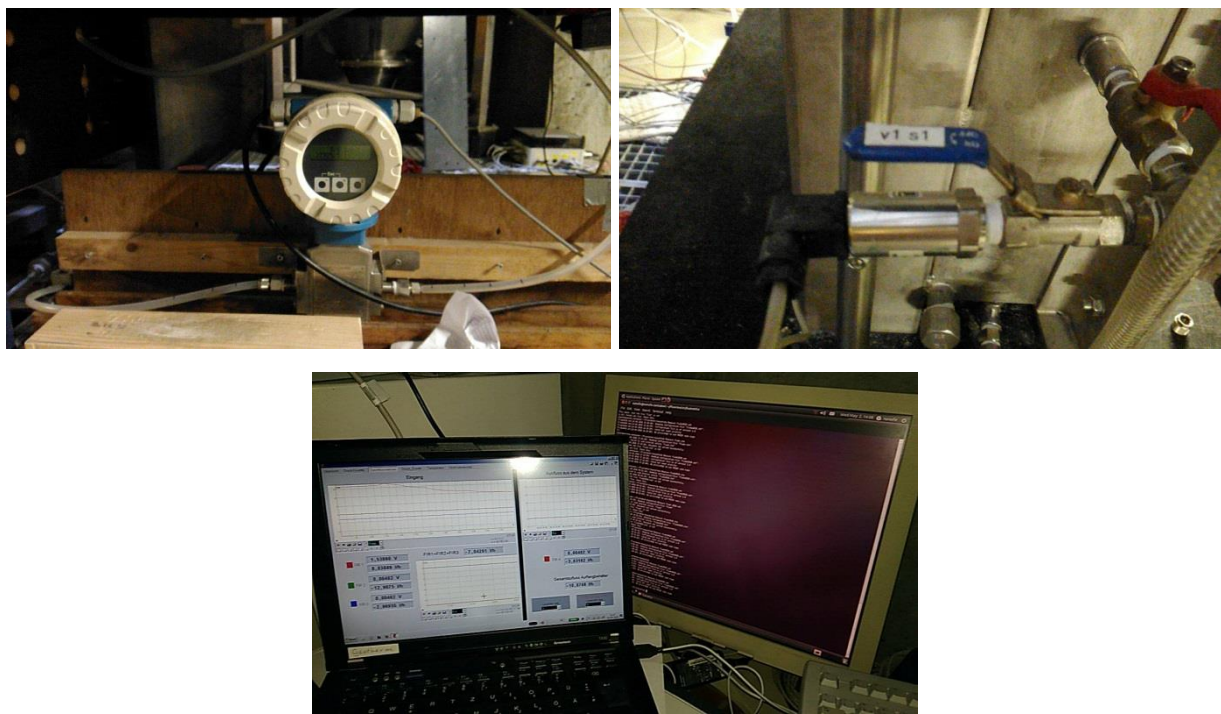


Figure 5.4 From left to right: magnetic inductive flow meter; pressure and temperature transducer and measure software

At the flume outflow, wells W4, W5, and W6 have fiber-optic sensors, indispensable to perform a tracer tests with a low concentration of uranine (in the order of $\mu\text{g/L}$).

Each optical fiber shows two channels, the first called *gain* which returns a signal measuring the device-given ray that hits the water surface, and the second called *signal* which represents the answer of the impacted surface and changes depending on the uranine concentration. The fluorescence signal is calculated by normalizing signal to gain.

5. TRACER TESTS

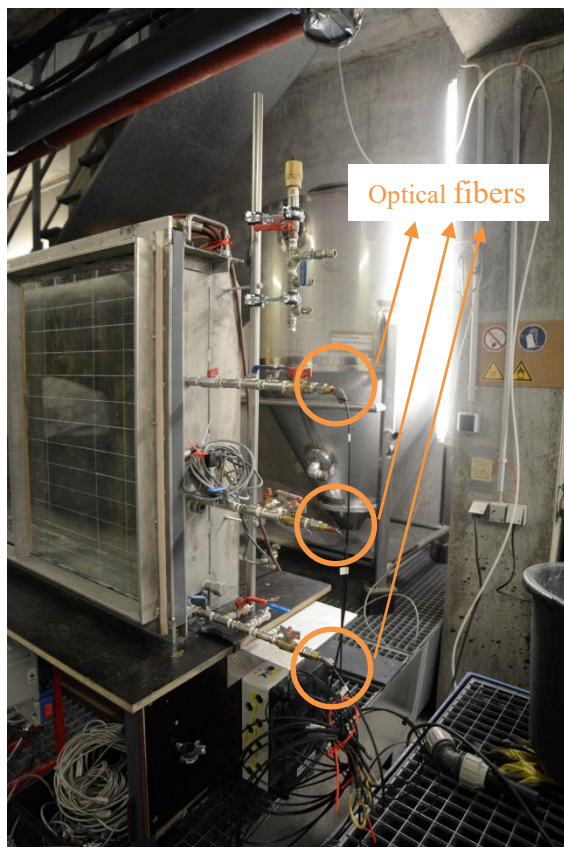


Figure 5.5 Optical fibers in wells 4, 5 and 6

5.1.1 Filling of the flume

The flume has different sands layers, they have synthesized in the Table 5.1:

Table 5.1 Flume's layers from the top to the bottom

Layer Flume	
1 cm	Geba
1 cm	Troptogel
0,5 cm	Bentonite
1,5	Geba
63,5 cm	Dorsilit n°8
2 cm	Geba

The sands are poured in the flume with the aid of a funnel which allows it to be filled along the entire length.



Figure 5.6 Flume filling with the use of a funnel (on the left), and sand compaction (on the right)

To have a homogeneous density in the flume, the sand is compacted every 15 cm by hitting a wooden block with a hammer.

To set up a confined aquifer, two impermeable layers are made. Their purpose is to avoid preferential pathways in the upper and lower extremities of the flume. This is achievable using fine sands.

In the bottom of the flume, there is 2 cm of GEBA. On the top, the flume has a mixture of sands: 1,5 cm of GEBA, 0,5 cm of bentonite in powder, 0,5 cm of a gelatinous mixture Troptogel and 0,5 cm of GEBA (Table 5.1).



Figure 5.7 From left to right: GEBA, Dorsilit n°8 bentonite and bentonite in powder

Table 5.2 Properties of GEBA sand

Properties of GEBA sand	
Form	Round shaped
Color	Grey/white /off white
Grain density (g/cm³)	2,65
Average grain (mm)	0,13
Mineralogical composition of GEBA sand	
Quartz (w/w%)	98
Clay Minerals (w/w%)	1,4
Mica (w/w%)	0,1
Residual Minerals (w/w%)	0,5

In the end, between these two impermeable layers, there is Dorsilit n°8. The properties of this sand are described in the Table 5.3.

Table 5.3 Properties of Dorsilit n°8

Physical properties	
Trade name	DORSILIT n°8
Grain Shape	Round
Grain Density	2,65 g/cm ³
Grain size	0,3-0,8 mm
Chemical properties	
SiO₂	ca. 98,9 w/w%
Fe₂O₃	ca. 0,01 w/w%
Al₂O₃	ca. 0,55 w/w%
TiO₂	ca. 0,04 w/w%

With some equations it is possible to calculate the porosity of the flume:

$$\rho_{bulk} = \frac{M_{sand}}{V_{bulk}} \quad (4)$$

$$n = 1 - \frac{\rho_{bulk}}{\rho_{grain}} \quad (5)$$

$$PV = n * V_{\text{bulk}} \quad (6)$$

The values calculated can be seen in Table 5.4.

Table 5.4 Parameters of the bed

Bulk dimension	M bulk (g)	122.760,5
	H (cm)	63,5
	B (cm)	12
	L (cm)	100
Dorsilit n°8	V bulk (cm ³)	76.200
	Bulk density (g/cm ³)	1,61103
Dorsilit n°8	Grain Density (g/cm ³)	2,65
	Porosity	0,39

With the equations 4, 5 and 6, it is possible to estimate the porosity and consequently, the pore volume (PV). In this phase, the flume has air in its pores but a confined aquifer is an environment without air and oxygen. For this reason, before filling with degassed water, another step was necessary.

To displace the air, CO₂ was used. It has a density higher than the air thus, the air is pushed on the top of the flume and not yet sealed. Furthermore, the CO₂ dissolves when in contact with water.

With a safety factor of 1,5 applied to the pore volume, 45L of CO₂ was injected in the flume from the valve 7 in Figure 5.1 (1L/min for 45 minutes).



Figure 5.8 Injection of CO₂

After that, it is possible to seal the top of the flume with a lid leaning on a waterproof tape and starting to fill the flume with degassed water and a flow of 1,5L/h.

5.2 Tracer test with optical fiber

The first test was completed with a concentration of 1000µg/L of uranine that is visible with using optical fibers.

100mL of uranine is injected for 10 seconds in a port placed before the three in-flow wells (valve7 Figure 5.1).

Before performing the test it was necessary to calibrate the optical fiber. The procedure was quite simple:

- Recording of signals without uranine;
- Injection of uranine (10 ml with a concentration of 1000 µg/L) in all the wells with optical fibers (valves 23, 26 and 29 Figure 4.1);
- Recording of signals with uranine;
- Calibration with two values of concentration 0 µg/L and 1000 µg/L.

The optical fibers in the wells 4 and 5 worked perfectly. In well 6, the constant value of concentration equal to zero changed. For this reason, we had to repeat the calibration for the W06 optical fiber.

After that, the test started using a flow of 9,06L/h. The results are shown in the Figure 5.9.

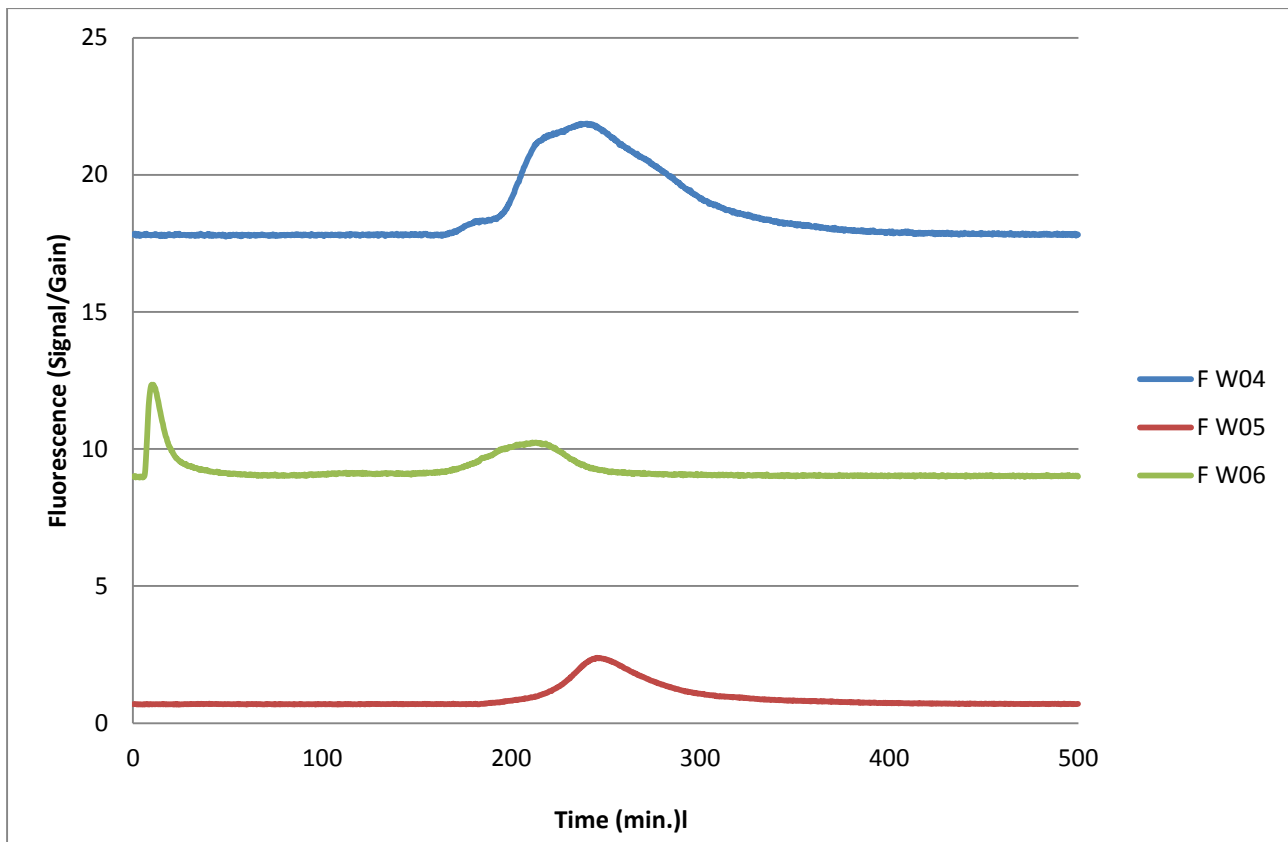


Figure 5.9 Fluorescence vs time: test with optical fiber

In well 6 the optical fiber shows a high signal in a short time. This may be due to a not excellent operation of the optical fiber in well 6 as the signal had shown some variations in the calibration test.

In addition, we made more calibration tests respective to the other wells. Therefore some uranine concentration of these tests could still remain near well 6.

With the calibration, we obtain the Figure 5.10.

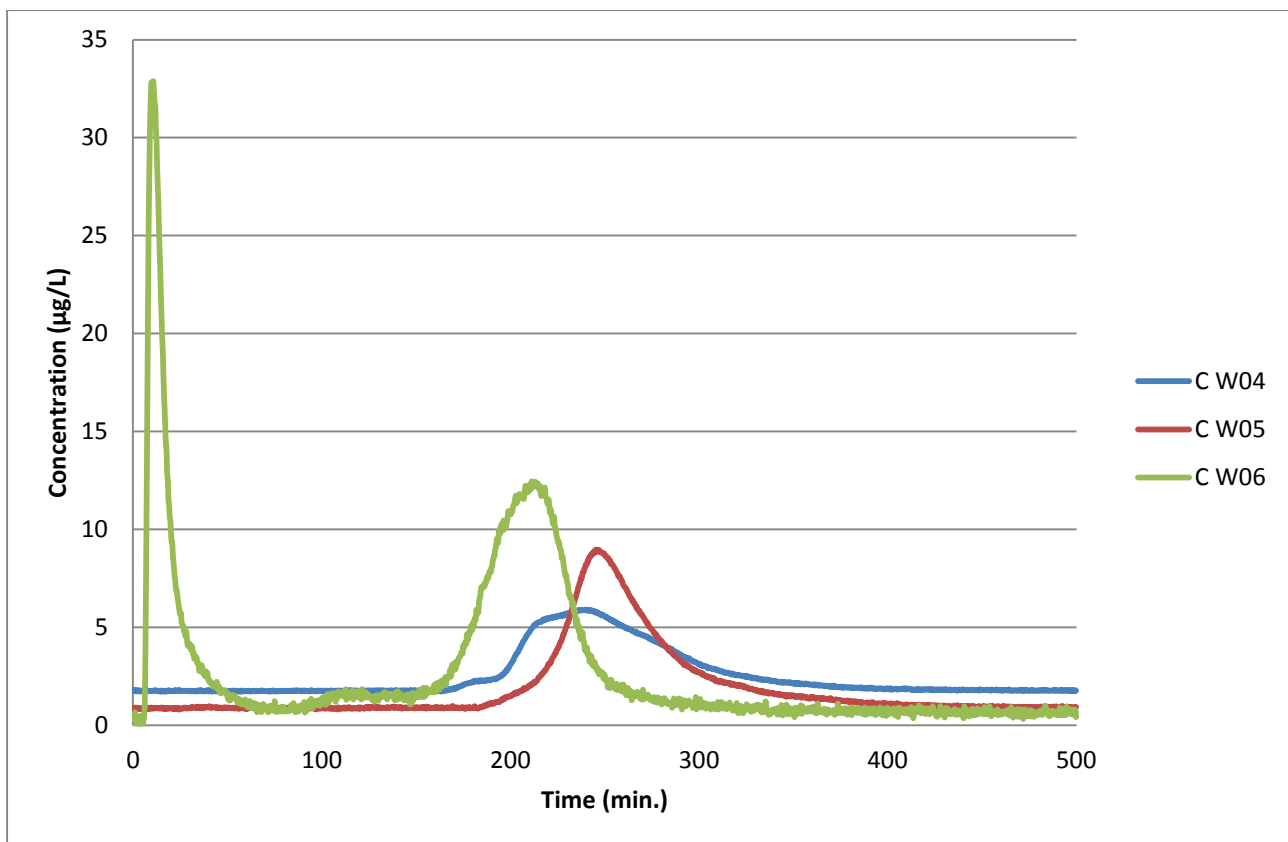


Figure 5.10 Concentration vs time: test with optical fiber

Not considering the anomaly explained above, it is possible to deduce that the peaks are very close to each other. Furthermore, the uranine arrived first on the top well (W06 with 208 minutes) and with a slight delay in the other two wells (W04 with 239 minutes and W05 with 245 minutes).

With these graphics and some formulas, it is possible to calculate the porosity and the hydraulic conductivity of the flume.

The Darcy velocity is the incoming flow divided for the cross-section.

$$v_d = \frac{Q}{A} \quad (7)$$

The pores velocity was obtained like the length of the flume divided for the average time of travel of the uranine in the flume.

$$v_e = \frac{L}{t_{av}} \quad (8)$$

With the result of equations 7 and 8, the porosity was calculated with the equation 9.

5. TRACER TESTS

$$n = \frac{v_d}{v_e} \quad (9)$$

In the end, it is possible to check the value of the hydraulic conductivity of the flume.

$$K = \frac{v_d}{i} = \frac{v_d * L}{\Delta h} \quad (10)$$

The calculations and the results are shown in the Table 5.5.

Table 5.5 Result of the tracer test: porosity and hydraulic conductivity

Tracer test			
1000 µg/L			
A (dm ²)	7,68	t _m (min)	230,6
Q (L/h)	9,06	v _e (m/s)	7,22E-05
v _d (m/s)	3,28E-05	n	0,45
t ₄ (min)	239	Δh (m)	0,38
t ₅ (min)	245	i	0,3875
t ₆ (min)	208	K (m/s)	8,6E-05

It is possible to calculate the conductivity of the different layers to observe possible preferential pathways. Therefore, with the help of the Equation 9 and 10, it is possible to calculate the hydraulic conductivities for each layer.

Table 5.6 Hydraulic conductivity in each well

	v _e (m/s)	v _d (m/s)	Δh (m)	i	K
W04	6,9735E-05	3,16E-05			8,27E-05
W05	6,80272E-05	3,09E-05			8,07E-05
W06	8,01282E-05	3,63E-05	0,3823875	0,382388	9,5E-05

The values are in the same range, this means that there are no clear pathways and the average hydraulic conductivity is equal to $8,57 \cdot 10^{-5} \text{s}^{-1}$.

5.3 Visual tracer test

100 mL of uranine with a concentration of 2 g/L for 10 seconds was injected in the visual test.

The first step was to cover the flume and create a dark room. The passage of the uranine was visible thanks to neon lamps.

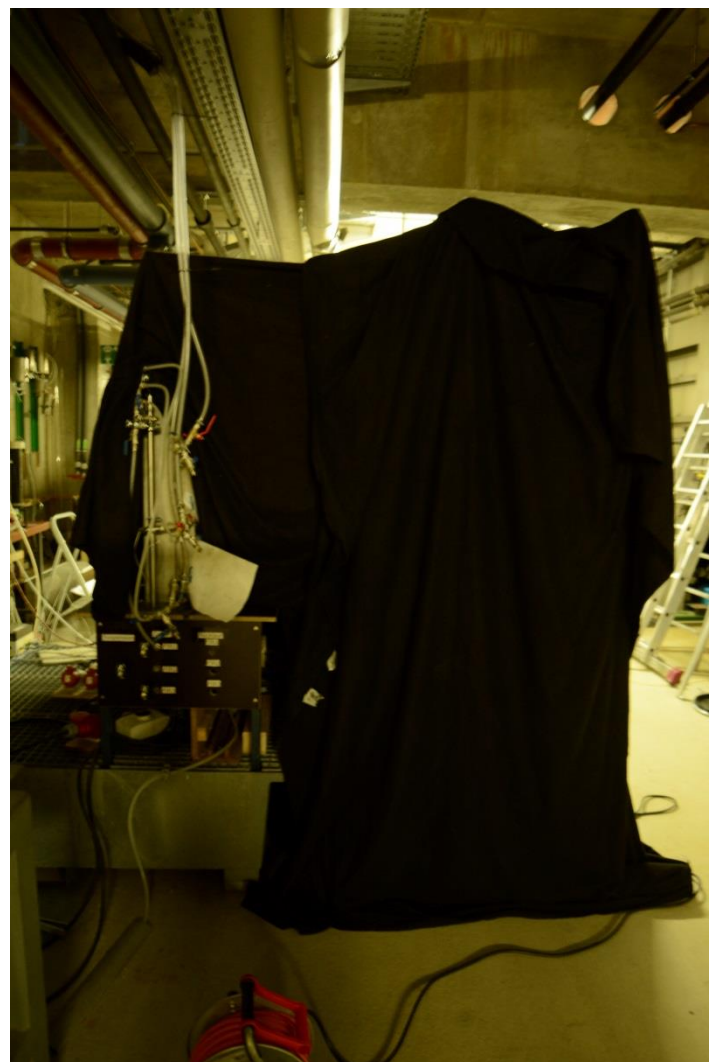
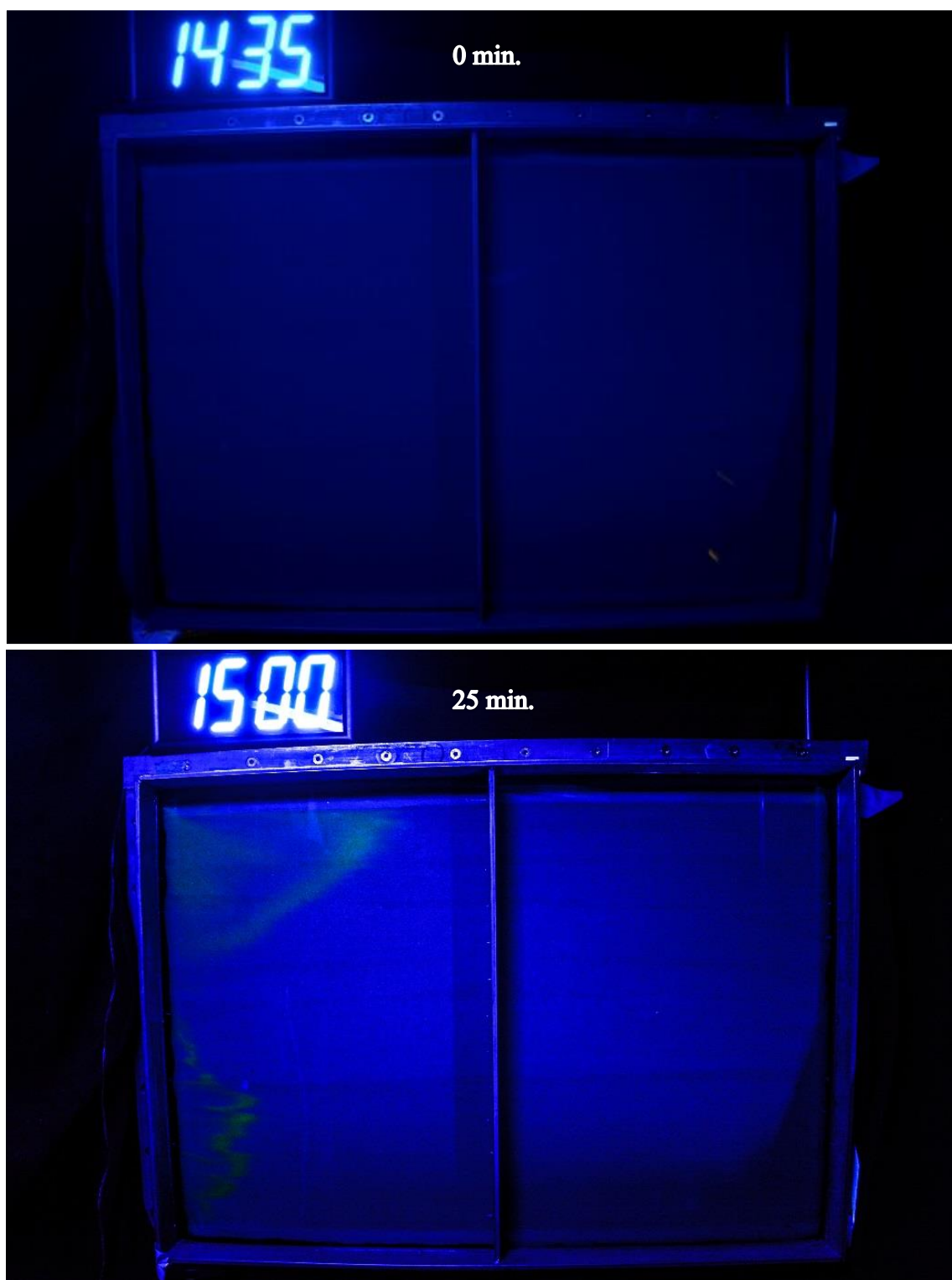
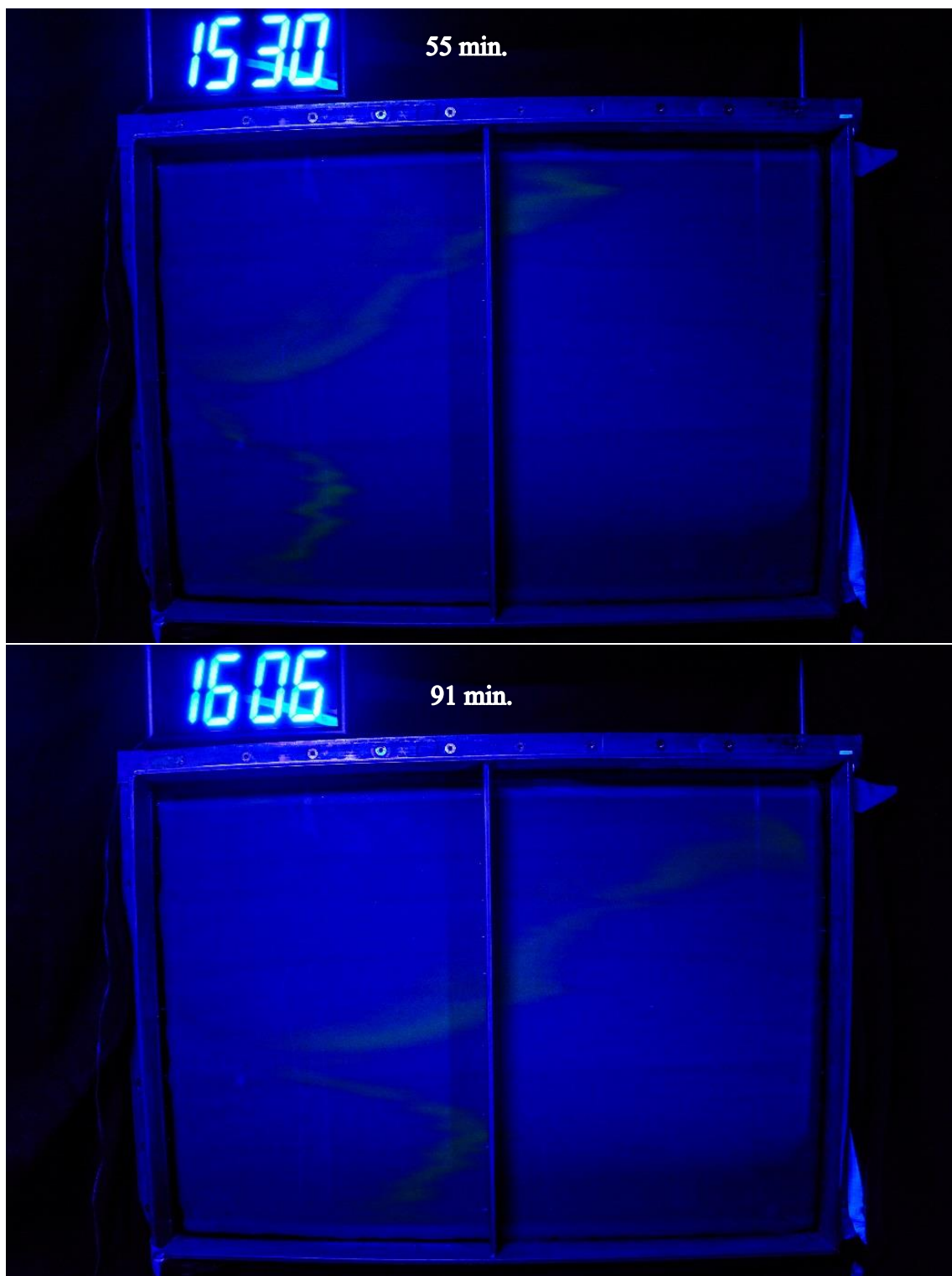


Figure 5.11 dark room

It is possible to observe a time lapse of the visual test in the Figure 5.12.





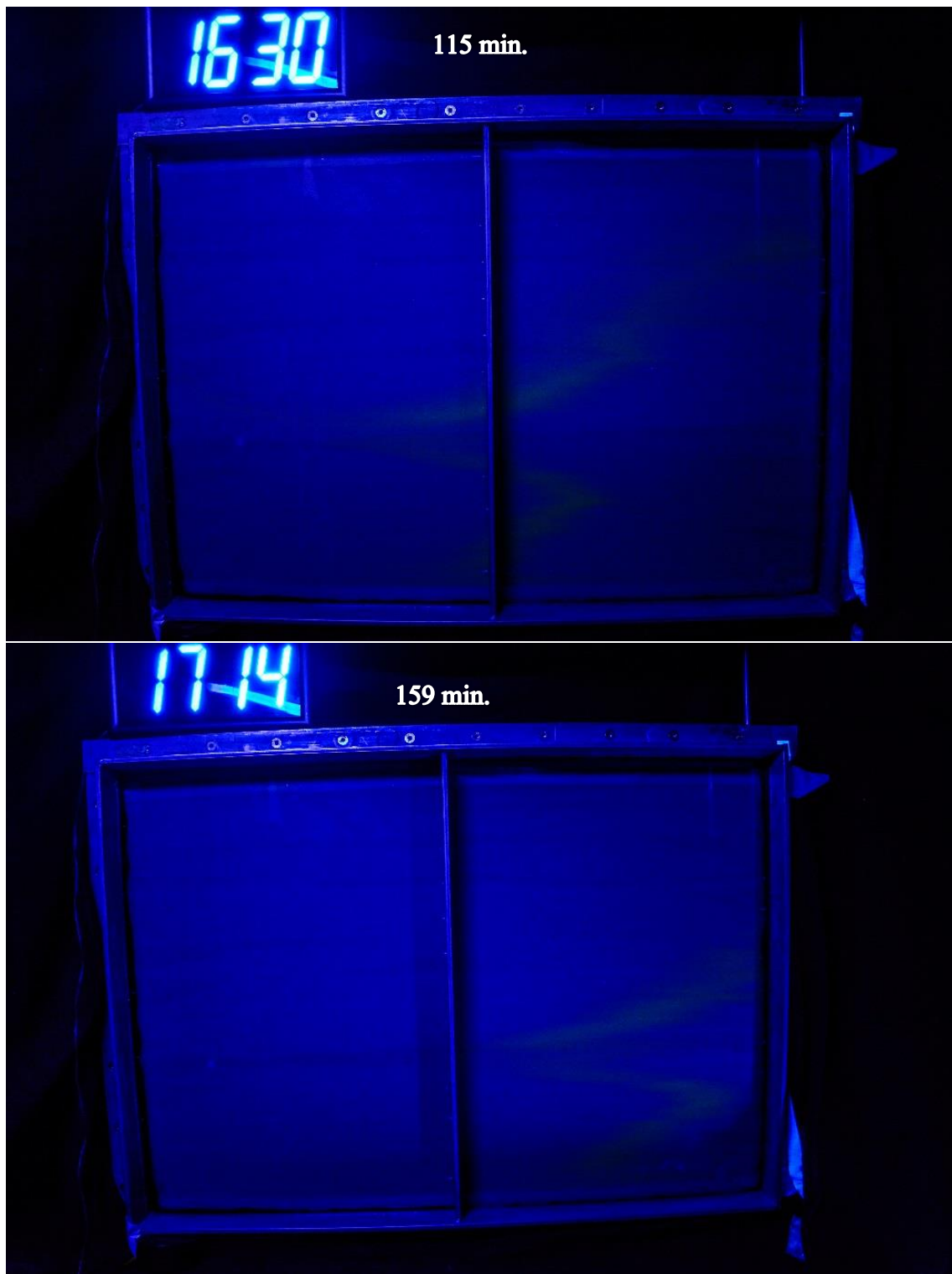


Figure 5.12 Visual test time lapse

The in-flow was increased to 16,3L/h, it is faster than the test with optical fibers due to observe a faster transport.

In Figure 5.12 are shown the different moment of the test:

- The test has started (14:35);
- Arrive of the uranine in the well 6 (16:06);
- Arrive of the uranine in the wells 4 and 5 (17:14).

The visual test gives the same results of the optical fiber test. The uranine arrives first in the top of the flume and after 68 minutes in the other ports simultaneously.

Using the Equation 7, 8 and 9 the porosity was calculated.

Table 5.7 Porosity evaluation with the visual test

Visual test 2g/L uranine	
A (dm ²)	7,68
Q (L/h)	16,3
Vd (m/s)	5,89E-05
τ4 (min)	159
τ5 (min)	159
τ6 (min)	91
τm (min)	136,33
Ve (m/s)	0,00013
n	0,45

It is possible observing that the value of porosity is equal for all the tests.

In the end, it is possible to evaluate the diffusion coefficient of the flume.

Ignoring the colloid deposition due to the uranine features and for the dimension of the flume it is possible to write the equation (3) with the Ogata and Banks where C is the concentration, x the position of the suspension and t the time.

$$\frac{C(x, t)}{C_0} = \frac{1}{2} \left\{ erfc \left[\frac{x - v_e t}{2\sqrt{D_x t}} \right] + exp \left(\frac{v_e x}{D_x} \right) erfc \left[\frac{x - v_e t}{2\sqrt{D_x t}} \right] \right\} \quad (11)$$

To calculate the coefficient of dispersivity (D_x) was taken the average values of the arrival time and of the velocity.

The equation 11 was used for the test with a concentration of 1000µg/L of uranine and the results was:

$$D_x = 0,005 \text{ m}^2/\text{s}$$

6 EXPERIMENT

Concluded the tracer tests, it was possible to start with the experiment planning. The boundary conditions are:

- Inflow: constant flow. Injection of the suspension in a central port located at the back of the flume.

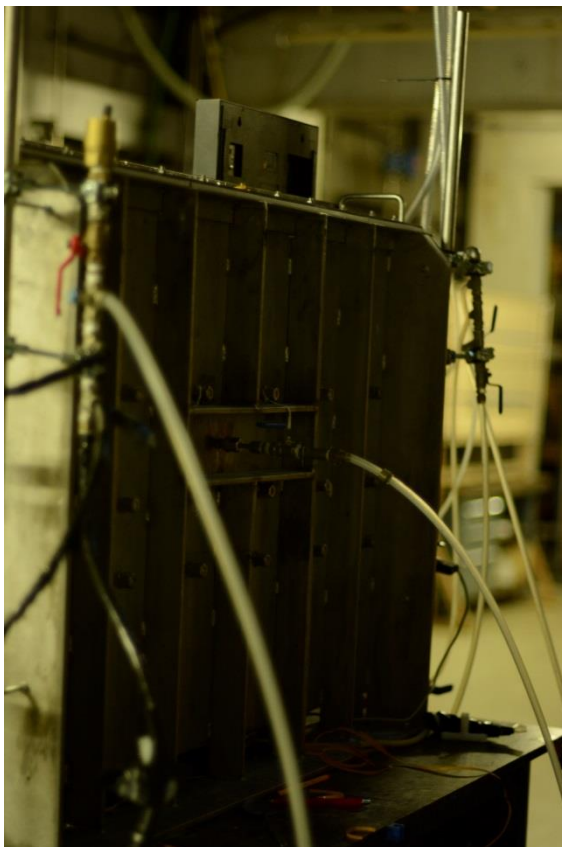


Figure 6.1 Central port located at the back of the flume

- Outflow: constant head for all the wells.

As mentioned in the previous chapters, the purpose is to study the spread of a Carbon Iron, water and, CMC in the flume to evaluate the TOC and the total iron.

Nonetheless, three visual tests were performed to have a qualitative comparison:

- Water solution: injection of water and uranine (1mg/L);
- CMC solution: injection of water, uranine and, CMC (1mg/L of uranine and 2g/L of CMC);
- CI solution: injection of 2g/L of CMC and 20g/L of CI.

The results of the first step were used to plan the injection set-up.

6.1 Injection set-up

The Figure 6.1 shows the project of the injection set-up.

INJECTION SET UP

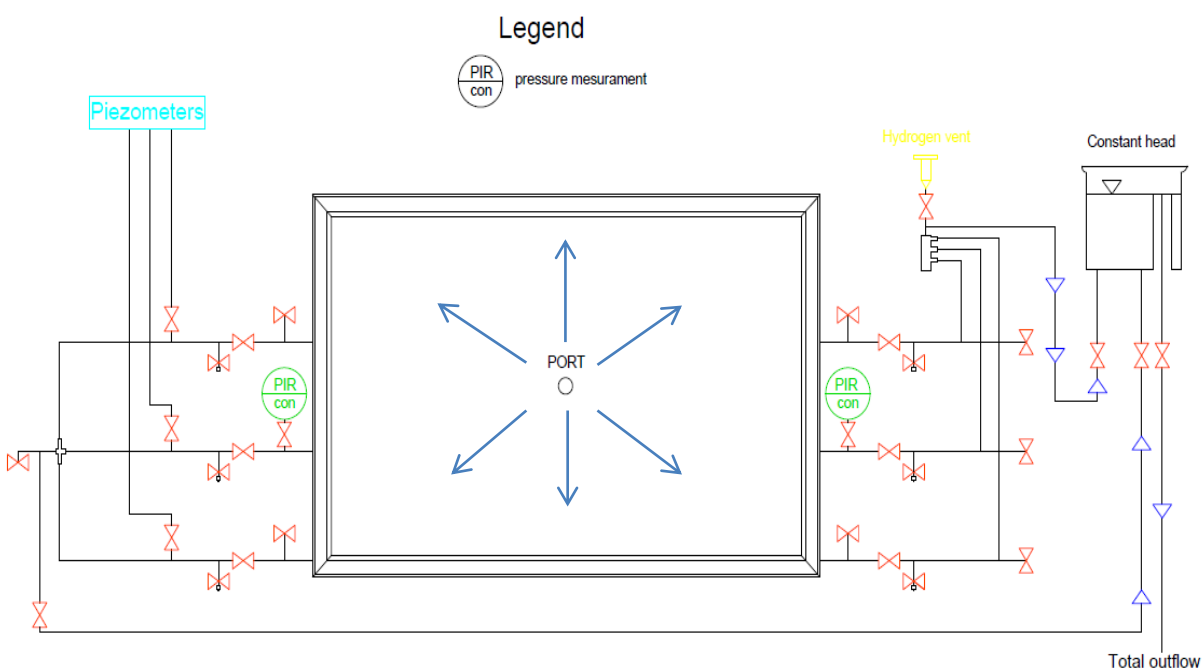


Figure 6.2 Injection set-up, the blue arrows show the flow direction

In this set-up the wells on the left side (W1, W2, and W3 in Figure 5.2) are not connected with the pump (YTRON-Z homogenizer-shear pump) of the base-flow but they are connected to the constant head (as W4, W5 and W6 of the Figure 5.2).

A peristaltic pump (Watson-Marlow 323 Figure 6.3) allows the injection in the central port located in the back of the flume.

The hoses employed in the peristaltic pump are made of VITON® fluoroelastomer with an internal diameter equal to 6,4mm. The velocity of injection is 96 rpm equal to 19,2L/h



Figure 6.3 Peristaltic pump

The test made in 2014 was carried out using four injection doors. To have comparable condition a discharge rate equal to the sum of those injected in the four ports (4,8L/h each) was used here, equal to 19,2L/h.

6.1.1 Suspension preparation

The suspensions with uranine were prepared by means of a mixer.



Figure 6.4 Preparation of uranine suspensions with a mixer (turrax9)

Since it was necessary to limit as much as possible the oxygen content in the Carbon Iron suspension, another mixing methodology was used: a concrete machine, with a re-circulation system to avoid sedimentation phenomena, was used to this purpose. Moreover, a lid wood was added on the top of the concrete machine in order to fill the mixing area with the inert gas Argon.

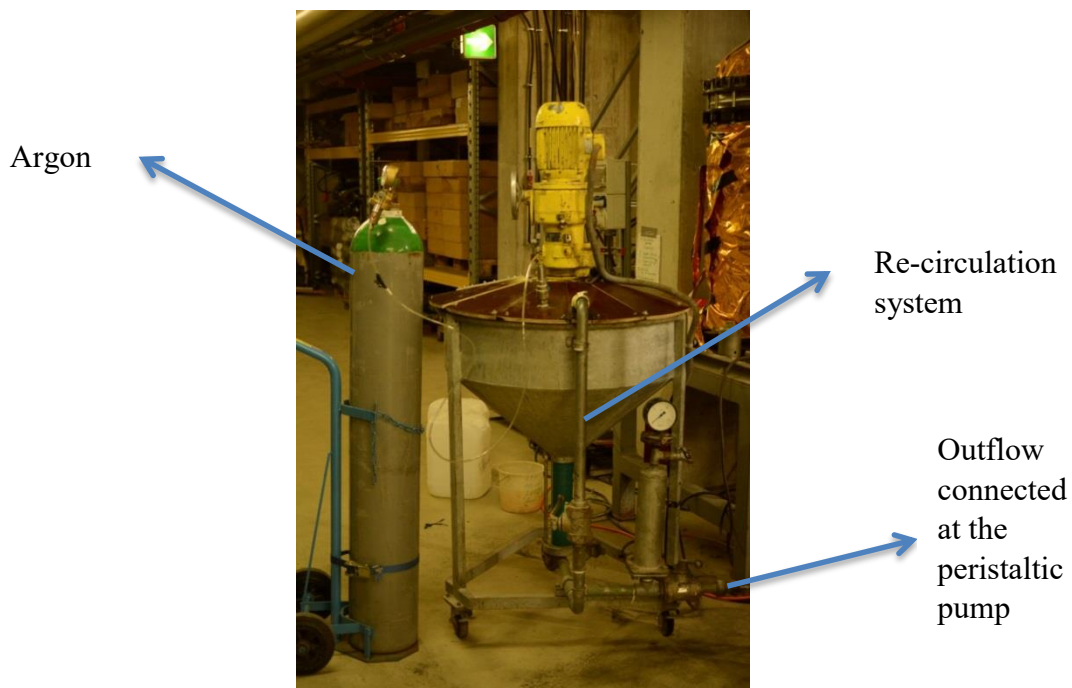


Figure 6.5 Concrete machine used to prepare the CI suspension

6. EXPERIMENT

The oxygen concentration and the temperature of the suspension were checked with by means of HQd fiel case.



Figure 6.6 HQd fiel case: oxygen and temperature meter

The values of oxygen concentration and temperature are shown in the Table 6.1.

Table 6.1 Values of oxygen concentration and temperature during the mixing phase

Mixing time	Oxygen Con.	Temperature
min.	mg/L	°C
30	0,21	23
60	0,17	23,3
90	0,13	24

6.2 Injection

During the injection, the base flow was stopped to focus just on the injection.

The three different injections have some common points:

- Volume injected equal to 8,1705L;
- Sample collection during the experiment to control that the injected suspension remained entirely within the flume. The samples were taken by the outflow of the constant head;
- Study of the spread area with the retention factor.

The spread area is evaluated visually how the external perimeter of the solutions and of the suspension.

The spread area was controlled with the use of Autocad and the same fixed focal-length lens of 35mm was used to avoid image distortion problems. The procedure was inserting the pictures on Autocad in the correct scale and after the areas were obtained by drawing polylines because Autocad returned the value of interest.

Using the following equation it was possible to relate the pore volumes occupied with the spreading area.

$$PV = \frac{Q \cdot t}{PV_{tot}} \quad (12)$$

In the Equation 12 the different values are:

- PV: pore volume occupy;
- Q: injection flow due to the peristaltic pump;
- t: time of the injection;
- PV_{tot}: total pore volume.

6.2.1 Water and uranine injection

The first injection was a solution of uranine in degassed water, with a concentration of 1g/L of the tracer.

Pressure measurements were taken connecting the tube in the central port with a piezometer.

During the injection, water samples were taken from the outflow to check that the tracer was not reaching the boundaries of the system.

The Figure 6.8 shows the result of the injection.

Pressure measure of water and uranine injection

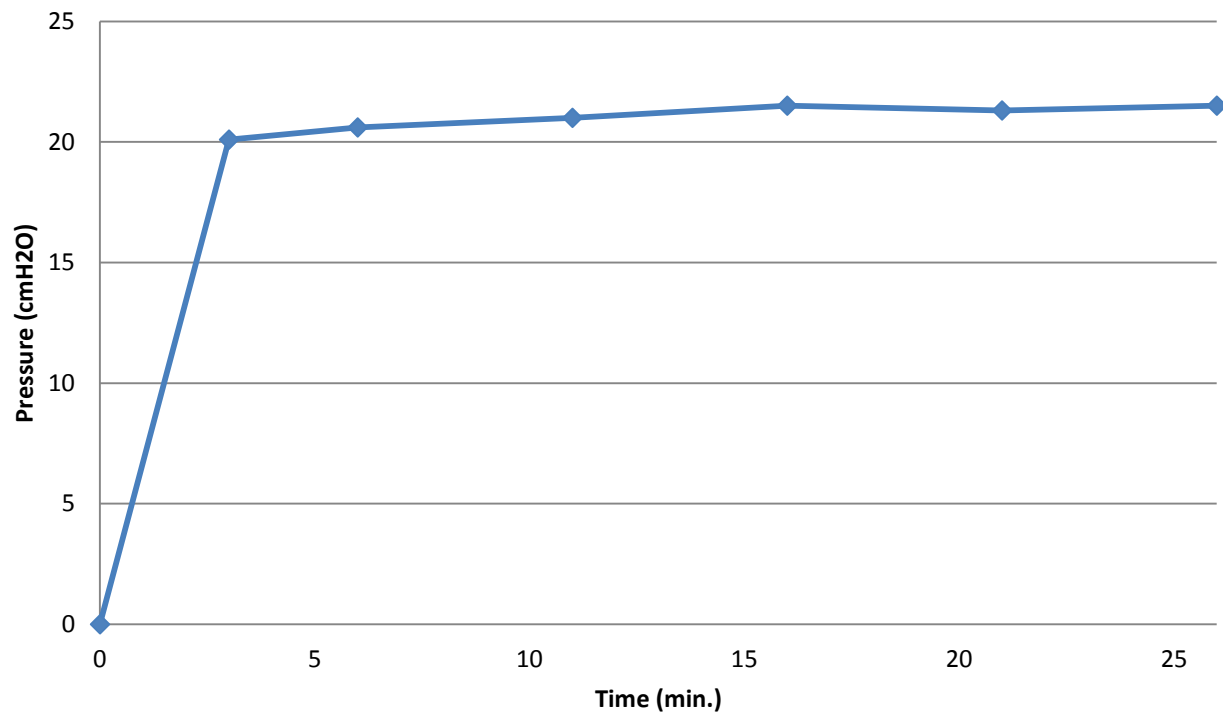


Figure 6.7 Pressure measure (Δh) of water and uranine injection

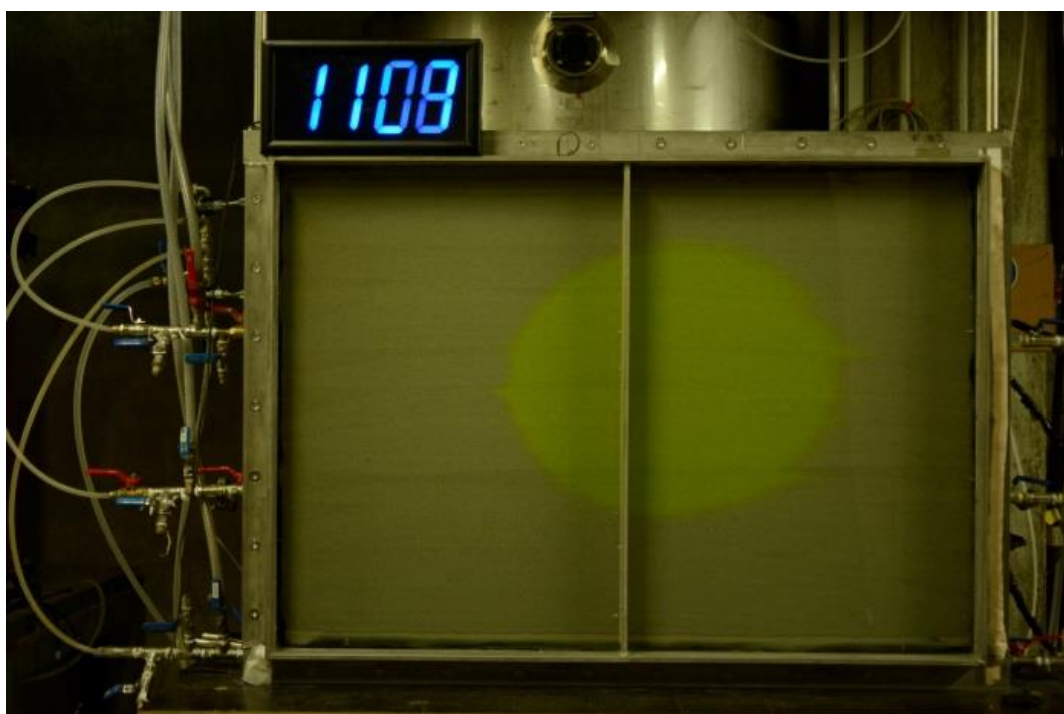


Figure 6.8 Uranine and water injection after 24 minutes

6. EXPERIMENT

It is possible to notice that the final area is bigger in the right than the left side due to a difference of 10mbar of pressure between the two outlets, resulting in a limited residual base flow. The pressure measurements showed an average pressure respectively of 62mbar 72mbar. This pressure difference occurs also in the next tests.

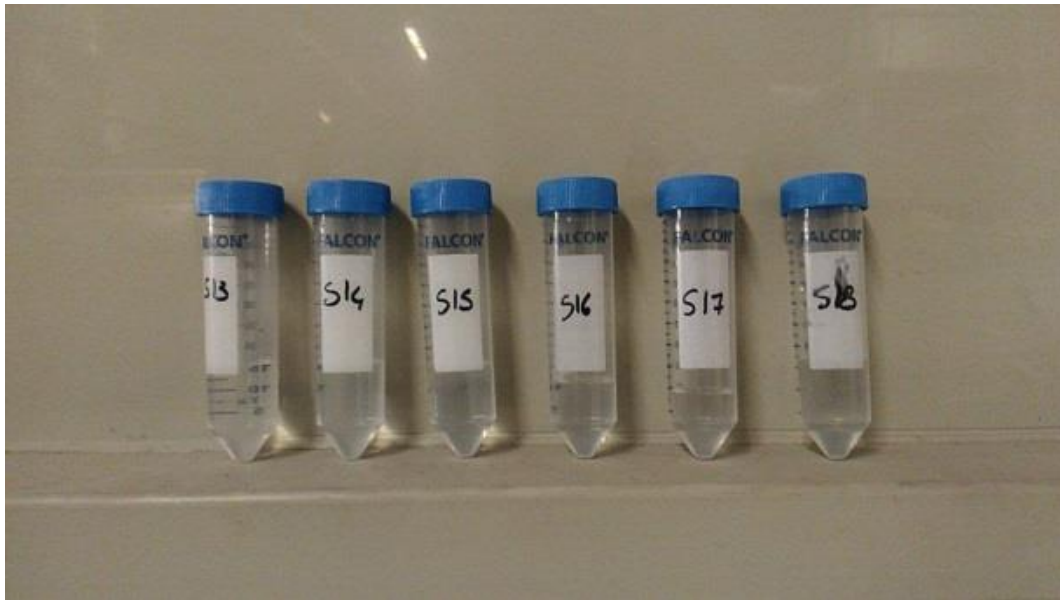


Figure 6.9 Outflow samples: uranine solution

In Figure 6.9 is clear that there is not uranine in the samples, this means that all the solution remains in the flume.

The last figure shows how the pore volume is occupied in the flume, the time relation is included in the graph thanks to the Equation 12.

6. EXPERIMENT

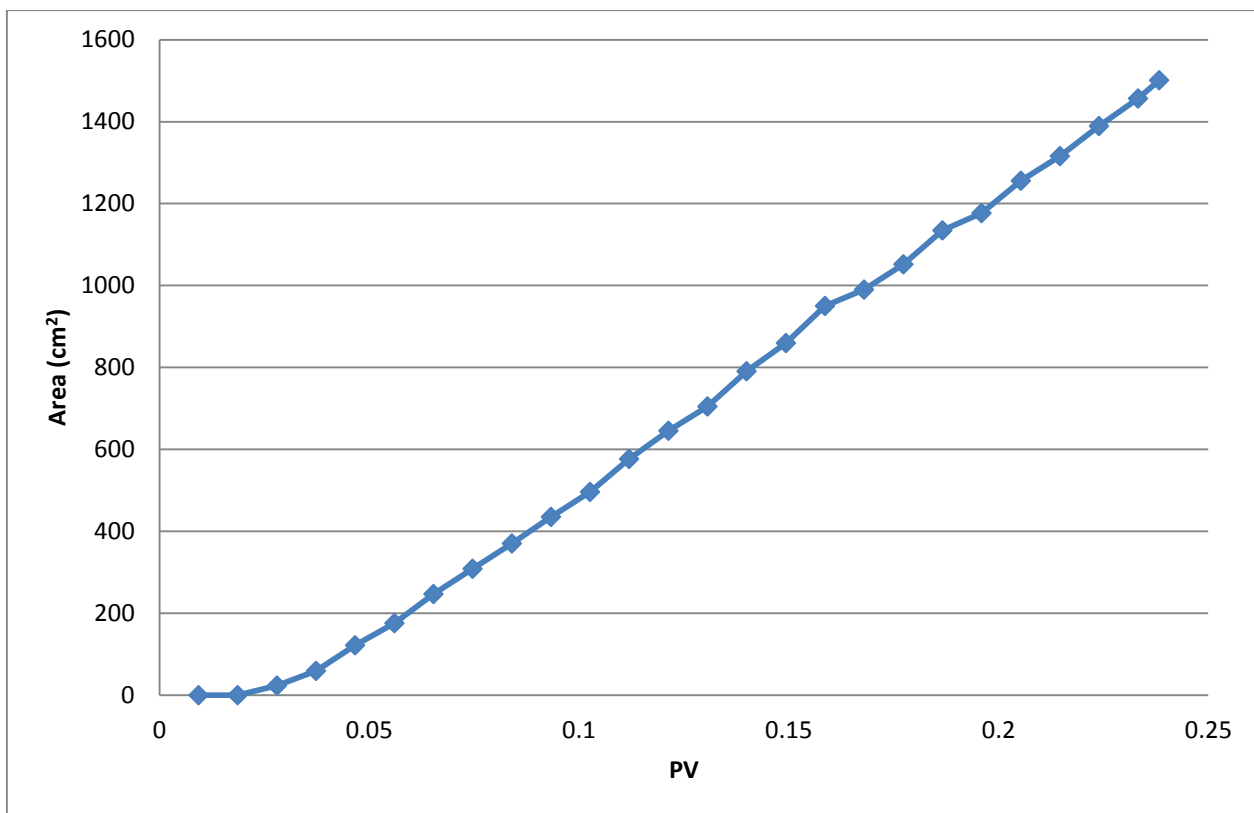


Figure 6.10 Spread with injection of water and uranine (24% of PV fill up)

6.2.2 Water, uranine and CMC injection

The solution in this test is composed of degassed water, 1g/L of uranine and 2g/L of CMC.

The injection follows the same procedure of the Water and uranine injection.

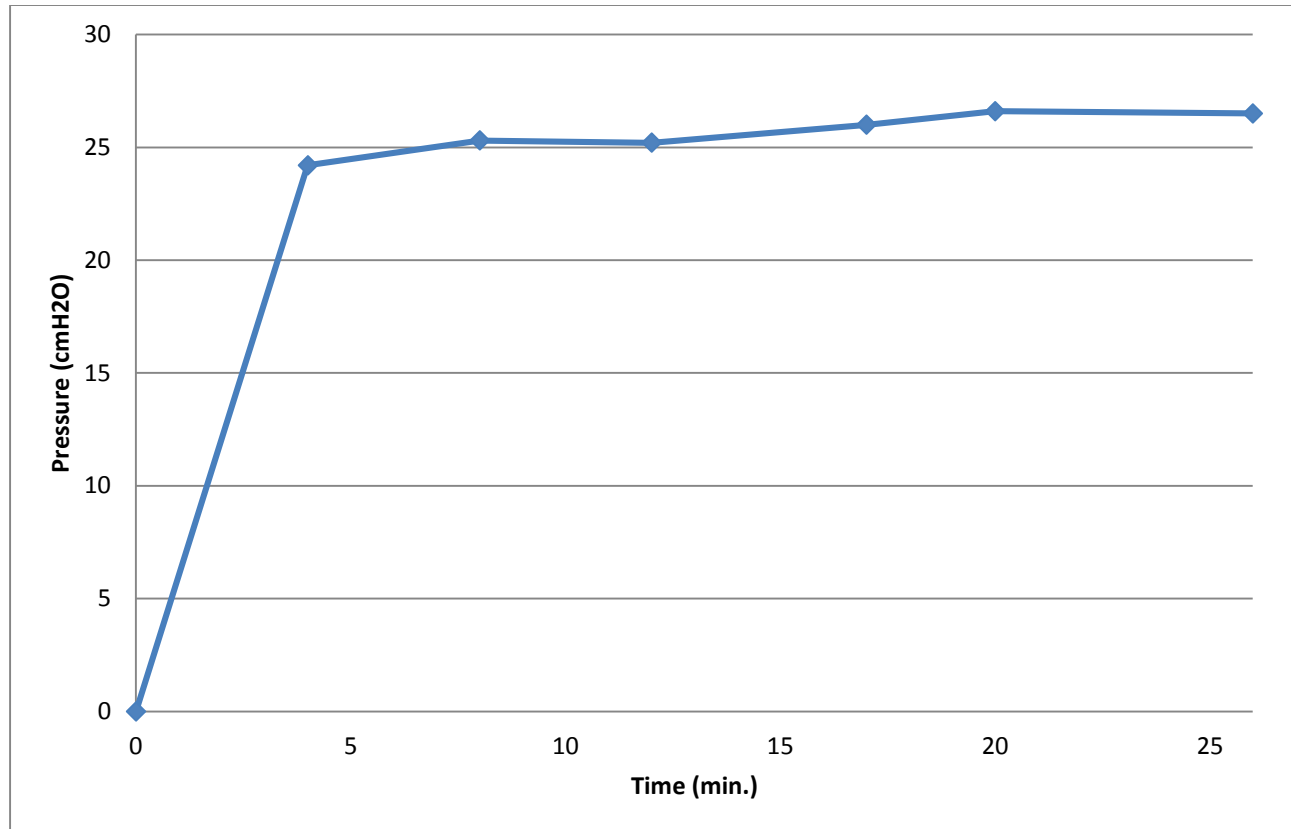


Figure 6.11 Pressure measure (Δh) of water, uranine and CMC injection

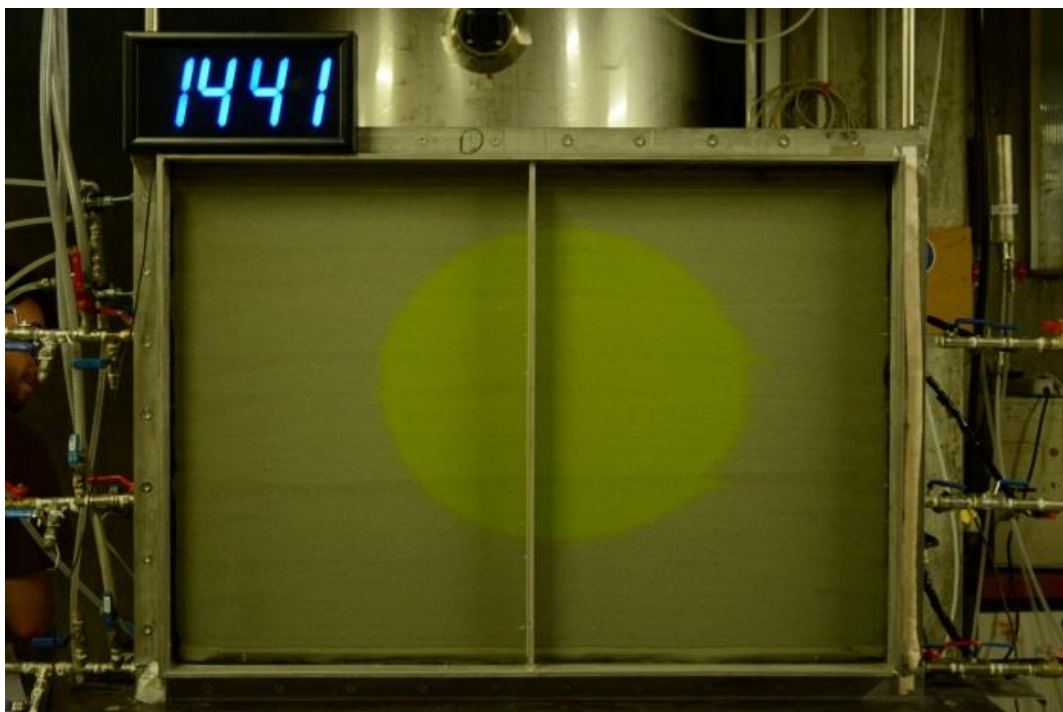


Figure 6.12 Water, uranine and CMC injection after 24 minutes

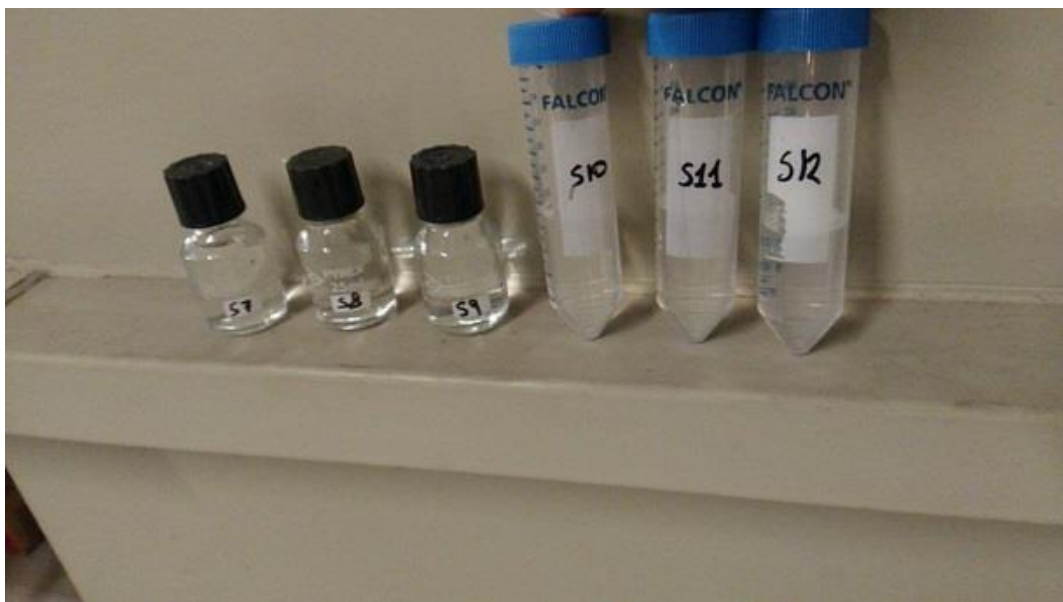


Figure 6.13 Outflow samples: CMC solution

Also in this injection, the outflow is water without uranine, this means that the CMC remained inside the flume.

With the equation 12 we obtained the Figure 6.14.

Spread with injection of water uranine and CMC

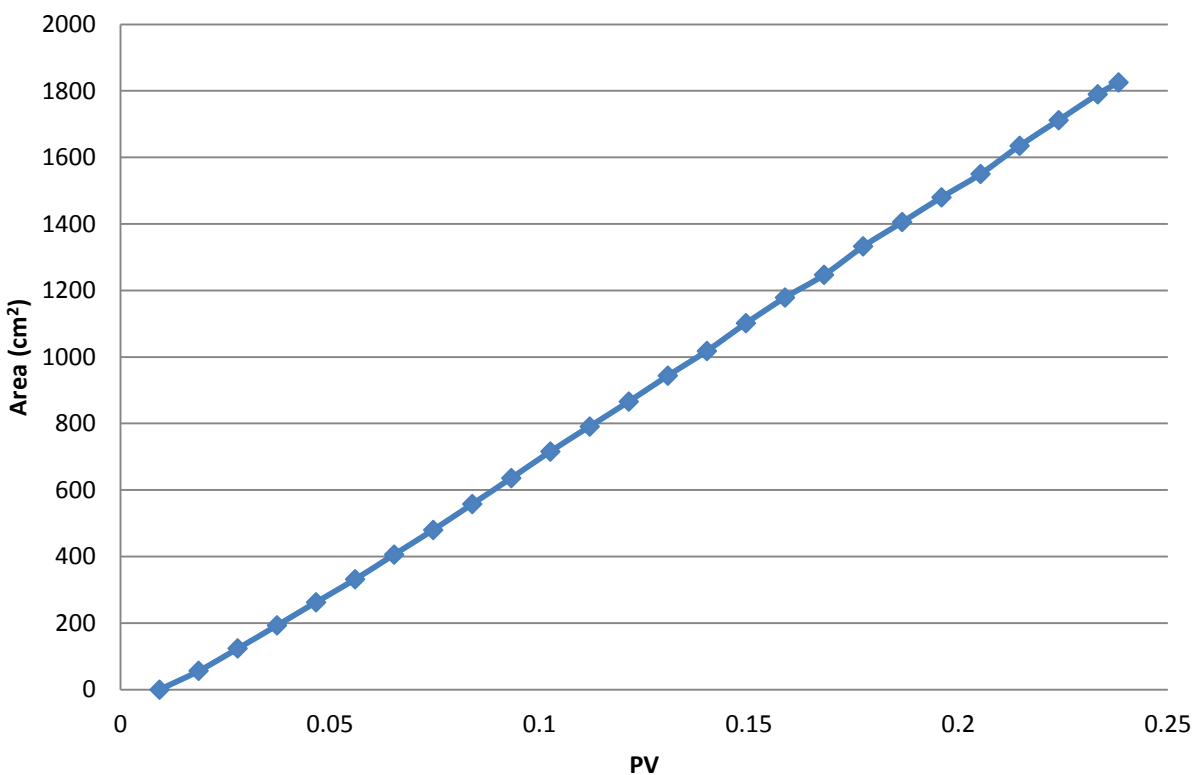


Figure 6.14 Spread with injection of water uranine and CMC

6.2.3 CI and CMC injection

The last injection was a 20g/L Carbon Iron and 2g/L CMC suspension.

Pressure measurements for this tests are not complete because of technical issues. During this test, the pressure became quickly higher than the maximum water height recordable by the equipment (400 cmH₂O). In a second stage of the test, the piezometer was replaced by a pressure gauge with a maximum recordable value equal to 1bar, which was overcome quickly causing the breakage of the instrument.

Nevertheless, the experiment was concluded and all the Carbon Iron remained inside the flume, as it is possible to see in the Figure 6.15.

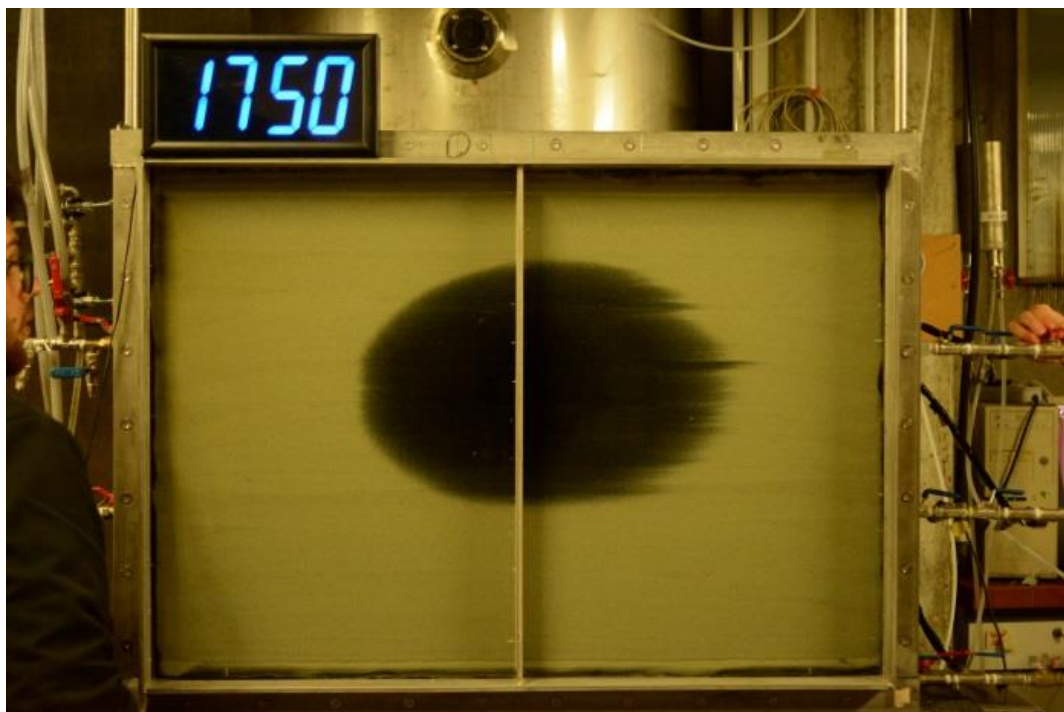


Figure 6.15 CI and CMC injection



Figure 6.16 Outflow samples: CI and CMC suspension

As in the previous chapters, the equation 12 was used to obtain the graph in the Figure 6.17.

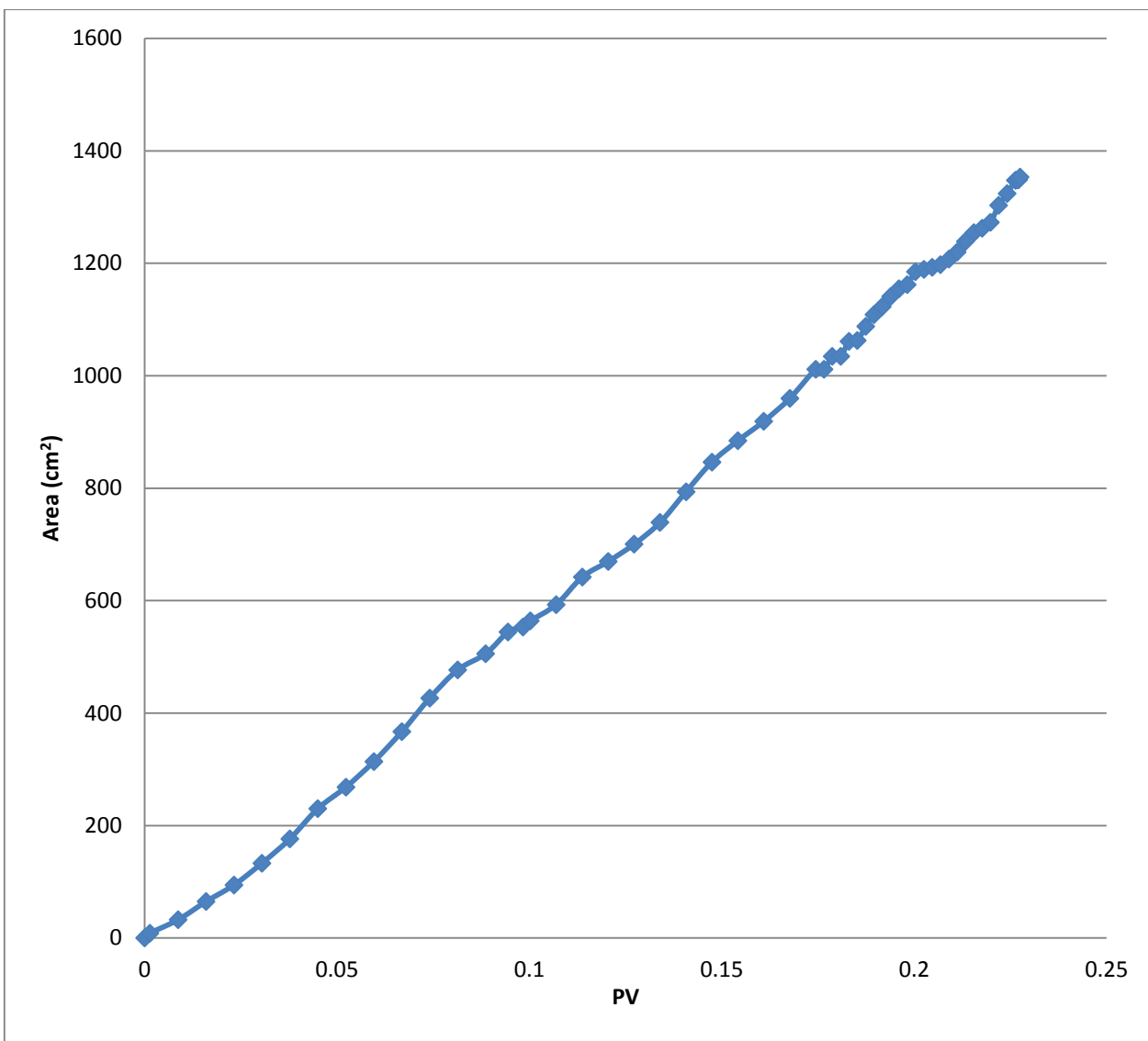


Figure 6.17 Spread with injection of CI and CMC

In the Figure 6.17 is possible to observe that the graph shows some anomalies.

The areas where the points are closer to each other represent a little area increase in a bigger fraction in the time.

Moreover, it is possible to notice that the final area is bigger in the right than the left side because of a difference of 10mbar of pressure between the two outlets. The pressure measurements showed an average pressure respectively of 62mbar 72mbar.

6.2.4 Comparison of the result

The different tests were compared with the retention factor equation:

$$R = \frac{A_{spr.} \cdot B \cdot n}{V_{inj.}} \cdot \alpha \quad (13)$$

Whose parameters are:

- R: retention factor;
- $A_{spr.}$: solution expansion area;
- B: thickness of the flume;
- n: porosity of the flume;
- $V_{inj.}$: volume injected in the tests;
- α : correction coefficient.

The water and uranine suspension must have a retention factor equal to 1 because the uranine do not change the water features. Consequently, it is possible to evaluate a correction coefficient with the relation between the R calculated and the R imposed. This correction coefficient (α) was used to evaluate the final retention factor also for the CMC and uranine solution and for the CI and CMC suspension.

$$\alpha = \frac{1}{R_{water+uranine}} = 1,09$$

Table 6.2 Retention factor for the different suspensions

	V_{inj}	B	A_{spread}	n	R
	L	dm	dm²	-	-
uranine solution	8,1705	1,2	13,89	0,45	1
CMC and uranine solution	8,1705	1,2	17,12	0,45	1,23
CI and CMC suspension	8,1705	1,2	13,53	0,45	0,97

Table 6.2 gives this result:

$$R_{CI} < R_{uranine+water} < R_{CMC+uranine}$$

In Figure 6.18 it is possible to observe how the pore volume was occupied from the different suspensions. It is important to say that the CI line changes its aspect because along the test it is possible divided two moment: the first one with a perfect operation and the second one, with the reduction of the outflow value.

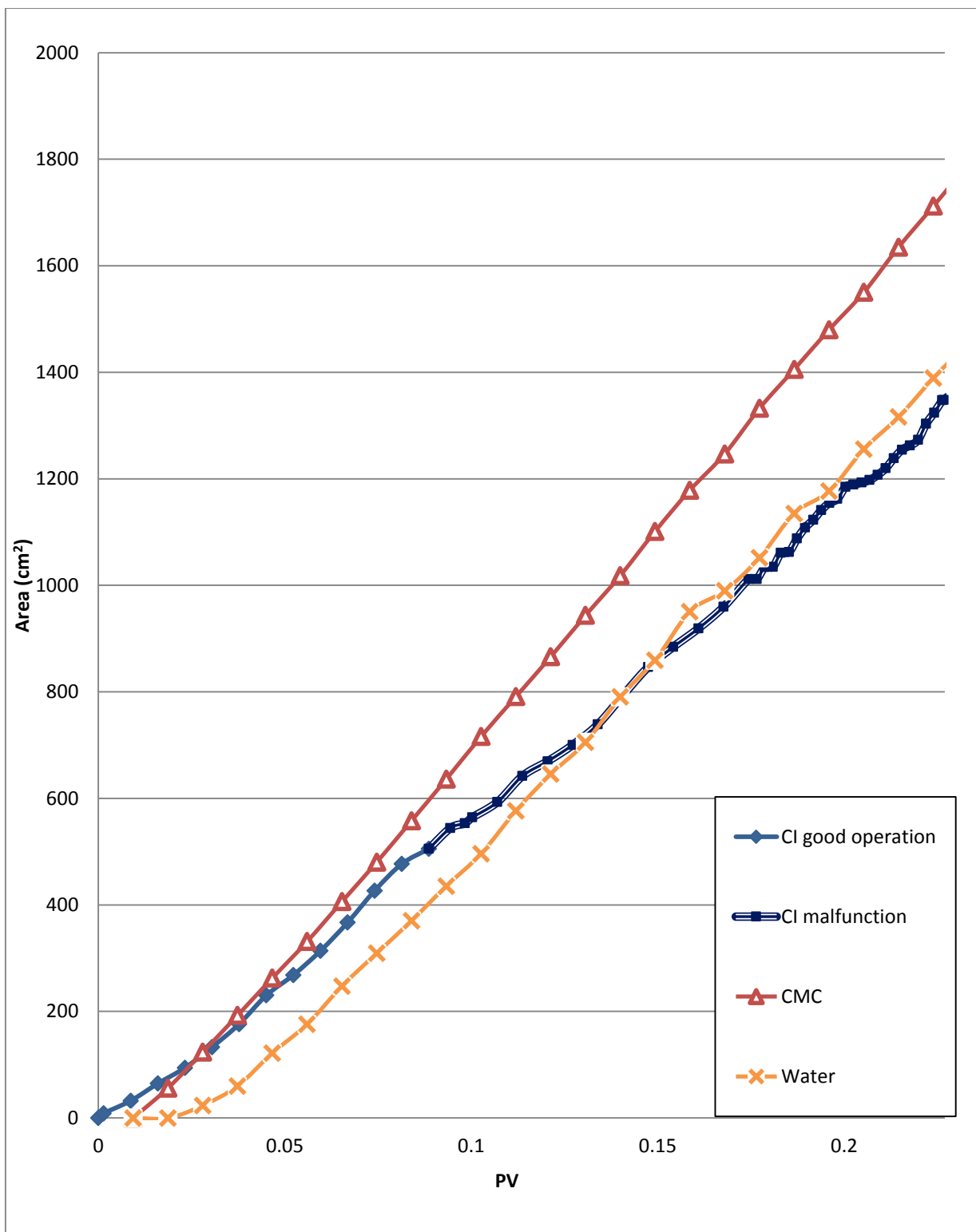


Figure 6.18 Spread areas of the three different suspensions

6. EXPERIMENT

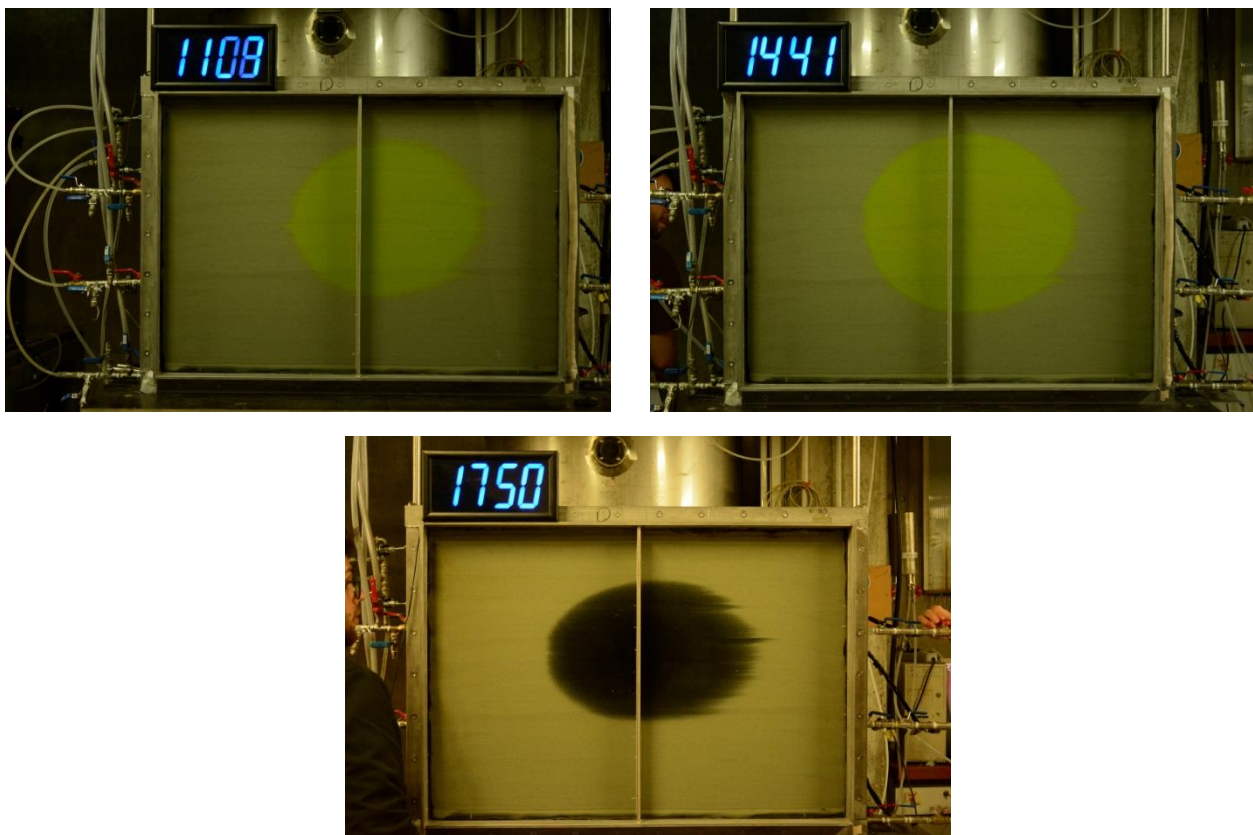


Figure 6.19 From left to right: final area occupied by the water and uranine; CMC suspension; CI suspension

The Figure 6.18 shows that the solutions (uranine and uranine + CMC) are perfectly comparable, but it is not possible for the CI suspension where there are two different trends, the first one of good operation and the second one of malfunction.

The first things that are quite obviously are the dimension of the different areas for the two solutions.

How already said in chapter 4, the diffusion coefficient (D) of a liquid substance is connected with the temperature and the viscosity through the Stokes-Einstein equation and it is known the different diffusion coefficient for the different solutions:

$$D = \frac{kT}{6\pi\eta r} \quad (14)$$

$$D_{CMC} < D_{water}$$

Where:

- k is the Boltzman constant;
- η is the solvent viscosity;
- r is the radius of the diffusing particles;

6. EXPERIMENT

- T is the temperature.

Comparing the CMC and water suspensions diffusion in the Figure 6.19 is possible to notice that a higher value of the diffusion coefficient does not mean a bigger spread.

In the Figure 6.20 is represented the concentration compared to the distance traveled in a specific time for a generic injection test, the point $x = 0$ is the injection point.

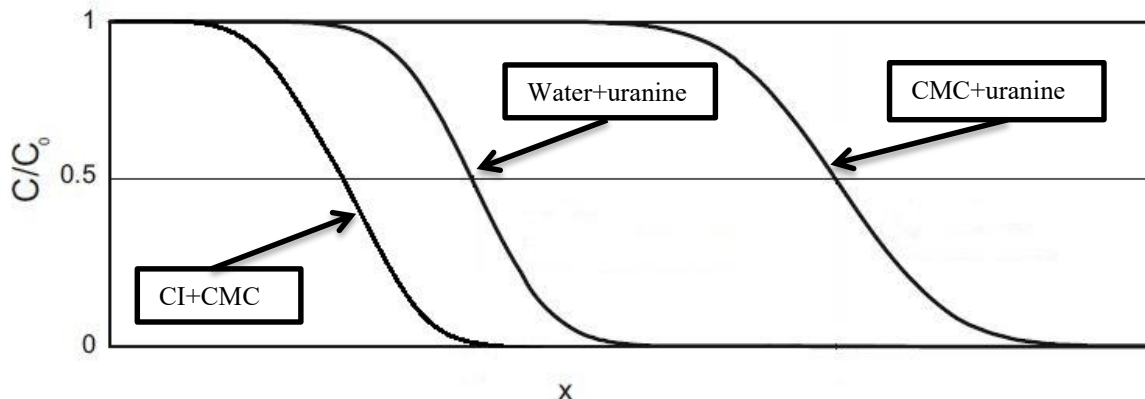


Figure 6.20 Breakthrough curves for different suspension and for the solution modified from (Di Molfetta & Sethi, 2012)

Therefore, the Figure 6.19 shows that the uranine solution spread is between the CMC solution and the CI suspension.

Obviously, CI suspension is slower than uranine solution ($R_{CI} < R_{water+uranine}$) because the suspension particles tie to the surface of the pore in the flume.

However, this not happens for the CMC solution that has a bigger spread in the same time of the injection ($R_{water+uranine} < R_{CMC+uranine}$) because the CMC is a polymer. The polymer chains are long agglomeration of molecules and they tend to do entanglements. These agglomerations of molecules move together through the bigger pores of the flume avoiding the smaller one. Consequently, the final visible spread area for the CMC solution is the largest between the others.

In the end, to validate further that the CMC solution has higher values of viscosity of the water and uranine, the pressure of the two experiments can be compared thanks to the Darcy's law:

$$Q = \frac{kA}{\eta} \left(\frac{\partial h}{\partial x} \right) \quad (15)$$

In the (15) the parameters are:

- Q: flow in the tube;
- A: cross section in the tube;
- η : viscosity;
- k: permeability;

6. EXPERIMENT

- $\partial h/\partial x$: pressure variation.

In the injection experiment was used the same flow for the solutions consequently, the results of the equation 15 must be the same. Then, to have equal flow values if the pressure increases in an experiment also the viscosity must increase to keep the same Q values. So, the pressure of injection will be higher in the solution with a bigger viscosity. In the end, the results achieved in chapter 4 are the same as the comparison between pressures and it is observable in the Figure 6.21.

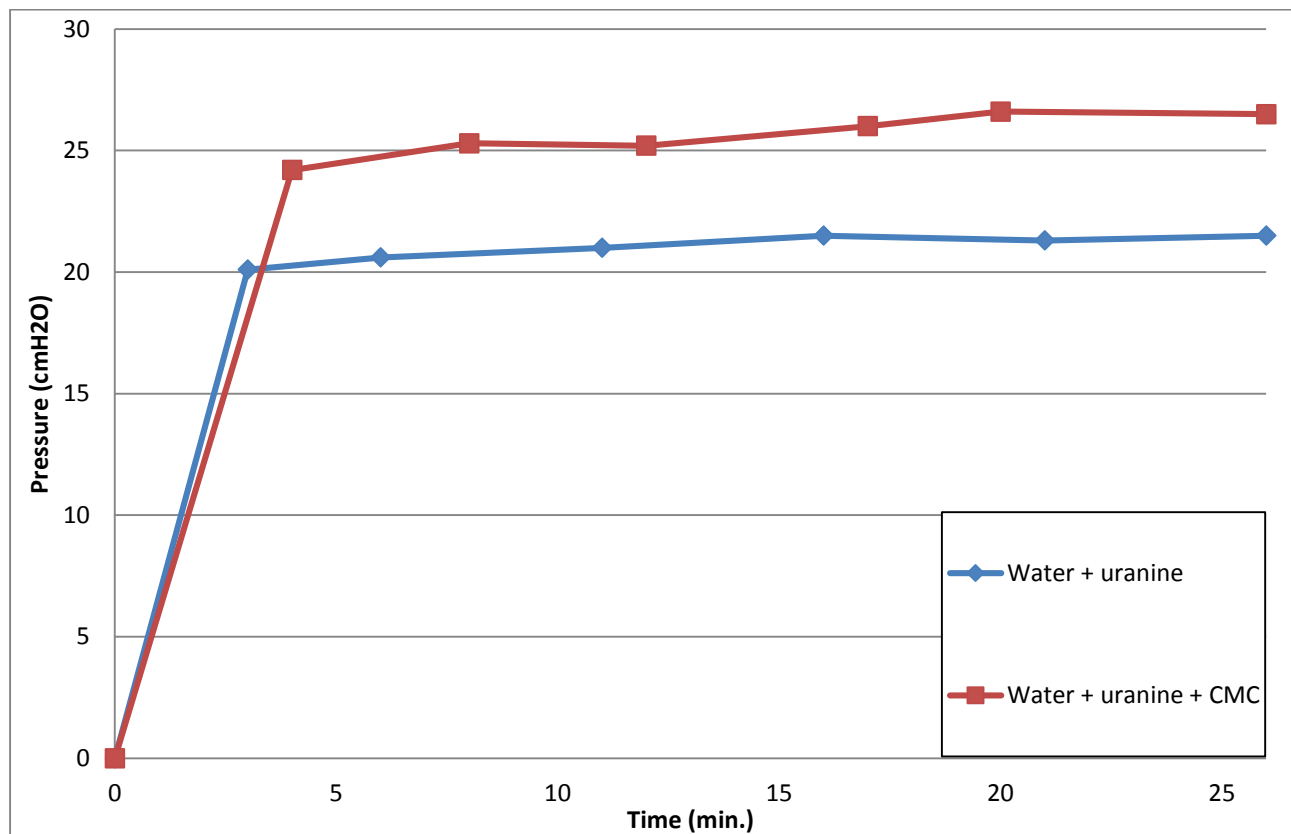


Figure 6.21 Pressure measurements (Δh) during the injection of the two solutions

In the end, it is possible to say that the pressure differences between the left and the right side of the flume (62mbar and 72mbar respectively) bring two different Darcy velocity in the two different sides. Consequently, the flow change in the flume too.

In Table 6.3 the two different Darcy velocity were evaluated thanks to the equation 10 and also to the pressure measurements.

6. EXPERIMENT

Table 6.3 Evaluation of the Darcy velocity in the two side of the flume: P is the pressure, L is half length of the flume, i is the hydraulic gradient, k is the permeability coefficient and vd is the Darcy velocity

water + uranine								
K	Average Pressure in the injection point	P _{left side}	P _{right side}	L	i _{left side}	i _{right side}	vd _{left}	vd _{right}
m/s	cmH20	cmH20	cmH20	cm	-	-	m/s	m/s
8.6E-05	108	73.42	63.22	50	0.69	0.89	6E-05	7.7E-05
water + uranine + CMC								
K	Average Pressure in the injection point	P _{left side}	P _{right side}	L	i _{left side}	i _{right side}	vd _{left}	vd _{right}
m/s	cmH20	cmH20	cmH20	cm	-	-	m/s	m/s
8.6E-05	112.65	73.42	63.22	50	0.78	0.99	7E-05	8.5E-05

The results show that the velocity in the right side is higher than the left side of the flume consequently, also the flow has the same behavior.

6.3 Sample collection

After the injection of Carbon Iron solution was necessary to drain the flume in order to preserve the particles distribution and the base-flow was not start up again.

During drainage, a partial movement of the suspension to the right side of the flume was observed, since the inlet drain was partly occluded during the test.

This phenomenon is observable in Figure 6.22.

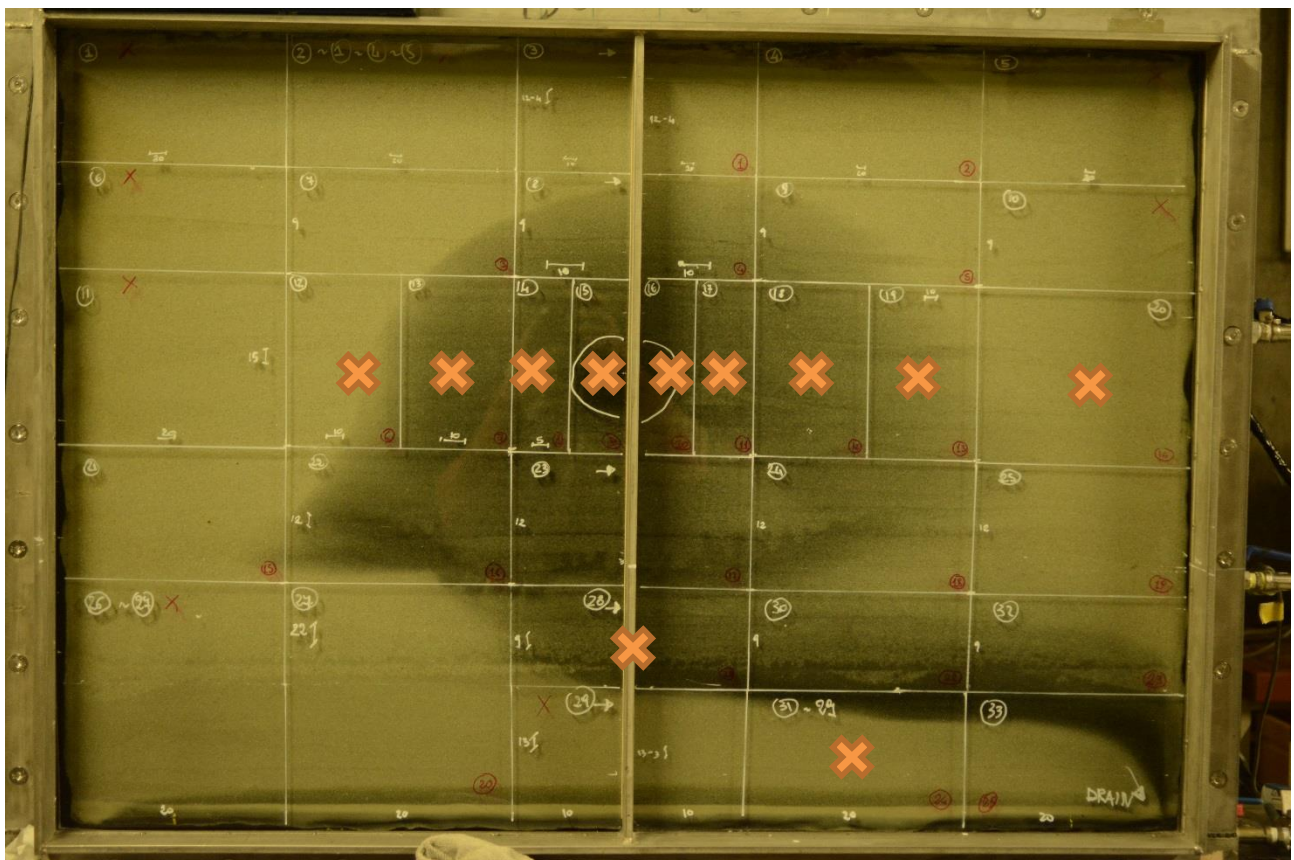


Figure 6.22 Draining of the flume, the orange x shows which samples were analyzed

Since the asymmetrical drainage caused a partial redistribution of the particles, sand samples to be analyzed for retained CI were collected along a horizontal line situated in the middle of the flume, to observe if the concentration of total iron was in acceptable concentration that is higher values in the center of the line and lower in the areas far from this central point.

Two additional samples were also collected in the lower part of the flume to quantify the particle re-distribution caused by the drainage.

Each sample was analyzed for total iron and total organic carbon concentration. A representative area was associated to each sample.

The measurement of the total iron was determined according to ISO 6332-1988, DIN 38406 E1-1:

1. The samples were weighed completely;
2. HCl was added;

6. EXPERIMENT

3. The samples were left 2 days to cool down;
4. Beaker glasses and folded filters were weighing;
5. The samples were filtered through weighed pleated filter;
6. The samples were transferred loss-free into the pleated filter;
7. The soils were washed with 1L of water;
8. Fold filter was dried in a beaker for 3 days in a drying cabinet at 105°C;
9. Samples were diluted individually in ultrapure water;
10. A defined volume was taken from the dilution and pipetted into a 10mL flask;
11. 0.5mL of ammonium acetate glacial acetic acid solution, 0.2mL of hydroxylammonium chloride and 0.2mL of 1,10-phenanthroline were added;
12. It was waiting 20 minutes for the reaction time;
13. The total iron measurements were taken with a photometer at 510nm.

For the TOC the procedure was:

1. The samples were dried in a cabinet at 105°C;
2. The samples were all ground (380rpm for 20 minutes) with agate ball mill;
3. The samples were individually weighed and measured in TOC crucibles with IR detector.
With a temperature ramp it was calculated only the TC, thus the CMC and Activated carbon were possible.

The used devices were:

- TC: TOC from SHIMADZU, TOC-5000A + SSM;
- Total iron: Photometer by Perkin Elmer Lambda 14, cuvette quartz glass, 1cm

6.3.1 Total Iron values

The total mass of CI injected can be calculated via a mass balance.

Knowing that:

- The injected volume is equal to 8,1705L;
- The Carbon Iron is composed for 22,3% of total iron (*Appendix 2*);
- The suspension is 20g/L of CI.

It is possible to write:

$$Fe_{tot, max} = C_{CI} \cdot V_{inj} \cdot 22,3\% = 36,16g$$

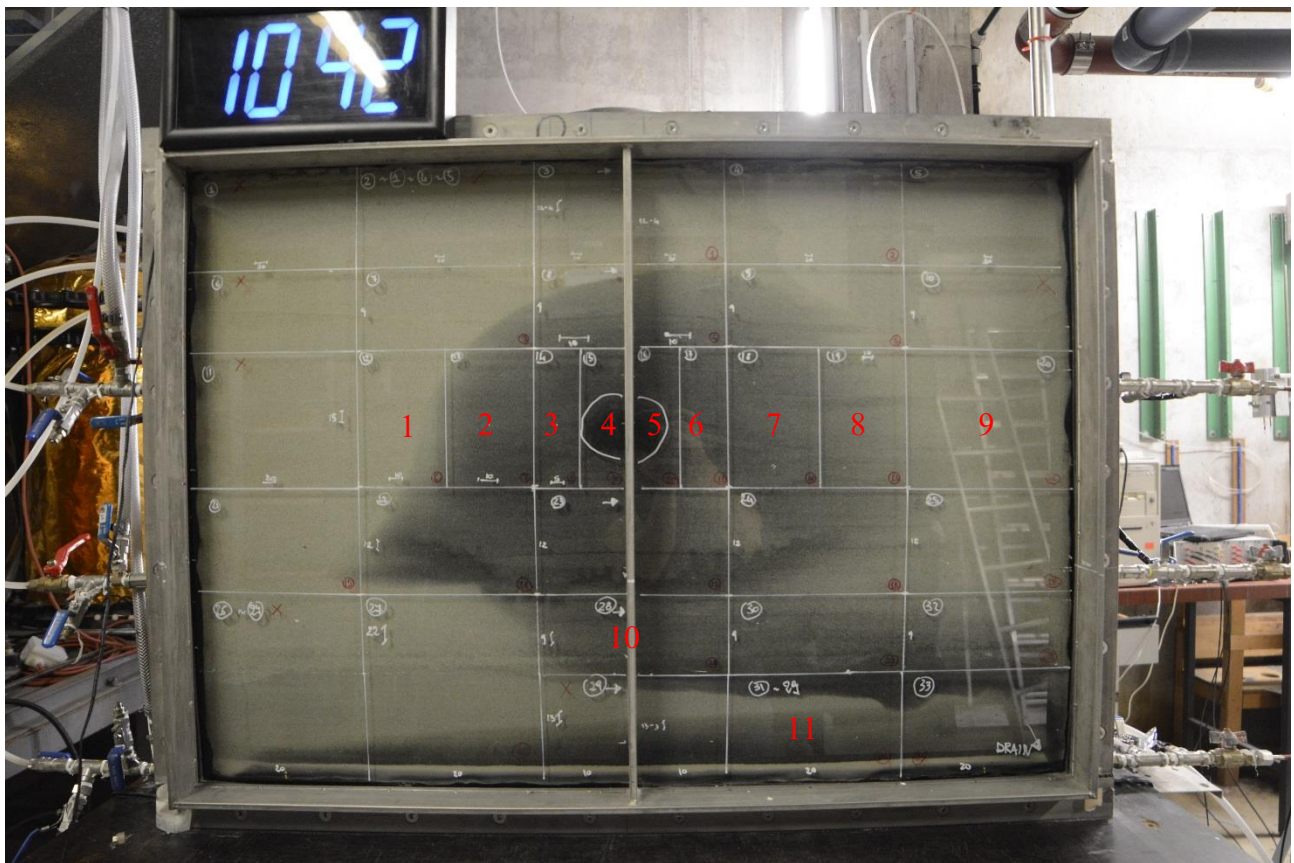


Figure 6.23 Numeration of the analyzed samples

Knowing the final area of the CI spread it is possible to estimate the iron concentration expected:

$$C_{Fetot} = \frac{Fe_{tot,max}}{n \cdot V_{spread} \cdot \rho_{bulk}} = 3,08g/Kg$$

In almost all the areas the concentration of iron is higher than this value, for this reason, it is possible to considerate the total iron values correct.

The total iron concentrations are reported in the Table 6.4.

6. EXPERIMENT

Table 6.4 Concentration and absolute values in the flume samples

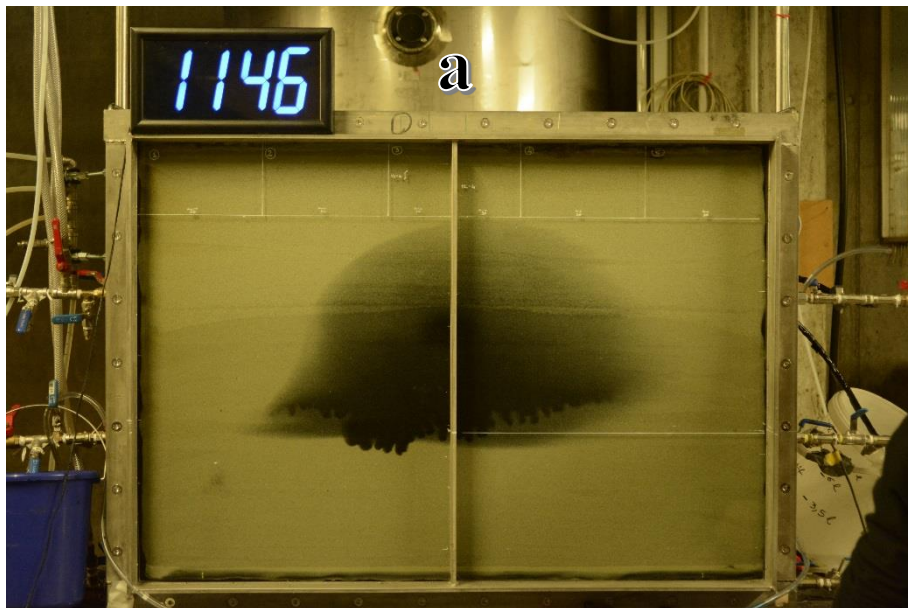
N° Sample	Concentration (g/Kg)	Iron mass in the collect sample (g)
1	0,19	0,008
2	9,25	0,320
3	89,33	2,988
4	87,52	2,941
5	107,61	4,559
6	15,65	0,947
7	1,28	0,085
8	0,39	0,023
9	0,25	0,014
10	0,04	0,002
11	0,03	0,003

As expected, the concentration of total iron is higher in the areas near the injection well and it decreases with the distance.

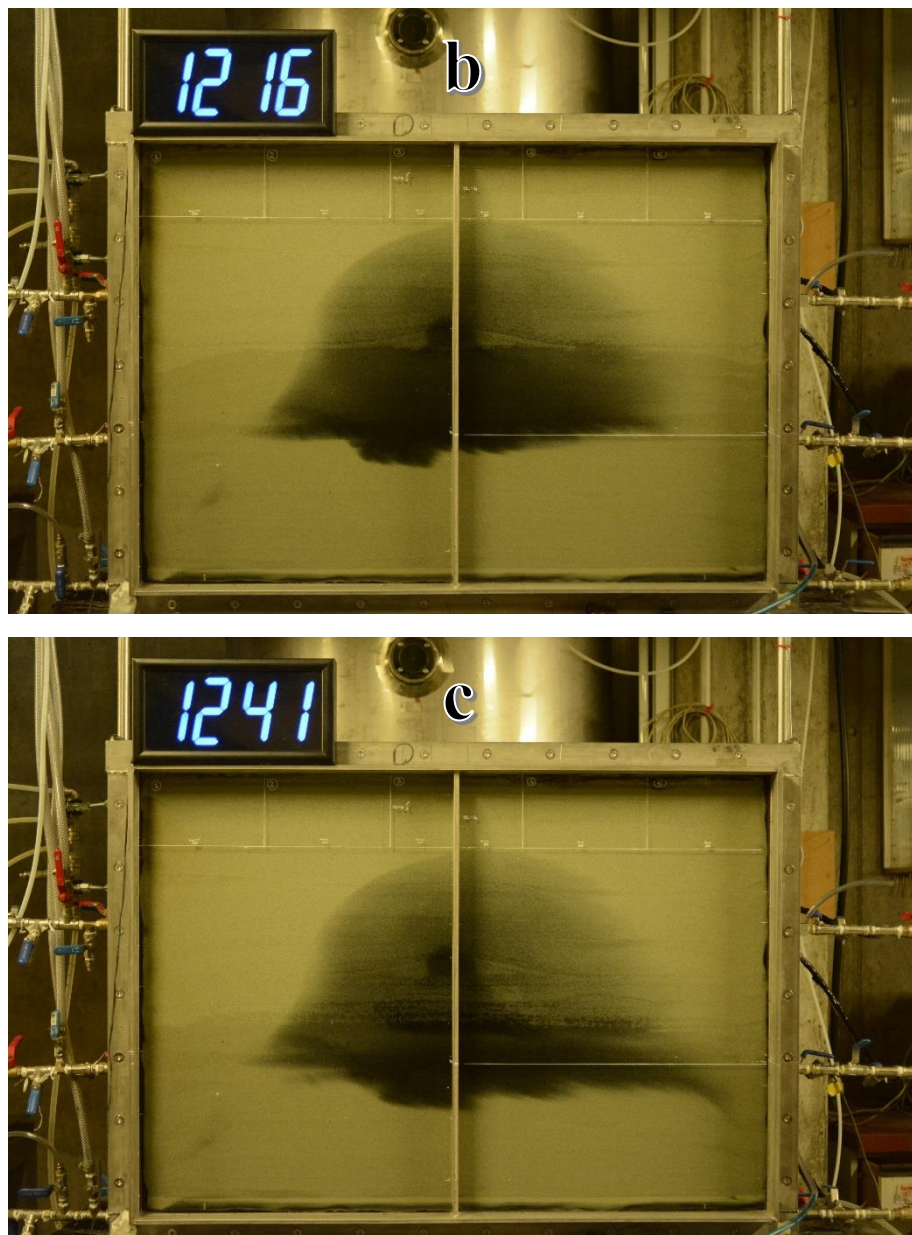
The iron concentration in the samples 10 and 11 in the Figure 6.23 depend by two phenomena:

- Sample 10: the iron in this in the area depend by the drainage that occurs in the flume;
- Sample 11: the iron in this area increases with the time due to the gravity force.

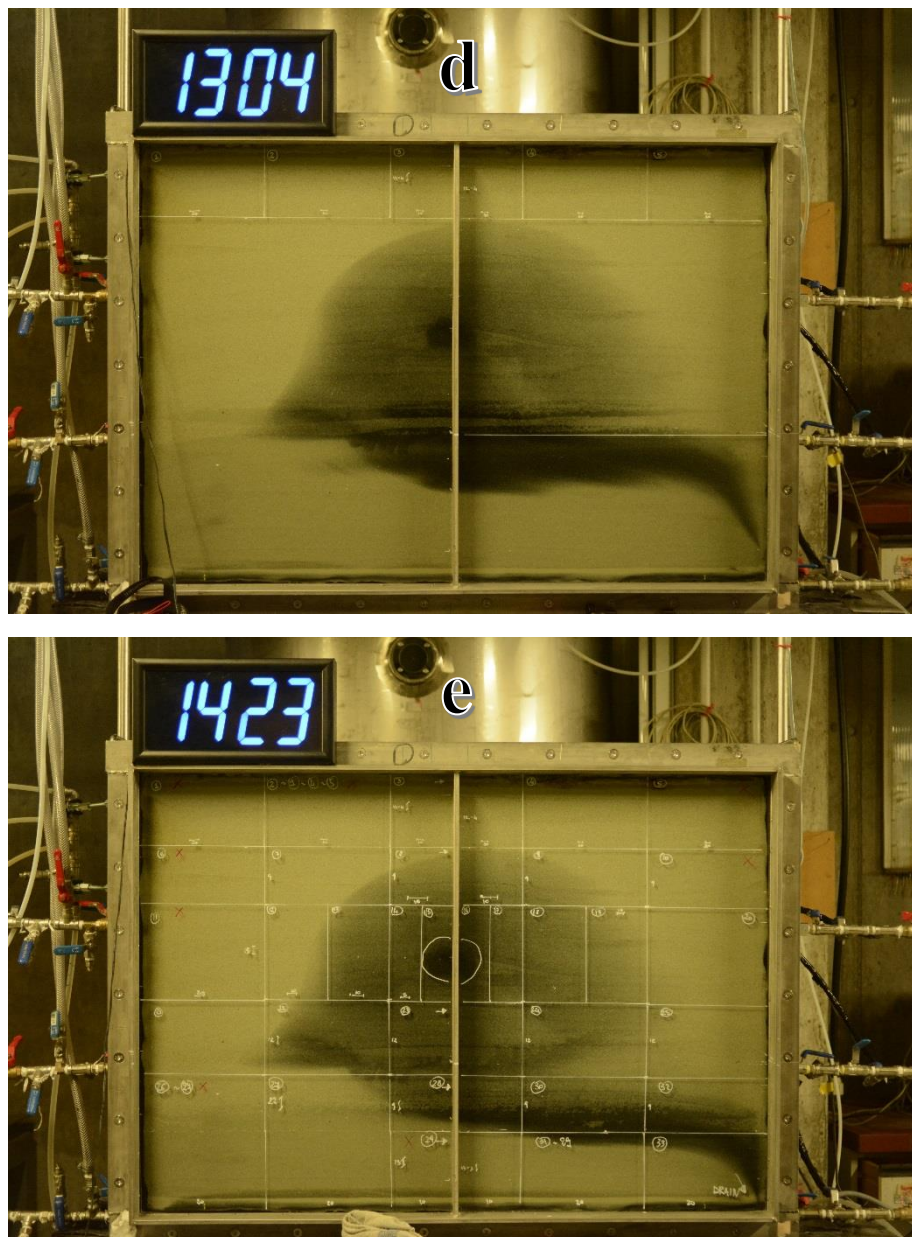
These two hypotheses can take true observing the Figure 6.24.



6. EXPERIMENT



6. EXPERIMENT



6. EXPERIMENT

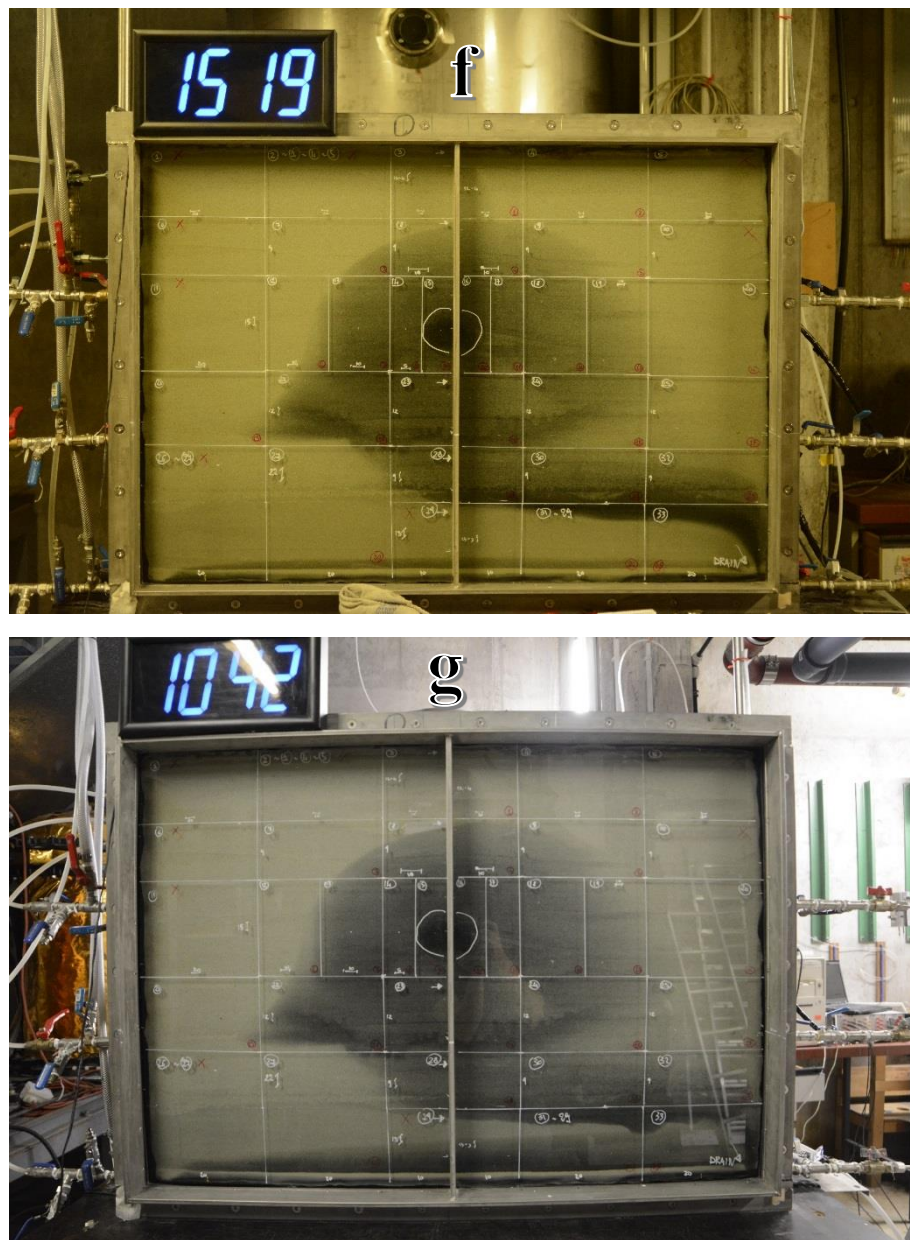


Figure 6.24 Time lapse of the draining process

In the Figure 6.24 it is important to notice some pictures:

- The picture “a” was taken one day after the injection experiment of CI with all the wells open;
- The picture “f” was taken the same day and, at that moment, all the wells were closed;
- The picture “g” was taken two days after the injection test before starting the sample collection.

So, the Figure 6.24 shows that the sedimentation in the bottom occurs when the wells are closed and for this reason, it is possible to considerate the sample in the bottom of the flume as the result of the gravity effect.

This means that the iron particles have a mobilization after the injection.

6. EXPERIMENT

In the end, it is also possible to say that the sum of the absolute iron in the flume is equal to 11,9g. It is an acceptable value in comparison with the maximum total iron previously measured (36,16g).

6.3.2 Total Organic Carbon values

The Total Organic Carbon concentration measured for this test includes both CMC and activated carbon particles present in CI.

From these data it is possible to evaluate if, as hypothesized based in sedimentation tests, a partial separation between the iron particles and the activated carbon happens, and how the carbon component of the suspension spread in the 2D aquifer.

The TOC values were measured in the same areas of the Figure 6.23.

The values are reported here as the ratio between the CMC and activated carbon values.

Initially, it is possible to compare the concentration of total iron and activated carbon because the Carbon Iron particles are composed of 22,3% of iron and 50% of activated carbon so it is possible to write:

$$CI * 22,3\% = C_{Fe} \rightarrow C_{AC} = CI * 50\%$$

In the end, the missing part of the AC was multiplied with a correction factor.

The correction factor was evaluated with the concentration of TOC measurement in the sedimentation test for the suspension of 20g/L of CI and no CMC. (Table 3.4 Tes1-sample1) because in this sample the TOC is related just to the activated carbon. Thus, the correction factor (ϕ) is equal to the division between the TOC concentration and the CI concentration in the suspension:

$$\phi = \frac{TOC_{Test1,sample1}}{C_{CI}} = 0,192$$

Table 6.5 Evaluation of the missing concentration of activated carbon in the different areas

Nº Sample	C _{Fe} (g/Kg)	C _{CI} Evaluated (g/Kg)	C _{CA} evaluated (g/Kg)	C _{CA} measured (g/Kg)	%C _{CA} missing
1	0,19	0,85	0,43	0,017	18,43
2	9,25	41,48	20,74	1,171	18,11
3	89,33	400,58	200,29	3,263	18,88
4	87,52	392,47	196,23	4,447	18,76
5	107,61	482,56	241,28	5,376	18,77
6	15,65	70,18	35,09	1,282	18,49
7	1,28	5,74	2,87	0,287	17,27
8	0,39	1,75	0,87	0,129	16,36
9	0,25	1,12	0,56	0,014	18,72
10	0,04	0,18	0,09	0,114	-5,20
11	0,03	0,13	0,07	0,041	7,49

6. EXPERIMENT

Almost all the values of activated carbon are lower than the expected concentration, particularly in the area near the injection well. The only values where the AC is a good concentration is in the sample 10.

Therefore, it is possible to say that:

1. The activated carbon has a higher mobility than the iron particles;
2. The drain phenomenon is stronger in the areas near the injection well how is clear by the time lapse in the Figure 6.24.
3. The high concentration of activated carbon in the area 10 of the Figure 6.23 is due to drain phenomenon that allows a migration of activated carbon particles and some of these particles sediment in the area 10 increasing the concentration AC value.

Moreover, the missing concentration of activated carbon is higher in the right side than the left side of the flume because this last one had a clogging phenomenon, so the right side had a stronger draining flow.

In the end, it is possible to compare the concentration of CMC and AC in the different areas.

The number of samples is related with the Figure 6.23.

Table 6.6 TOC: concentration of CMC and AC and their ratio in the flume

Nº Sample	Concentration CMC (mg/Kg)	Concentration AC (mg/kg)	Ratio (C_{CMC}/C_{AC})
1	0,023	0,017	1,35
2	0,548	1,171	0,47
3	3,194	3,263	0,98
4	3,925	4,447	0,88
5	4,649	5,376	0,86
6	0,835	1,282	0,65
7	0,181	0,287	0,63
8	0,101	0,129	0,78
9	0,02	0,014	1,47
10	0,071	0,114	0,62
11	0,106	0,041	2,59

6. EXPERIMENT

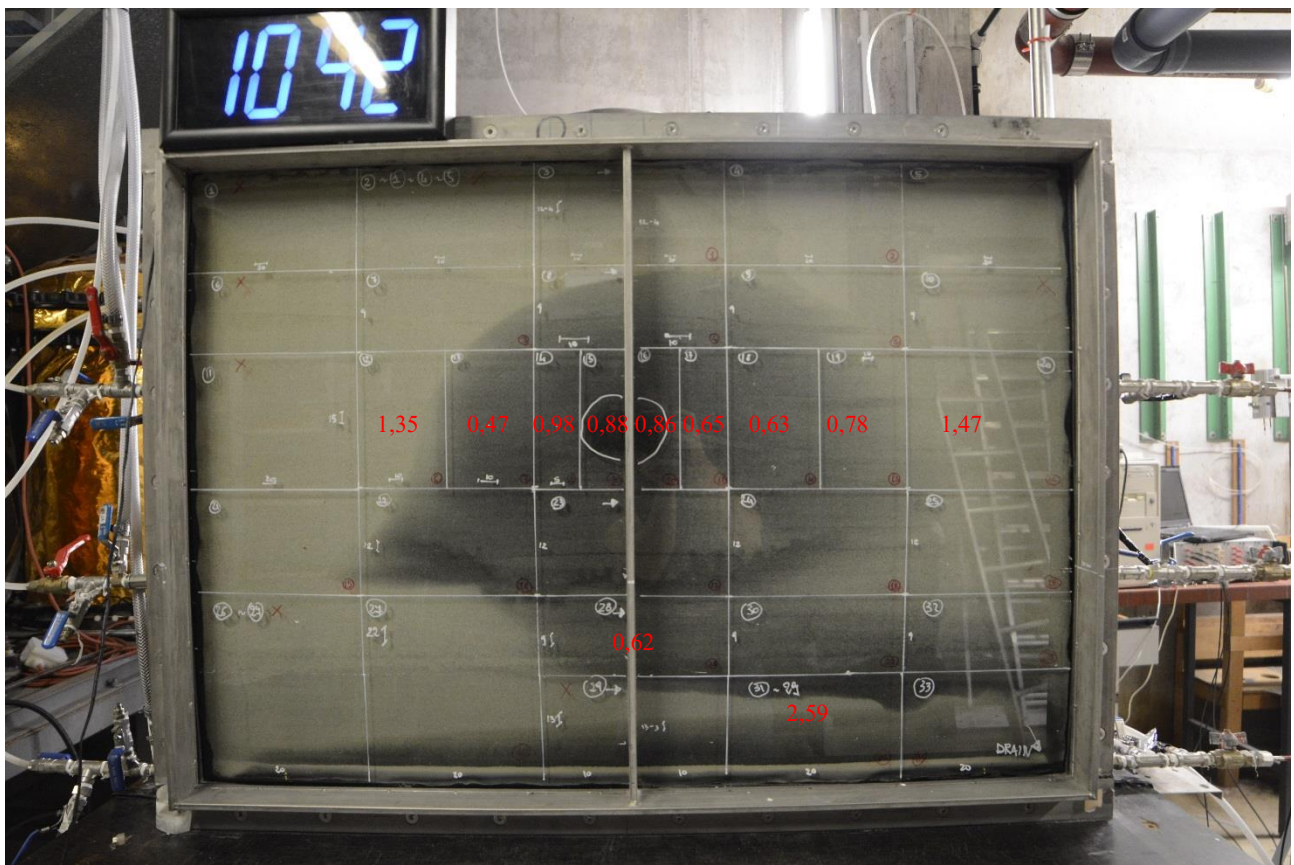


Figure 6.25 Ratio between the CMC and AC concentration

It is noticeable that near of the injection point the values are quite similar and near to the value 1 and in the extremity we have higher values of CMC. This happens because the CMC has a higher mobility, so in the first part of the draining process it arrives more than the activated carbon in the flume extremity and, at the end of the draining process in that areas there is a slow flow how already observed studying the relation between the iron and the activated carbon.

In the bottom areas, we have two different values. The first ratio is equal to 0,62 that means a higher value of activated carbon. This happens because the area had a fast flow so, the more mobile CMC goes in the outlet.

In the end, the last bottom area of the flume shows a very high value of CMC than the AC. This means that when all the wells were closed the gravity effect act more on the CMC than the activated carbon.

7 CONCLUSION

The work conducted in the VEGAS evidenced several new aspects related to preparation and injection of Carbon Iron, extremely relevant for its field applications.

The rheological measurements demonstrated that the viscosity of the CMC solution without AC is higher than the suspension because the CMC ties with the activated carbon of the CI.

The results of the TOC and Total Iron measurements in the flume experiments confirmed the preliminary hypothesis, based in sedimentation tests, the iron particles are not fully and irreversibly bonded to the activated carbon. This result is in agreement with previous hypothesis proposed by the producer to explain a partial separation of iron nanoparticles and activated carbon observed in some cases in previous studies, but never investigated into details before.

The flume injection experiment evidence that, as reasonably expected, the mobility of CMC is higher than the CI, and that the iron particles have a higher capacity to be retained in the flume compared to activated carbon, which is beneficial for the field application of the material, when it is desired to have iron particles retained in the soil after injection, and not indefinitely mobile in the subsurface.

Based on the results of this study, it is possible to conclude that the use of this material in the field is potentially extremely effective, even if would be necessary carry out further tests to obtain a complete picture of CI mobility and injectability in large scale and field-like conditions. In particular, it would be beneficial to run additional injection tests at a CMC concentration lower than the dose used here: the results evidenced that, when using 2g/L of CMC the suspension is quite prone to density-driven flow, thus causing a transport of CI still suspended in pore water toward the bottom regions.

APPENDIX AND BIBLIOGRAPHY

Appendix 1, sedimentation test procedure:

DATE: SEPT 2004

Particle Size Analysis (Hydrometer Method)

1. Application

The percentage of sand, silt and clay in the inorganic fraction of soil is measured in this procedure. The method is based on Stoke's law governing the rate of sedimentation of particles suspended in water.

2. Summary of Methods

The sample is treated with sodium hexametaphosphate to complex Ca^{++} , Al^{3+} , Fe^{3+} , and other cations that bind clay and silt particles into aggregates. Organic matter is suspended in this solution. The density of the soil suspension is determined with a hydrometer calibrated to read in grams of solids per liter after the sand settles out and again after the silt settles. Corrections are made for the density and temperature of the dispersing solution.

3. Safety

Each chemical compound should be treated as a potential health hazard. The laboratory is responsible for maintaining a current awareness file of OSHA regulations regarding the safe handling of the chemicals specified in this method. A reference file of material handling data sheets should be made available to all personnel involved in the chemical analysis.

4. Interferences

The principal source of error in this procedure is the incomplete dispersion of soil clays. These clays are cemented by various chemical agents and organic matter into aggregates of larger size. Failure to effect complete dispersion results in low values for clay and high values for silt and sand. The rate of sedimentation also is affected by temperature and the density of the dispersing solution.

5. Apparatus and Materials

- 5.1 Glass cylinders, 1000-ml capacity
- 5.2 Thermometer, Fahrenheit
- 5.3 Hydrometer, Bouyoucos (Fisherbrand Model # 14-331-5c)
- 5.4 Electric mixer with dispersing cup
- 5.5 Plunger
- 5.6 Balance sensitive to $\pm 0.01\text{g}$

6. Reagents

- 6.1 Dispersing solution, 5%: Dissolve 50 g of sodium hexametaphosphate, $\text{Na}_6(\text{PO}_3)_6$ in deionized water and dilute to 1 liter.

7. Methods

- 7.1 Mix 100 ml of the 5% dispersing solution and 880 ml of deionized water in a 1000 ml cylinder. This mixture is the blank. (Note: 100 ml + 880 ml = 980 ml. This blank is not diluted to 1000 ml; the other 20 ml is the volume occupied by 50 g of soil.).
- 7.2 Weigh 25-50 g of soil and transfer to a dispersing cup. Record weight to $\pm 0.01\text{g}$.
- 7.3 Add 100-ml of 5% dispersing solution.
- 7.4 Attach dispersing cup to mixer and mix the sample for 30 – 60 sec.
- 7.5 Transfer the suspension quantitatively from the dispersing cup to a 1000 ml cylinder.
- 7.6 Fill to the 1000-ml mark with deionized water equilibrated to room temperature, or allow to stand overnight to equilibrate.
- 7.7 At the beginning of each set, record the temperature, and the hydrometer reading of the blank, using the procedure described below.
- 7.8 To determine the density insert plunger into suspension, and carefully mix for 30 sec. until a uniform suspension is obtained. Remove plunger (begin 40 second timer) and gently insert the hydrometer into the suspension.
- 7.9 Record the hydrometer reading at 40 sec. This is the amount of silt plus clay suspended. The sand has settled to the bottom of the cylinder by this time. (Repeat 7.8 – 7.9 for each sample)
- 7.10 Record the hydrometer reading again after 6 hours, 52 minutes. This is the amount of clay in suspension. The silt has settled to the bottom of the cylinder by this time.

Appendix 2, CI properties from producer:



Helmholtz-Zentrum für Umweltforschung GmbH – UFZ | Permoserstraße 15 | 04318 Leipzig

Juergen Braun, Ph.D.
Universität Stuttgart
IWS/VEGAS
70569 Stuttgart Germany
Pfaffenwaldring 61

Dr. Robert Köhler
Department
Technische Umweltchemie

Tel. ++49 (0)341 235 1573
oder 1762

Leipzig, 12.2.2018

Fax ++49(0)341 235 1471
robert.koehler@ufz.de

Lieber Herr Braun,
wir konnten ca. 2,76 kg Carboiron herstellen, die Sie portioniert zu ca. 300 g unter Ar- Atmosphäre und in Beuteln verpackt in den Plastikeimern im Paket finden.

Beutel 1	299,25	mg
Beutel 2	300,75	mg
Beutel 3	299,35	mg
Beutel 4	299,6	mg
Beutel 5	299,75	mg
Beutel 6	302,15	mg
Beutel 7	303,22	mg
Beutel 8	299,4	mg
Beutel 9	358,73	mg
Σ	2762,2	mg

Helmholtz-Zentrum für
Umweltforschung GmbH – UFZ

Sitz der Gesellschaft: Leipzig

Permoserstraße 15
04318 Leipzig
PF 500136
04301 Leipzig
Tel +49 341 235-0
Fax +49 341 235-2791

info@ufz.de
www.ufz.de

Registergericht: Amtsgericht Leipzig
Handelsregister Nr. B 4703

Vorsitzender des Aufsichtsrats:
MinR Wilfried Kraus

Wissenschaftlicher Geschäftsführer:
Prof. Dr. Georg Teutsch

Administrativer Geschäftsführer:
Dr. Andreas Schmidl

Bankverbindung:
HypoVereinsbank Leipzig
BLZ 860 200 86
Kto.-Nr. 5080 186 136
Swift(BIC)-Code HYVEDEM 495
IBAN-Nr. DE12860200865080186136
UST-Ident-Nr. DE 141 507 065
Steuer-Nr. 232/124/00416

Als Primärpartikel verwendeten wir Pulsorb-Aktivkohle RD 90 mit einem $d_{50} < 1,5 \mu\text{m}$ - also ein bisschen größer als das Material, welches Sie schon einmal von uns bekamen. Der Fe(0)-Gehalt der Gesamtcharge beträgt 22,3 Ma.-%. Den Kohlenstoffgehalt muss ich noch bestimmen und liefern ihn per mail baldigst nach.

Gestatten Sie uns noch ein paar Anmerkungen zur Verwendung und zu den Eigenschaften dieser CI-Charge:

Im carbothermischen Prozess verbucken/verhaken die Partikel gern. Diese Verbackungen lassen sich aber durch gute Suspendierung mit dem Ultra-Turrax lösen, so dass dann wieder die Primärpartikel vorliegen.

Ohne intensive Suspendierung sollte nicht gearbeitet werden!

Das UFZ ist validiert nach EMAS –
Geprüftes Umweltmanagement

APPENDIX AND BIBLIOGRAPHY

Seite 2



Neben der chemischen Charakterisierung, haben wir uns auch das Sedimentationsverhalten angesehen. Dazu haben wir die Proben so vorbereitet, wie es im Feld vor einer Injektion gemacht würde: Suspendierung der Partikel, CMC-Zugabe (vorgelöst) und intensive Dispergierung. Wir haben in den Sedimentationsversuchen wieder den Effekt gesehen, dass es nicht ein völliges Gleichlaufen von Kohlenstoff und Eisen gibt. Das hat sich jetzt für die carbothermisch hergestellten Proben so bestätigt, obwohl akribisch beim Tränken darauf geachtet wurde, dass das Eisensalz in das Porenvolumen eingebracht wurde. Das hatte aber für die neulich im Feld von Intrapore eingesetzte Charge keine Abstriche am Ergebnis bedeutet. Die hier vorliegende Charge ist auch schon nach einer neuen angepassten Methode hergestellt worden und ist in Wasser (natürlich wieder unter anoxischen Bedingungen arbeiten!) sehr korrosionsstabil. Für eventuelle Reaktivitätsuntersuchungen muss man deshalb darauf achten, dass für die Produktanalytik nicht nur nach Ethan und Ethen geschaut wird, sondern auch Ethin mit einbezogen wird, das anfänglich bevorzugt entsteht. Außerdem wird es eine deutliche leachbare Chloridmenge geben, die man beim Bilanzieren mit beachten muss. Wir haben aber nun nicht mehr den Effekt gehabt, dass sich H₂-Blasen bilden und so Umströmungen auftreten.

Gern können Sie mich bei auftretenden Fragen kontaktieren.

Mit freundlichen Grüßen auch von Katrin M.

A handwritten signature in blue ink, appearing to read "Katrin M." followed by a date.

Bibliography

- (s.d.). Available at National Geographic Society:
<https://www.nationalgeographic.org/encyclopedia/aquifer/>
- (s.d.). Available at ENCYCLOPAEDIA BRITANNICA:
<https://www.britannica.com/technology/water-supply-system/Surface-water-and-groundwater>
- (s.d.). Available at proekosrl: <https://www.proekosrl.com/shop/cmc-carbossimeticellulosa-grado-tecnico-100-gr/>
- Abita, A., Palumbo, V., Costa, N., Nicolosi, M., & Pellerino, S. (2017, August 24). *ARPA*. Available at <http://www.apa.sicilia.it/wp-content/uploads/2017/08/report-monitoraggio-corpi-idrici-2016-.pdf>
- ahin, S. E. (2011, September 13). Quantification of pore-size spectrums by solute breakthrough curves. *Copernicus Publications*, p. 8397.
- Arle, J., Blondzik, K., Claussen, U., Dufferk, A., Grimm, S., Hilliges, F., . . . Leujak, W. (2013). *Water Resource Management in Germany Part 2 -water quality-*. Berlin: Umwelt Bundesamt.
- Atkins, P. (2000). *The Elements of Physical Chemistry With Applications in Biology*. New York: W.H: Freeman and company.
- Boulding, J. (1996). *EPA ENVIRONMENTAL ENGINEERING SOURCEBOOK*. Cheòsea, Michigan: Ann Arbor Press, Inc.
- Britannica, T. e. (s.d.). Tratto da Encyclopaedia Britannica:
<https://www.britannica.com/science/magnetic-susceptibility>
- Di Molfetta, R., & Sethi, R. (2012). *Ingegneria degli acquiferi*. Springer Verlag.
- Erşahin, S. (2011, September 13). Quantification of pore-size spectrums by solute breakthrough curves. *Copernicus Publications*, p. 8397.
- Giannelli, G. (2014). *Small Flume Experiment for the Transport Evaluation of Carbon-Iron Particles in a Confined Aquifer*.
- Greenlee, L., Lawler, D., Freeman, B., Marrot, B., & Moulin, P. (2009). Reverse osmosis desalination: Water sources, technology, and today's challenges. *Water Research*, 2317-2348.

- Konijn, B., Sanderink, O., & Kruyt, N. (2014). Experimental study of the viscosity of suspensions: Effect of solid fraction, particle size and suspending liquid. In *Powder Technology* (p. Volume 266, Pages 61-69). L.-S. Fan (The Ohio State University, USA).
- Kretzschmar, R., Borkovec, M., Grolimund, D., & Elimelech, M. (1999). MOBILE SUBSURFACE COLLOIDS AND THEIR ROLE IN CONTAMINANT TRANSPORT. *Academic Press*, p. 121-169.
- multiphysics CYCLOPEDIA*. (2015, January 14). Available at:
<https://www.comsol.com/multiphysics/diffusion-coefficient>.
- R.Gavaskar, A. (1999, August 12). Design and construction techniques for permeable reactive barriers. *Journal of Hazardous Materials*.
- R.Gavaskar, A. (1999). Design and construction techniques for permeable reactive barriers. *Journal of Hazardous Materials*, 41-71.
- Sweeney, R., & Harries, N. (2016). *A Guide to Nanoparticles for the Remediation of Contaminated Sites*. CL:AIRE.
- Tosco, T., Bianco, C., & Sethi, R. (2018). An Integrated Experimental and Modeling Approach to Assess the Mobility of Iron-based Nanoparticles in groundwater System. In N. Q. Marta I. Litter, *Iron Nanomaterials for Water and Soil Treatment*. Pan Stanford.
- Tosco, T., Gastone, F., Luna, M., & Sethi, R. (2015). *MICRO E NANOPARTICELLE DI FERRO PER LA BONIFICA DI ACQUIFERI CONTAMINATI: DAL LABORATORIO ALL'APPLICAZIONE IN CAMPO*.
- Vanzetti, C., Giangoglio, N., & Sesia, E. (2016, January). *Arpa Piemonte*.
- Zangheri, P. (2000). *L'acqua sotterranea: una risorsa nascosta. Pozzi, acquiferi e falde nella provincia di Venezia*. Villorba (Treviso): Centro Internazionale civiltà dell'Acqua.